Universiteit Utrecht

Adriana M. Currin Sala
MSc Thesis
supervised by
Prof.Dr. Martyn Drury
Dr. Côme Lefebvre

June 2014

STRUCTURAL AND METAMORPHIC EVOLUTION OF THE ERICEK AREA (SE TURKEY) NEAR THE SÜRGÜ FAULT, NORTH OF BERIT MOUNTAIN, IN CONTEXT OF EURASIA-AFRICA COLLISION

Acknowledgements

Firstly thanks to Côme Lefebvre and Donna Whitney of the University of Minnesota for accepting my proposal to work on objectives related to the CD-CAT project. Many thanks to Côme for supervision as well as providing samples, field data and invaluable guidance along the project. Satellite imagery used in the regional map is copyright of DigitalGlobe, Inc. and provided through the Polar Geospatial Center (University of Minnesota - Twin Cities)

Many thanks to my supervisor Martyn Drury of Universiteit Utrecht for his support and guidance and for teaching me so much and showing me a new way of looking at microstructural analysis.

Also to Gill Pennock of Universiteit Utrecht for being so helpful and also guiding me in organisational matters and support in follow-up meetings and help in SEM.

To all the other staff and lecturers at Universiteit Utrecht that I've had the pleasure to learn from and have made my outlook on Geology so different from before, including Herman van Roermund, Chris Spiers, Oliver Plümper, Liviu Matenco, Hans de Bresser, Manfred van Bergen and Paul Meijer.

Many thanks to Gemma Alias of the University of Barcelona for her advice, showing me how to go about a research project in the first place and pass on her enthusiasm for petrology and metamorphism. Also to Montserrat Liesa, for fuelling my motivation and teaching me so much. In addition, thanks to all those other lecturers at UB who contributed to my geological learning.

And to all those friends, colleagues and family who have offered their invaluable support throughout this task.

Adriana Currin Sala, June 2014

Table of Contents

Abstract

In the current setting of SE-Anatolian escape tectonics, the Ericek area, N of Berit mountain, is integrated by tectonic stacking of units near a palaeo-suture zone. These units record a history of oceanic closure, back-arc rifting and plate collision. Late Cretaceous to Eocene magmatism and intermediate-to-high temperature metamorphism is found to intrude into the complex nappe-stacking system found at Berit Mountain.In addition, Plio-Quaternary Sürgü Fault Zone (SFZ) is a localized strike-slip system that cuts the study area as a small branch of larger-scale escape tectonics. Both the study of intrusions and their relationship to metapelitic and calcitic host rocks and the study of units affected by later faulting can give insight into the tectono-metamorphic evolution of the study area. The following study employs petrological and microstructural tools, such as light microscopy and SEM, to explore the aforementioned two issues. Metapelites are confirmed to be affected by a contact metamorphic aureole of the intrusive batholiths, showing biotite, cordierite (syn-foliation) and andalusite (post-foliation) as index minerals. The timing of events and metamorphic growth correlate to late-to-post orogenic intrusive activity. No clear isograds have been traced, but changes in mineral composition within the contact aureole are attributed to thermal metamorphism and chemical availability. In addition, granitic samples from the Berit group some km apart on either side of the study area have different characteristics, both in nature of the granitic batholith and of the surrounding country rock. This could be attributed to different timing of intrusion. On the other hand,studied fault rocks confirm the action of the more modern strike-slip Sürgü Fault Zone (SFZ) on Jurassic, Eocene and Miocene lithologies, indicating its later occurrence. Pseudotachylite veins have been searched for in fault rocks, but grain-size reduction has proven to be the main mechanism of deformation in place of frictional melting. However, available microstructural evidence is still insufficient for confirmation.

1. Introduction

The collision of the African-Arabian plate with Eurasia induced the development of two major strike-slip faults in the north and east of the Anatolian peninsula. The Eastern Anatolian Fault Zone (EAFZ) is a major sinistral fault system which runs across the south-east of the peninsula, extending from the easternmost Mediterranean to the East Anatolian plateau or collision zone.In this collision zone the EAFZ converges with the dextral Northern Anatolian Fault Zone (NAFZ), that runs parallel to the southern coast of the Black Sea. The motion these two major strike-slip zones accommodates the shortening from collision between the Eurasian and Arabian-African plates (Şengör *et al.*, 1985). The Anatolian plate is wedged in between the latter two and as a result of their collision is subject to westward displacement. The northward subduction of the African plate beneath Eurasia started in the Late Cretaceous, with the closure of the Neotethyan ocean. The existence of this ocean is marked by outcropping Late Cretaceous ophiolitic sequences in south-eastern Anatolia, providing evidence for the presence of a spreading ridge prior to plate collision (Yilmaz et al, 1993; Göncüoglu, 2010). The tectonic evolution of south-eastern Anatolia is still a matter of discussion and requires further study especially concerning later stages of subduction and onset of continental collision.

It is important to consider the mechanisms responsible for the formation of escape tectonics to acommodate shortening and the relationship of tectonic events to magmatic activity in order to understand the overall structural evolution of SE Anatolia. In addition, the complex context of such geological processes should be taken into account, since the Anatolian plate islocated betweenthe collision zone of Arabia and Eurasia in the East and an extensionalsetting to the west in the Aegean sea.

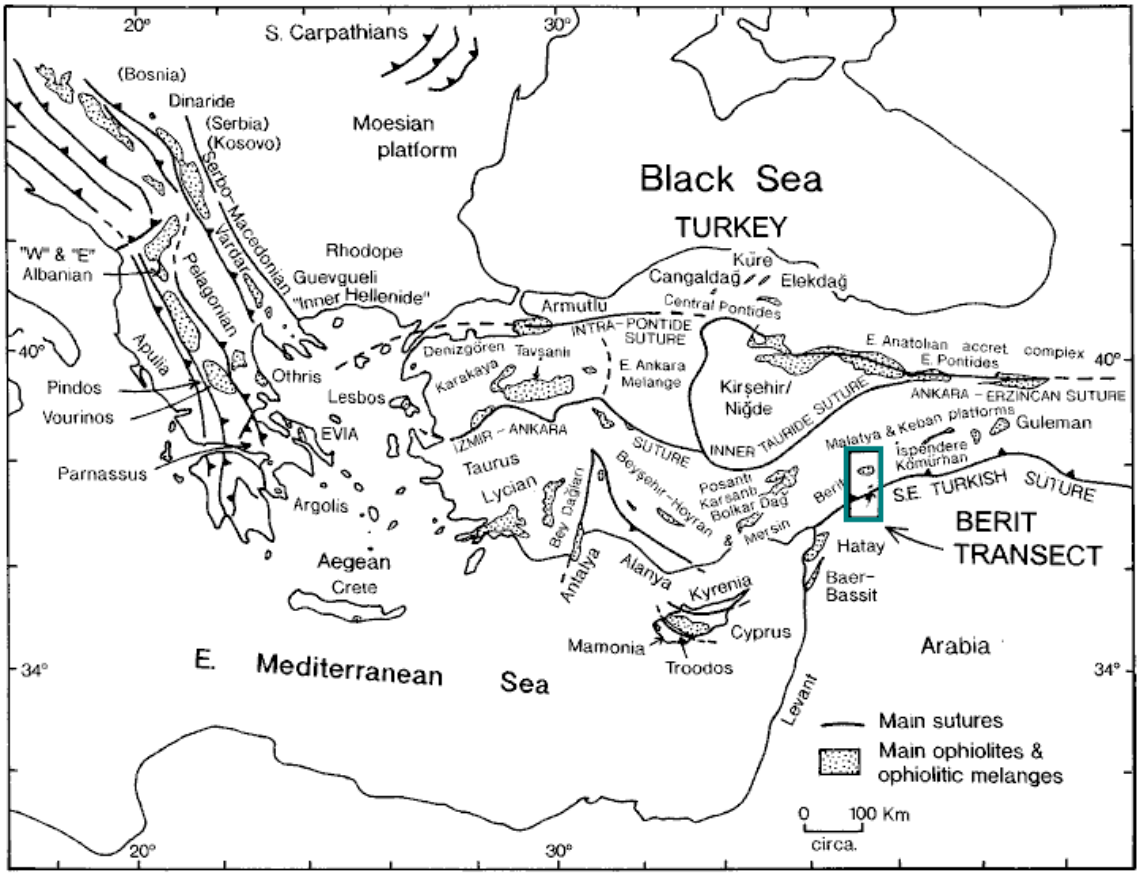

Figure 1.1 –*Map of the Eastern Mediterranean showing the main tectonic divisionsin the Aegean and Anatolian areas. Location of the study area is found within theblue rectangle. Modified from Robertson (2006).*

Study area

The area near the village of Ericek is made up of a sequence of E-W-trending thrust sheets of southward vergence, granitic intrusions and cross-cutting strike-slip faults. The Sürgü fault is a branch of the aforementioned Eastern Anatolian Fault and the thrusts are part of the nappe-stacks that result from collision of the African-Arabian and Eurasian plates. This area is therefore the setting of an apparent transition of strain localization mechanisms between a thrusting regime and a strike-slipfaulting context.The timing of this transition is key to the understanding of the tectonic evolution of the area.

1.1. Research approach

The study of this area has been divided into two lines of research concerning:

a) (Eocene)magmatism and high-temperature (HT)metamorphism incorporated into the complex nappe-stacking system found at Berit Mountain.

b) A localized strike-slip system that developed with escape tectonics which cuts through the aforementioned nappe-stacks:the Sürgü Fault.

The aim of this project is to study the structural and metamorphic evolution of the area, involving the relation between the Berit Mountain (composed of superimposed tectonic slices) in the south and the dextral Sürgü Fault Zone (SFZ) in the North. In order to achieve this, the nature of metamorphism should be assessed and the implication of local problems should be understood at a regional scale.

Problem statements

- The tectonic-scale deformation history and plate configuration of SE Anatolia needs to be constrained further.
- The sequence of tectonic, magmatic and metamorphic events in the vicinity of the village of Ericek requires more in-depth understanding at a local scale and in its large-scale tectonic context.

Research questions

- *What is the **relation**, **origin** and **age** between magmatic and metamorphic eventsin the vicinity of Ericek and in SE Anatolia?*
- *Why is **magmatism** in SE Anatolia, mainly **localized** at the vicinity of the Surgu Fault (Karaoglanet al. 2013)?*
- *What are the **metamorphic** and **deformational conditions** of the area and sampled rocks?*
- *What is the **role** and the **age** of the Sürgü fault?*
- *What **degree of fault activity** is observable in the microstructures of the sampled rocks?*
- *Can **seismic vs. aseismic** fault rocks and microstructures be recognised in the fault zone?*
- *Are there any indicators for **exhumation** in the area?*

Objectives

a) Mapping of potential metamorphic field gradient throughout the study area and major structures shaping the region through integration of petrological and field data.This will allow understanding the relationships between lithological units and give insight into the tectono-metamorphic evolution of the area.

b) Microstructural analysis of intermediate- to high-grade schists. This will show relationship between different lithological units and large-scale tectonic events.

c) Analysis of fault rocks within the Sürgü fault zone with special attention to rocks formed during seismic deformation, such as potential pseudotachylite and ultra-cataclasites.

d) Place the analysis of tectonic evolution of metamorphic, magmatic and fault rocks in the context oftheir tectonic setting and correlate to results exposed in the literature. This will allow understanding of the general tectonic-scale plate deformation and configuration.

In this study, results from the following methods are integrated: structural analysis of different lithological units using field data and stereographic projection; light microscopy analysis of available thin sections; SEM study of pyroclastic fault rocks. The data available includes hand specimens, thin sections, structural field measurements, field photographs, SEM imagery and chemical analyses (qualitative and semi-quantitative). The study did not include any results of LT-geochronological information since data was not yet available and therefore timing of exhumation of analysed lithologies could not be estimated. In addition, previous research plans of analysing deformation of apatite crystals related to fission-track dating methods were not carried out due to insufficient availability of the trace mineral.

1.2. Geological Setting

1.2.1. Structure

Berit Mountain is located in SE Anatolia (Fig. 1), between the western portion of the EAFZ in the South and the Tauride thrust belt in the North, which trends NE-SW in this sector. The northern part of the study area is affected by a dextral strike-slip fault, the Sürgü Fault, which branches off the sinistral East Anatolian Fault to the West (Koç and Kaymakci, 2013).The different lithological units in this area are arranged in a sequence of E-W-trending thrust sheets of southward motion (Perinçek & Kozlu, 1984), which can be found as tectonic windows with the present topography (Karaoğlan*et al.*, 2013). The thrust sheets of this area are emplaced at different timesbetween Late Cretaceous and pre-Mid Miocene (Perincek, 1984). Some normal faults affect the area in a NW-SE and SW-NE direction, oblique to thrusting, possibly related to extension periods during closure of the Neotethyan ocean (Kuscu, 2010). Reactivation of thrust sheets took place in the Plio-Quaternary in the form of strike-slip faulting (Karaoglan, 2013). The contacts between lithologies are mostly of tectonic nature.

As mentioned earlier in the Introduction, the area near the village of Ericek is dominated by Alpine nappe-stacking of different pre-Cenozoic units of platform carbonates, pelites and ophiolites. These units are intruded by granitic batholiths and cross-cut by normal faults. Eocene and Miocene volcano-sedimentary units, clastics and platform carbonates are found overlying the thrusted lithologies. The whole area is cross-cut by the Sürgü fault, anE-W-trending Plio-Quaternary strike-slip fault zone (Robertson *et al.* 2006) (see map, Appendix 1).

1.2.2. Stratigraphy

The main units found in the study areacorrespond, from base to top, to the following tectono-stratigraphic units, arranged by age (Fig. 1.2).

The Andirin Limestone (and other pre-orogenic carbonate platforms of the Taurides)corresponds to Triassic-Jurassic rocks thrust above the Berit groupthat form a tectonic window on the hilltop of Berit Mountain. This unit is overlain by clastics related to closure of the Neotethyan ocean and onset of plate subduction (Kemaliye and Binboga formations:Perincek & Kozlu, 1984;Robertson *et al.*, 2006). The Andirin limestone is thrust over the Berit group.

The Berit group consists of meta-pelites, meta-ophiolite and granite intrusions. This unit is thrusted over the Maden group (Perinçek & Kozlu, 1984). The meta-pelitic part of the unit consists of mica schists and marble and limestone lenseswith some intercalated volcanics (Perinçek & Kozlu, 1984; Karaoğlan *et al.*, 2013).All three subgroups of this unitare intruded by calcalkaline granitoid bodies of either Late Cretaceous (Robertson *et al.*, 2006) or Middle Eocene age (if correlated to similar units located further East,dated by Karaoğlan *et al.*2013). The metamorphic evolution of the aforementionedpelitic lithologies is object of this study.

The Maden group is made up of Middle Eocene volcano-sedimentary formations. These lithologies crop out extensively to the North of the Sürgü fault (Perinçek & Kozlu, 1984) and to a lesser extent in the south of Ericek and the SFZ, where samples have been collected for analysis. This unit corresponds to calcalkaline to alkaline pyroclastics that originated from volcanism at a back-arc rift setting (Robertson *et al.* 2006).

The Kuzgun formation:this unit corresponds to Miocene hemipelagic clastic rocks and reefal limestones as well as intercalated volcanics (Perinçek & Kozlu, 1984).Limestones from this unit are sampled for analysis close to the Sürgü fault.

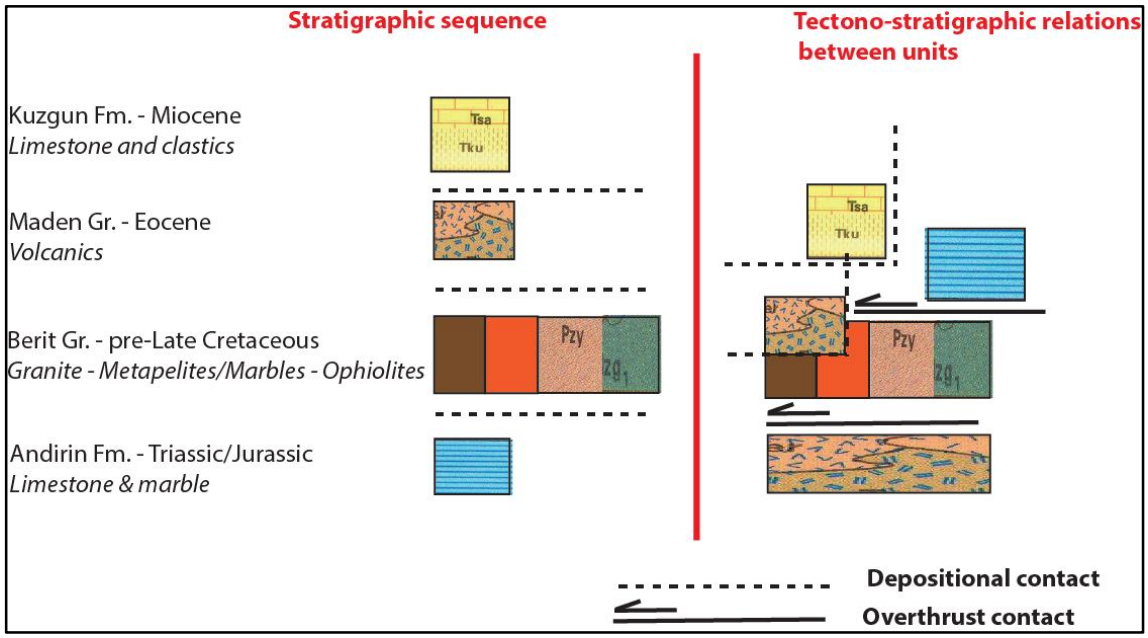

Figure 1.2 – *Sketch showing stratigraphical sequence of main units outcropping in the Ericek area.*

1.2.3. Magmatism

In the South-East Anatolian Orogenic Belt there are associated orogenic igneous rocks from plutonic to intrusive and extrusive nature, generally late to post-orogenic.There is a gradual change in composition from North to South, migrating from calcalkaline to alkaline in a southerly direction. This might be the consequence of variations in the motion and morphology of the subducting slab (Kuscu *et al.* 2010).

According to Kuscu et al (2010), intraplate magmatic events associated to subduction and collision in SE Anatolia often involve episodes of extension, although there is no consensus about the exact mechanisms causing uplift and volcanism. It is likely that extension may be caused by lithosphere delamination and/or variations in the subducting plate and upper mantle (Duggen *et al.* 2005) or due to slab roll-back (Wortel and Spakman, 2000). According to

Robertson *et al.* (2006) the extension that causes magmatism corresponds to back-arc within-plate extension.

Robertson *et al.* (2006) mention that granitic intrusions are largely absent further south of Berit Mountain. Karaoglan*et al.* (2013) report intrusions close to the Sürgü fault in a location area some tens of km further NE.In the Ericek area, granitic batholiths are found intruding pelitic and ophiolitic units of the Berit group.

According to Robertson *et al.* (2006), the granite found between the Sürgü fault and Berit mountain is sheared on its edges and cross-cut by aplite intrusions with a less deformed interior. In this study we refer to this granite as the granite of the western valley of the study area. Robertson *et al.* also mention smaller-scale granitic dykes intruding the metapelitic unit of the Berit group, such as that found adjacent to the hornfels sample described in this study (15D).

1.2.4. Metamorphism

Some of the lithological units in this area are found to have undergone metamorphism during closure of the Neotethyan ocean. This is the case of the metapelites and metaophiolites of the Berit Group, which crop out in this area (Perinçek & Kozlu, 1984). Equivalent units some 75 km further East have been found to be affected by high-temperature metamorphism, the temperature increase of which may have occurred due to subduction of an active mid-ocean ridge below a magmatic arc (Karaoğlan *et al.*, 2013). Contact metamorphism is likely to have occurred in the study area due to the presence of intrusive granitic bodies into metapelitic and limestone/marble host rocks.Age constraints on metamorphism still need to be confirmed in the Ericek area.

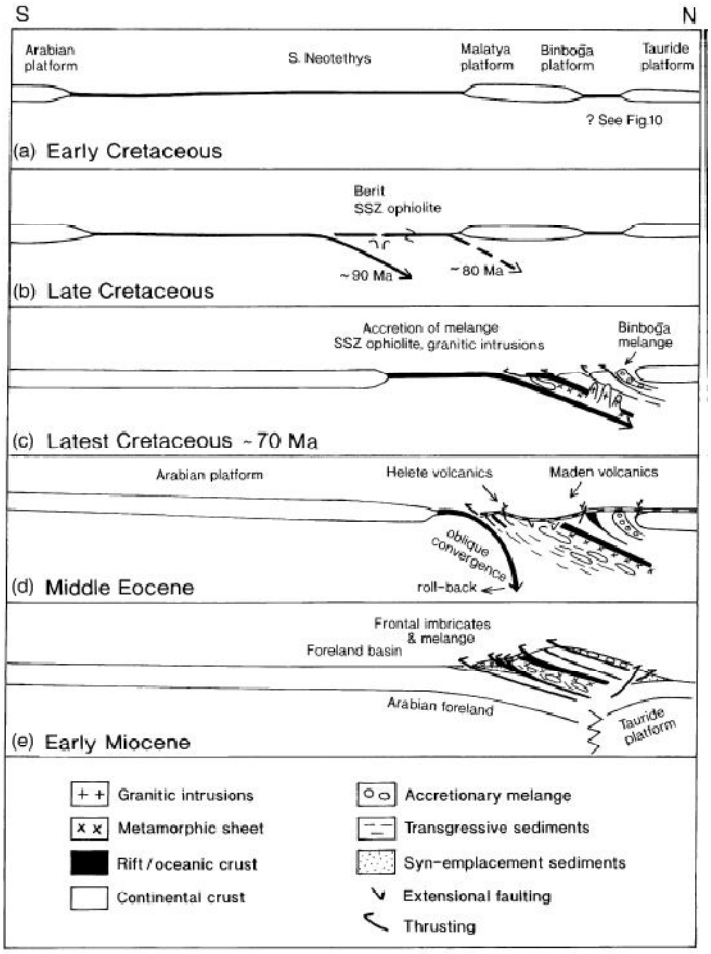

1.2.5. Alpine tectonic evolutionof the area

The following model is described by Robertson et al. (2006) on multi-phase convergence of Eurasia-Arabiabetween the Late Cretaceous and mid Miocene as part of the Alpine Orogeny.Ophiolites found in the study areawere generated in the Coniacian (Late Cretaceous) on a northward-subducting oceanic plate, some km south of the edge of the Tauride continent.

The latter continental crust overthrusted the Berit ophiolite and then was intruded by calc-alkaline granitic rocks.Closure of the Neotethyan ocean continued

Figure 1.3 –*Schematic diagram of different stages of tectonic plate configuration in SE Anatolia. Robertson et al. (2006).*

with progressive subduction until continental collision in the Miocene, with some extensional episodesdue to to back-arc basin formation. Slopes generated by thrusting gave rise to erosion and deposition of units.Further volcanism arose from extension (and normalfaults).

1.2.6. Geological hazards

South-eastern Turkey is an area of Earthquake hazards, despite the low activity related to the EAFZ in the last century, it is an active seismic zone (Nalbant *et al.* 2002). The Sürgü fault that cuts across the study area, being a branch of the EAFZ, is a potential earthquake hazard.

2. Results

The results obtained from the analysis of 18 thin sections are presented in this chapter. Samples have been studied with light microscopy and 2 of them with a JEOL tabletop scanning electron microscope (SEM). In the following section the aforementioned samples will be briefly described at a microscopical scale and will be discussed in their context, using field observations and structural data. The chapter is divided into two distinct sections: one involving lithologies affected by brittle deformation and related to the Sürgü strike-slip fault; another on analysis of metamorphosed sediments and their relation to granite intrusions. A geological map of the area has been elaborated on the basis of the Elbistan geological map (MTA, 1994)and updated with field measurements. This regional geological map includes lithological and structural information, as well as sampling locations (Appendix).

The study area is bound by the Sürgü fault in the North, which cuts across in an E-W direction. Two valleys can be distinguished, each of which is taken up by a plutonic body and sedimentary host rock. In the South Berit Mountain crops out with a tectonic window of metamorphosed limestone.

2.1. Metamorphism and magmatism in the Ericek area

This section describes the lithologies sampled in the metamorphosed sediments and granitic intrusions of the Berit group located between the Sürgu fault and Berit Mountain, SE Anatolia.Their location corresponds to the points in the map (Appendix 1), distinguishing between those lithologies sampled in the western and those from the eastern valley.A comparison between samples of the latter two valleys will be made in order to understand structural relations and timing of tectonic events. A more in-depth description and discussion is dedicated to the metapelites of the western valley and their relation to deformation and granitic intrusions. High resolution scans of each sample are available in the appendix.

2.1.1. Eastern valley – Granitic and sedimentary protoliths

2.1.1.1 Granite-derivedlithologies

This lithological unitcorresponds to the granite patch displayed in the geological map (Appendix 1).This description represents several samples taken from the aforementioned unit of plutonic origin, which display felsic compositions and microstructures resulting from ductile deformation. Compositions vary from almost purely quartzitic to quartzo-feldspathic with low percentages of plagioclase, biotite and muscovite. Matrix microstructures are generally integrated by equidimensional minerals elongated by shear and, on occasion, porphyroclasts of k-feldspar and veins or pores infilled with biotite and muscovite.The range of compositional variations give rise to different nomenclature for each of the samples: meta-syenogranite (18B), qtz-kfs-bt schist (18D), impure quartzite (18C and 18F).

Minerals: quartz, feldspar, plagioclase, biotite, muscovite, chlorite, epidote.

Microstructure: The samples with porphyroclasts are heteroblastic, with a matrix of plagioclase, quartz and feldspar and porphyroclasts of potassium feldspar and plagioclase (Fig. 2.1). Porphyroclasts range from 0.5 to 5 mm in grain size, are anhedral and have rough grain boundaries while those of matrixquartz look well defined, forming a granoblastic elongated microstructure in some areas.Both quartz (60-80%) and potassium feldspar (5-30%), both form elongated crystals of 70 to 200 μm in grain size that follow a preferred orientation along their

maximum elongation axis. Some of the samples are cross-cut by evenly-spaced cracks, some millimetres apart. Undulatory extinction is present in some quartz grains. Other mineralogies present are plagioclase (2-10%), biotite (0-5%) and muscovite (0-3%) in much lower abundance. Biotite and muscovite are around 50 μm in grain size and are found infilling cracks and in localized areas in interstitial spaces between quartz grains.Chlorite is also present as a secondary mineral in much lower abundance (0-0.5%).Some samples(18B) contain small amounts of epidote, that form isolated clusters of about 600 μm with andhedral shape.Samples richer in biotite may present compositional lamination/banding (18D).

The sample closest to the Sürgü fault (18F) presents both ductile and brittle structures, cross-cut by microfaults and microfolds also with quartz grains elongated up to 180 μm and only 30 μm wide.

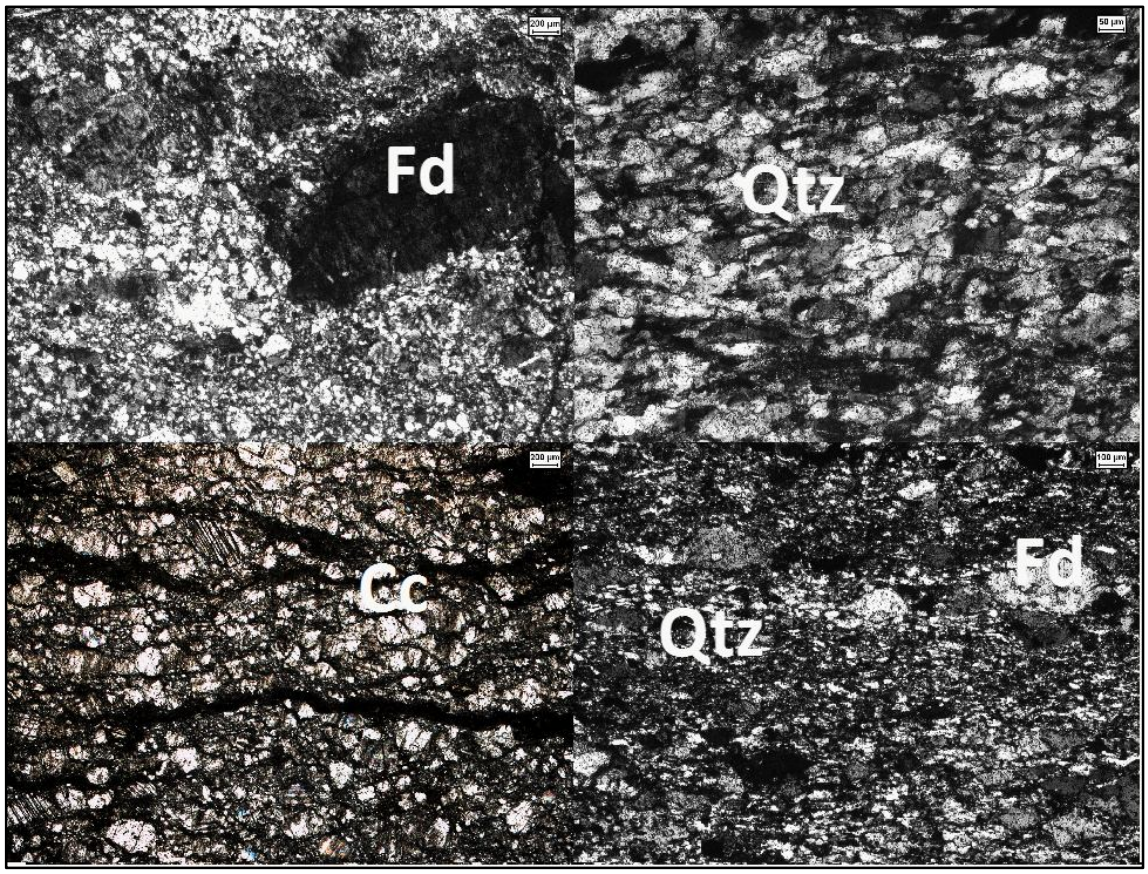

Figure 2.1 –*Microphotographs of samples 18B(top left), 18F (top right), 18E (marble-bottom left), 18C(bottom right).*

Interpretative comments: the protolith of this sample is a felsic granite which has undergone ductile shear and some brittle deformation, with a recrystallized (predominantly quartz) matrix and non-recrystallized porphyroclast formation. This granite has undergone ductile deformationin comparison to granite from W valley. In addition, its composition is remarkably different.

2.1.1.2 Marble

This lithology has been sampled some 300 m East of the granite area marked in the geological map (sample 18E, Appendix 2).

Minerals: calcite, opaque minerals.

Microstructure: It is foliated and mostly made up of well-formed sparitic calcite crystals of around 400 μm with smooth grain boundaries. The crystals display undulatory extinction and are moderately elongated, with some grains showing clast-like morphologies. Discontinuous bands of oxides are present parallel to foliation directions.

Interpretative comments: calcite shows clear signs ofrecrystallization such as regular grain boundaries and slightly elongated crystals (indicating growth coeval to deformation).Therefore this rock can be classified as a marble.

2.1.2. Western valley - Study of a contact metamorphic aureole on pelitic host rocks and other metamorphic lithologies

This section describes and discusses the microstructure and mineral content of six samples of the western valley of the area south of the village of Ericek using light microscopy studies (see location in map, Figs. 2.2. & 2.3). The aim of the research done in this chapter is to understand the relationship of these lithologies to the adjacent granitic body, the Sürgü fault and the nappe-stacking dynamics affecting the region. Emphasis will be made on a particular schist (sample 15E) as a key to unravel its tectono-metamorphic history and give insight into that of the other samples studied. Five samples correspond to metapelitic compositions and one to an impure marble. Microphotographs of each of these samples can be found in the appendix Mineral grain percentages have been obtained by visual estimation with the aid of charts by Compton, 1962.

The metapelitic sequence studied corresponds to foliated lithologies rich in phyllosilicates and quartz, some with aluminosilicates and cordierite. As these rocks approach the contact with the granite, recorded sizes of andalusite crystals show a noticeable increase with a decrease in mineral preferred orientation. This indicates the probable existence of a contact metamorphic aureole due to the intrusion of the adjacent granitic body and subsequent thermal metamorphism. The sample of impure marble has been used to assess degree of recrystallization and foliation orientation. Descriptions are arranged by proximity to batholith, from furthest to closest.

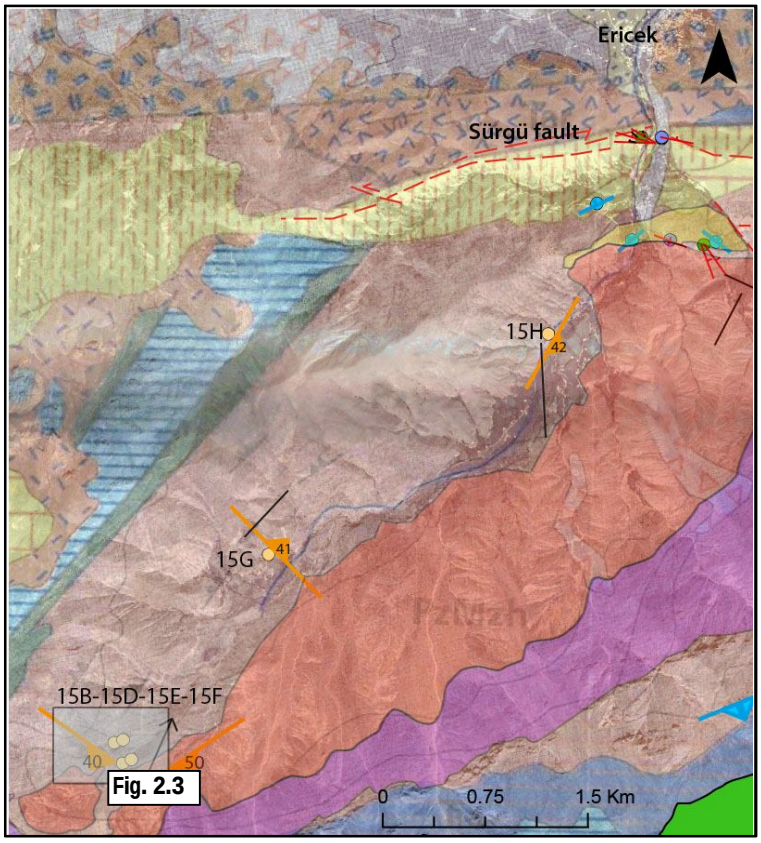

Figure 2.2 –*Map of the western valley of the study area with location of sampling points. Rectangle corresponds to zoomed in map (Fig. 2.3).See map legend (Appendix1). Modified from MTA (1994).*

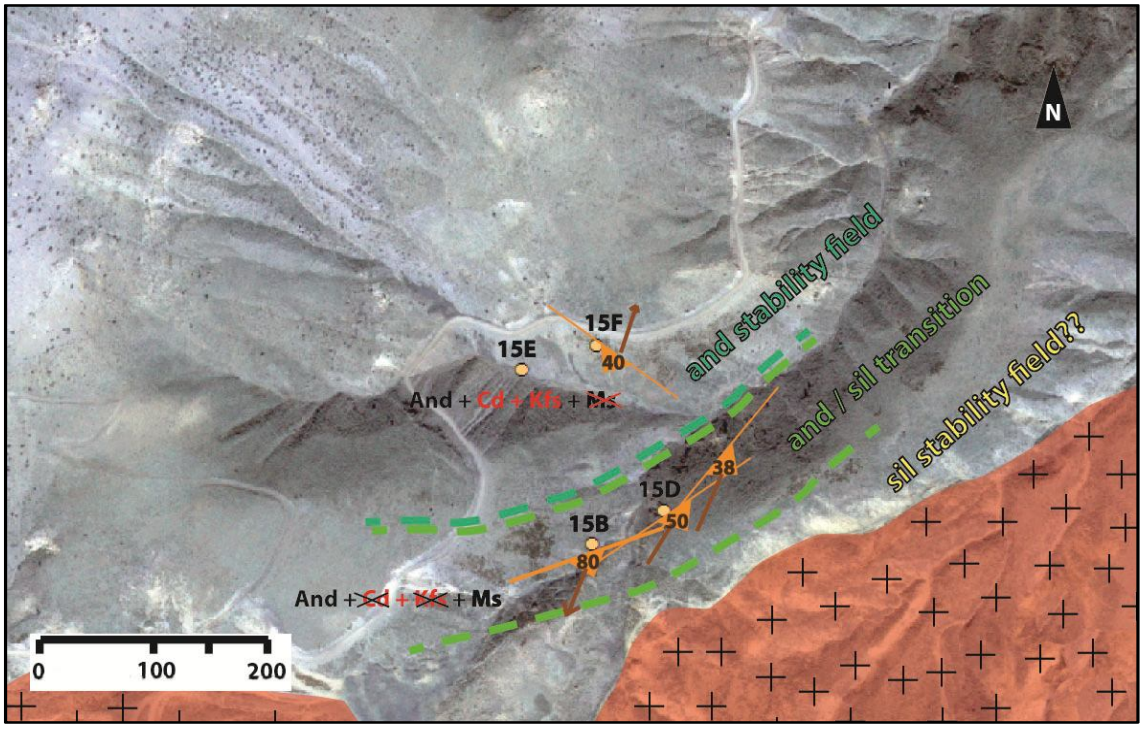

Figure 2.3 –*Detailedmap of the SW edge of the western valley of the study area with location of sampling points, structural information and hypothetical isograds (dashed lines).Foliation (orange), mineral lineation (brown arrows).*

2.1.2.1 Monzogranite – 17E

This sample was taken from an outcrop in the western valley of study area, close to Sürgü Fault and Ericek village on a branch of the fault discovered.

This lithology corresponds to a monzo-granite made up of potassium feldspar (45%), plagioclase (30%), quartz (20%), biotite (3.5%, grain size 0.6 mm), muscovite (0.5%). Plagioclase crystals are euhedral and range from 0.4 to 2 mm in grain size. The latter have concentric zoning and some grains show lamellar twinning. The cores of plagioclase crystals are generally almost completely altered to sericite and are often oxidized. Some of the potassium feldspar grains contain perthites. This rock presents pervasive fractures, a lot of which are filled with calcite (1%).

This granite is brecciated and shows clear signs of deformation from the SFZ.

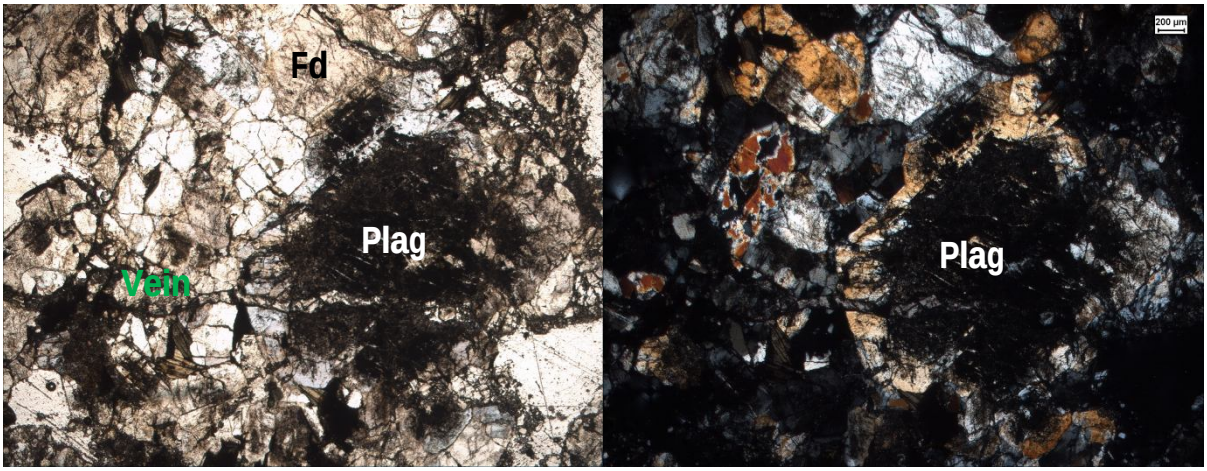

Figure 2.4 –*Microphotograph (Leica microscope) of sample 17E, monzogranite.Left: ppl, right: ppx (high birefringence due to thick cut of thin section). Grains are brecciated. Plagioclase displays a sericitized core. The sample is cross-cut by veins.*

2.1.2.2 - Qtz – bt – and spotted phyllite (15G)

Distance from granite: 620 metres.

Description in hand specimen: inequidimensional rock sample with clear compositional layering, alternate millimetric darker and lighter laminae. A lightly anastomosing foliation is apparent. This lithology is grey and brownish on the outside and greyish in fresh cut. Foliation surfaces show a lustre distinct of phyllosilicate minerals with a preferred orientation.

Mineralogy

Major minerals: quartz (70%), biotite (20%), muscovite (6%), andalusite (4%)

Secondary minerals:opaque minerals.

Microstructure

Rock with compositional layering made up of a quartz matrix with some biotite-rich layers (Fig. 2.6). Quartz is around 0.1 mm in grain size. Biotite grains are inequidimensional and show a preferred orientation that defines a foliation accommodated around porphyroblasts or clusters of quartz. Veins infilled with brown material in ppl cross-cut the thin section. This material may be an iron oxide such as hematite.

Porphyroblasts of andalusite are broken and sheared. Quartz clusters are found in the same manner as andalusite porphyroblasts, possibly as a replacement.

The aforementioned heterogeneities may account for ductile foliation and further growth of porphyroblasts with an increase in geothermal gradient. Protolith may correspond to a fine-grained sandstone with coarse-grained sand lenses.

Stable mineral assemblage: qtz + bt + and + ms

Metamorphic facies: amphibolite (see Fig. 2.27)

Approximate stable P,T conditions (see petrogenetic grid, Fig.2.28-2.29): (0.14 GPa, 500°C)

Timing of deformation and metamorphic growth

Sample 15G				
Mineral	*Def.*		***D1***	
Biotite			----------	
Muscovite			----------	
Quartz		----------		
Plagioclase		----------		
Andalusite			----------	

Table 2.5 - *Paragenetic grid of 15G. Metamorphic minerals have grown syntectonically to deformation phase D1 which corresponds to foliation development.*

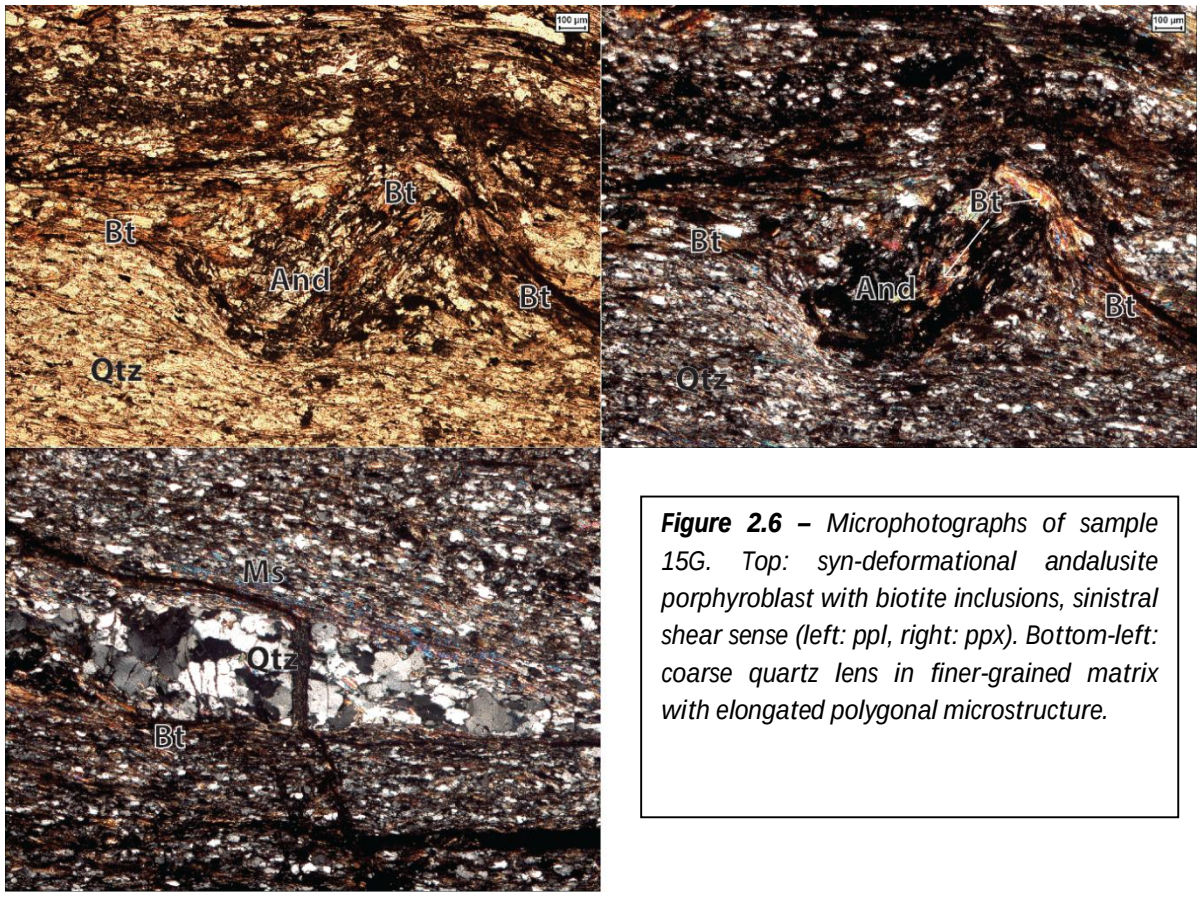

Figure 2.6 – *Microphotographs of sample 15G. Top: syn-deformational andalusite porphyroblast with biotite inclusions, sinistral shear sense (left: ppl, right: ppx). Bottom-left: coarse quartz lens in finer-grained matrix with elongated polygonal microstructure.*

2.1.2.3 - Quartz - biotite - sillimanite - chlorite - muscovite schist (15H)

Distance from granite: 380 metres.

Description in hand specimen: sample of inequidimensional rock with penetrative foliation and greenish-grey colouring. The former is comprised of platy submillimetric minerals with a pale lustre. On one side the cross-section shows the hinge of an isoclinal fold.

Mineral content: quartz (45%), biotite (25%), sillimanite (15%), chlorite (10%), muscovite (5%).

Microstructure

This rock displays an overall foliated microstructure defined by prismatic sillimanite and inequidimensional phyllosilicates (namely, biotite, chlorite and muscovite). Sillimanite shows elongated prisms of around 3.5 mm in length and 0.1 wide with a preferred orientation parallel to the elongation axis of the mineral. Biotite shows a more random orientation and its subhedral flat prisms are 1 by 0.05 mm in grain size. Muscovite is integrated by subhedral inequidimensional and randomly oriented crystals of around 0.3 by 0.02 mm. Equidimensional matrix quartz grains (0.1 mm grain size) define a polygonal granoblastic microstructure (Fig. 2.7).

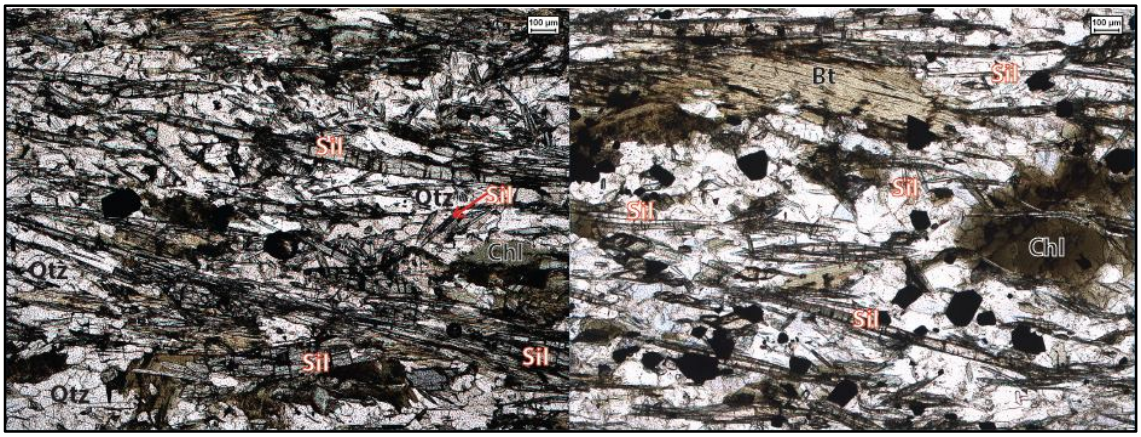

Figure 2.7 – *Microphotographs of qtz-bt-sil-chl-ms schist (sample 15H). Laths of sillimanite with preferred orientation are a characteristic feature of this lithology.*

Stable mineral assemblage: qtz + bt + ms + chl +sil

Metamorphic facies: amphibolite (see Fig. 2.27)

Approximate stable P,T conditions (see petrogenetic grid, Fig.2.28-2.29): (0.35 GPa, 520°C)

Timing of deformation and metamorphic growth

Sample 15H						
Mineral	*Def. Phase:*		*D1*		*D2*	
Biotite			----------			
Chlorite		----------				
Quartz		----------				
K-feldspar		----------				
Muscovite						----------
Sillimanite			----------			

Table 2.8 - *Paragenetic grid of qtz-bt-sil-chl-ms schist (sample 15H). D1 corresponds to an early formation o foliation and D2 indicates an isoclinal folding event of earlier foliation. Biotite and sillimanite have their long axis oriented in the direction of foliation whereas chlorite does not show enough evidence to have formed during the deformation phase. The fact that muscovite has a random orientation indicates likely formation later than both deformation phases.*

****This lithology is not affected by the contact aureole and followed a different P,T path from that of the other 4 metapelitic samples described in this chapter.***

2.1.2.4 - Impure marble

Distance from granite: 217 m

Description in hand specimen: Massive rock with millimetric lamination given by an foliated white material with intercalations of dark grey material. The white mineral makes up 95% of the composition. The spacing of the dark layers is of 0.5 to 1.5 cm. The latter form sigmoidal shapes.

Mineralogy: calcite (95%), quartz (2%), opaque minerals (3%)

Microstructure:

This lithology is made up of euhedral equidimensional calcite with lamellar twinning and polygonal grain boundaries. The well-formed nature of the calcite crystals indicated recrystallization. Some sigmoidal pockets of microgranular quartz can be found in thin layers parallel to foliation (Fig. 2.9).

This rock has undergone recrystallization dure to increase in the geothermal gradient and ductile deformation, however it has not suffered any mineral transformations.

**This rock will be excluded from the petrogenetic grid due to its almost monominerallic nature. There is not enough information to know whether calcite recrystallization took place due to contact metamorphism or regional metamorphism.*

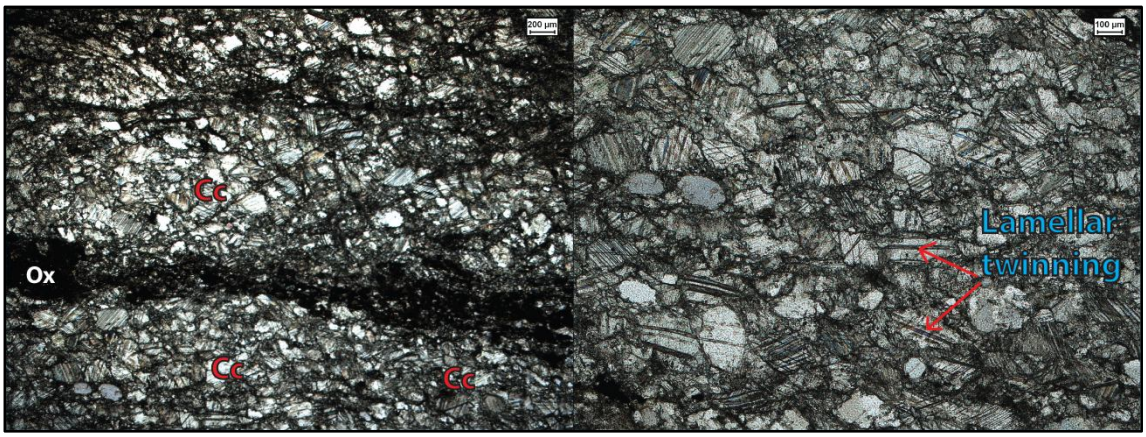

Figure 2.9 – *Microphotographs of impure marble (sample 15F). Crystals of well-formed sparitic calcite can be seen integrating the matrix. Calcite bands are separated by rows of oxides (left). Calcite crystals are slightly elongated and with regular grain boundaries forming a polygonal microstructure. The former show lamellar twinning.*

2.1.2.5 - Phyllite –hornfels transition (15B)

Distance from granite: 54.5 metres

Description in hand specimen: Inequidimensional hand specimen with compositional layering, lamination spaced from 0.2 to 5 mm apart, and foliation resulting in fissile planes. Colouring includes shades of brown, red, ocre and yellowish-green as external alteration. Fresh cut is blue, brown, grey and white. Foliation is defined by phyllosilicates, the tabular grains of which are oriented on the same plane, with all the crystals reflecting light towards the same preferred orientation, grain size of around 0.5 to 1 mm. Lighter-coloured layers are rich in quartz and feldspar, while darker layers are biotite-rich.

The surface of the sample is mottled with dark, greyish, patches. The latter correspond to round elongated porphyroblasts, generally elongated in the preferred orientation defined by phyllosilicates.

Mineral content

Major minerals: Quartz (42%), biotite (23%), orthoclase (12%), muscovite (10%), andalusite (6.5%), plagioclase (6%), sillimanite (0.5%).

Secondary minerals: opaque minerals.

Trace minerals: apatite.

Microstructure

Laminated lithology comprised of millimetric bands with compositional and textural differences. Each of these laminae is made up of a groundmass of biotite and quartz with alternate predominance, some muscovite and, in some layers, porphyroblasts of andalusite. The alternating layers described as follows can be distinguished as the main components of this lithology.

a) Thick phaneritic veins made up entirely of 0.5 to 1mm subhedral quartz grains and locally with plagioclase grains in addition (Fig. 2.10).

b) Laminae largely integrated by a matrix of anhedral grains of feldspar and quartz and inequidimensional biotite crystals either in chains of oriented grains or of criss-crossing orientations at 90-120º. Biotite prisms wrap around andalusite porphyroblasts. The latter grains are colourless, around 0.7 mm in size, showing two cleavage directions at roughly 90º, anhedral and with abundant biotite inclusions (Fig. 2. 10).

c) Layers with a groundmass of subhedral quartz and feldspar crystals (0.05 mm grain size) with some randomly-oriented biotite (0.8 x 0.08 mm in grain size) and muscovite grains (0.8 x 0.08-0.15 mm grain size) scattered across it. A small fraction of feldspar crystals present lamellar twinning, indicating the presence of plagioclase (Fig. 2.11).

*In locallized areas, thin laths of colourless sillimanite can be found overlaying other mineral grains such as quartz or biotite.

Interpretative remarks

Biotite and muscovite do not present preferred orientations in a large part of the sample. This heterogeneity accounts for the classification as transitional lithology between phyllite and hornfels. The external foliation that is apparent at outcrop scale may be a consequence of fine compositional layering, with fissile planes created by the difference in mineralogy and weakness of planes rich in phyllosilicates.

Stable mineral assemblage: bt + and +ms + cd + qtz

Relict minerals: plag + kfd

Facies: amphibolite facies (see Fig. 2.27).

Approximate stable P,T conditions (see petrogenetic grid, Fig.2.28-2.29): (0.15 GPa, 610°C)

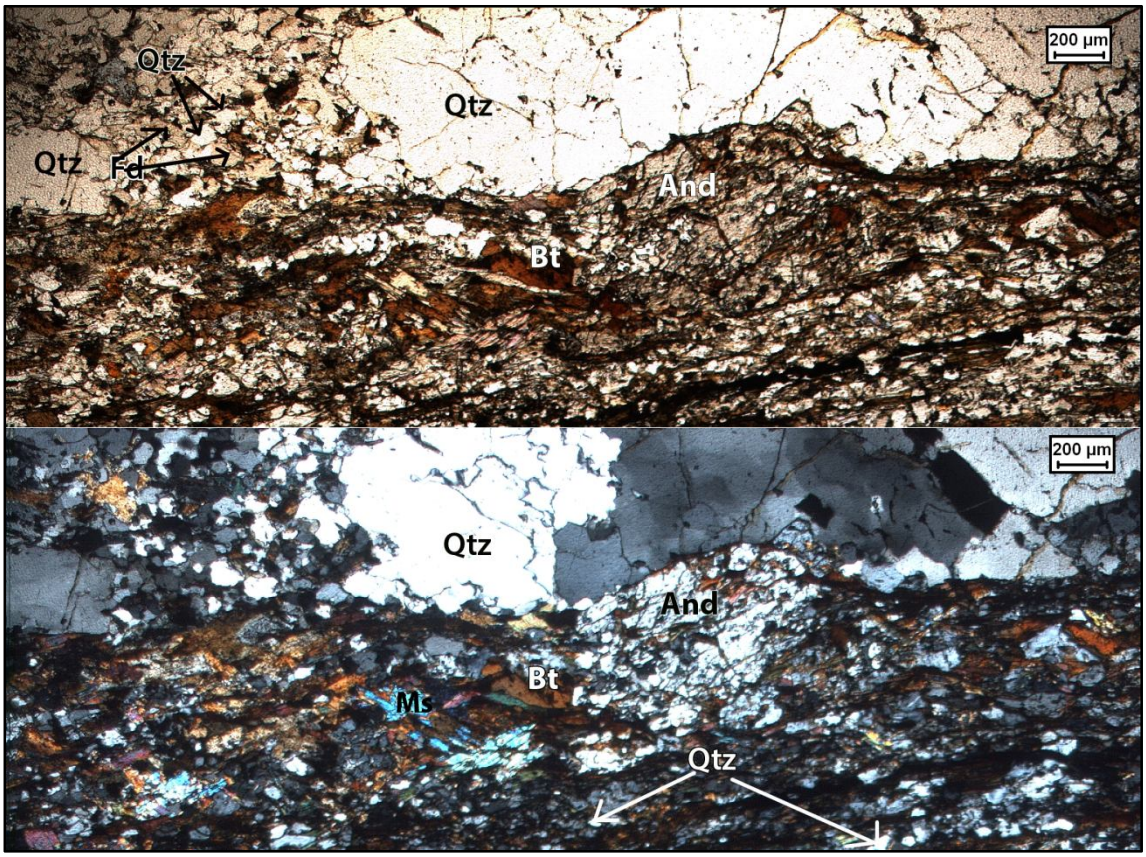

Figure 2.10 – *Microphotographs of phyllite –hornfels transition(sample 15B) in ppl (top) and ppx (bottom). Subhedral andalusite with small anhedral biotite inclusions can be seen overlapping the decussate microstructure of the matric phyllosilicates. Both biotite and muscovite are arranged in a random orientation. Qtz can be found in the matrix in small grains below 100 microns in grain size or in larger millimetric grains as part of a vein parallel to compositional lamination.*

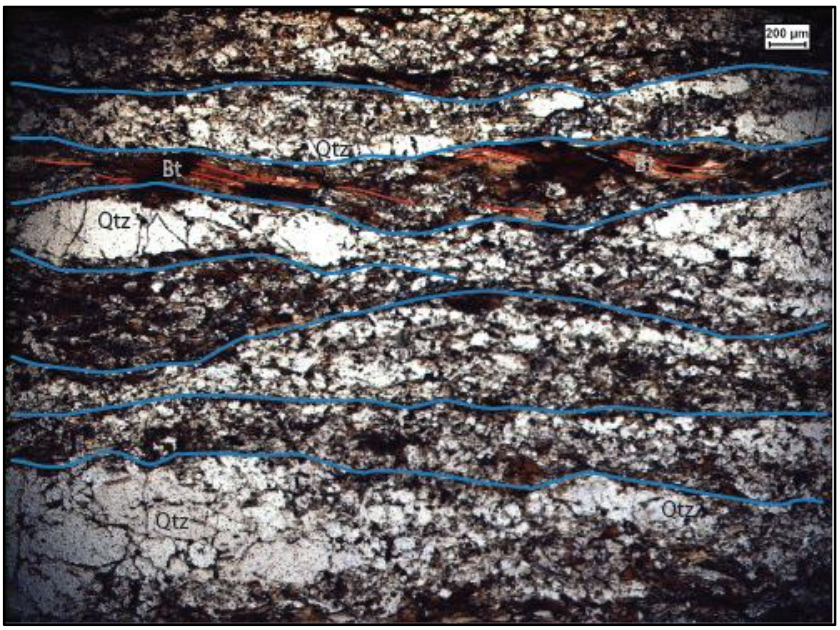

Figure 2.11 – *Microphotograph of phyllite – hornfels transition(sample 15B). Separations between textural or compositional domains are highlighted in blue. The slightly curved/anastomosing nature of the separations may indicate deformation or relict sedimentary structures. Bitotite shows a preferred orientation in the 3rd layer, so it is not always found randomly oriented as in the previous image (Fig. 2.10).*

Timing of deformation and metamorphic growth

Sample 15B				
Mineral	*Def. Phase*		*D1*	
Biotite			----------	--------
Muscovite				--------
Quartz		----------		
K-feldspar		----------		
Plagioclase		----------		
Andalusite				---------

Table 2.12 - *Paragenetic grid of 15B reflecting that biotite growth occurs in two different stages, first contemporarily to deformation phase D1 and after it. The latter is inferred from the two orientation trends of biotite in this lithology; a population of crystals with a preferred orientation and another randomly oriented group found together with muscovite, forming a decussate microstructure. Quartz, k-feldspar and plagioclase are inferred to be reequilibrations of relict minerals from protolith or injected by hydrothermal veins.*

2.1.2.5 - Cd – And – Bt spotted schist (15E)

***Note:** this lithology will be analyzed more in depth than the others given its greater interest applied to the study of porphyroblast-matrix relations*

Distance to granite:214 m

General description in hand specimen: The sample taken from this lithology is inequidimensional and foliated with brownish outer colouring with red oxidation. However, fresh cut is white with dark and blueish-grey grains. This lithology is dense and massive with a foliation anastomosing around large porphyroclasts. The groundmass is made up of submillimetric shiny platy minerals (biotite) showing a preferred orientation and white rounded minerals (k-feldspar and quartz). Dark elongated spots (biotite clusters) oriented with their long axis (around 1 mm) in the same direction as foliation. Large rounded porphyroclasts are visible in between foliation planes, slightly elongated in the direction of foliation, corresponding to cordierite. Their long axis is about 3-6 mm.

Mineral content

Major minerals: biotite (30%), k-feldspar (25%), cordierite (19%), quartz (10%), andalusite (8%), muscovite (2%)

Secondary minerals: pinite (3%), ilmenite (3%).

Trace minerals: apatite.

Microstructure

Inequigranular rock characterized by a foliated matrix of biotite, k-feldspar and quartz around 0.3 mm in length wrapping around deformed millimetric porphyroclasts of cordierite. Matrix foliation is a continuous schistosity (according to the classification after Powell 1979 and Borradaile *et al.* 1982), designated here as external schistosity ($\mathbf{S_e}$), mainly defined by biotite. $\mathbf{S_e}$ is anastomosing due to accommodation around cordierite porphyroclasts. Elongated submillimetric to millimetric porphyroblasts of andalusite are found surrounding the aforementioned cordierite porphyroclasts, occasionally found in the matrix without association to cordierite.

Biotite 1 is the main component of the foliated matrix, with crystals displaying a lattice preferred orientation. This generation of biotite presents a narrow tabular almost acicular habit, with subhedral grains. Grain sizes are up to 0.5 mm in length and 0.05 mm in thickness (Figs. 2.13, 14, 15).

Biotite 2 is found in elongated clusters with different random orientations, intercalated within the matrix foliation. These biotite clusters are about 1 mm long and 0.2 mm wide with a stretched elliptical morphology with narrow edges, sometimes shaped as a mineral fish. Most of the agglomerations are oxidated at their core by a titanium and iron oxide (ilmenite) (Figs. 2.13, 14).

Potassium feldspar is one of the main components of the matrix, forming elliptical grains of 0.1-0.2 mm and an aspect ratio of 0.6 with a tendency to develop ϕ and σ-clast morphologies. They contain narrow s-shaped biotite inclusions of the same dimensions as the biotite found in the matrix (Fig. 2.15).

Cordierite grains are found as deformed porphyroclasts enveloped by crystals of biotite with preferred orientation. Their sizes range between 1 and 6 mm in length and from 0.8 to 2.8 mm in width. These porphyroclasts contain inclusions of biotite that make up an internal schistosity ($\mathbf{S_i}$). $\mathbf{S_i}$ is generally sigmoidal and refracts from the schistosity of the matrix $\mathbf{S_e}$. The relationship between $\mathbf{S_i}$and $\mathbf{S_e}$is discussed further below, as well as kinematic criteria to interpret the growth of cordierite crystals. Cordierite also contains quartz inclusions and pinitized rims (Figs. 2.16, 17, 18).

Quartz is found in the matrix as small subhedral elliptical crystals of about 0.03 mm of grain size, following the generalized mineral lineation of the rock. It defines a granoblastic elongated microstructure in some sectors of the matrix such as in strain shadows of cordierite porphyroclasts (Fig. 2.13).

Andalusite is comprised of subhedral to euhedral prisms of 0.2 to 2 mm long and 0.3 mm wide with two visible cleavage directions at almost 90°. Andalusite grains are mostly located on the rims of larger cordierite porphyroclasts and on occasion surrounded by the matrix. These prisms often display a mimetic growth, being parallel to matrix foliation (Fig. 2.18).

Muscovite is found in the matrix with similar characteristics to biotite 1. However it only appears in very localized areas.

Stable mineral assemblage: bt + kfs + and + cd (+ qtz +ms)

Facies: amphibolite facies/pyroxene hornfels facies (see Fig. 2.27).

Approximate stable P,T conditions (see petrogenetic grid, Fig.2.28-2.29): (0.13 GPa, 640°C)

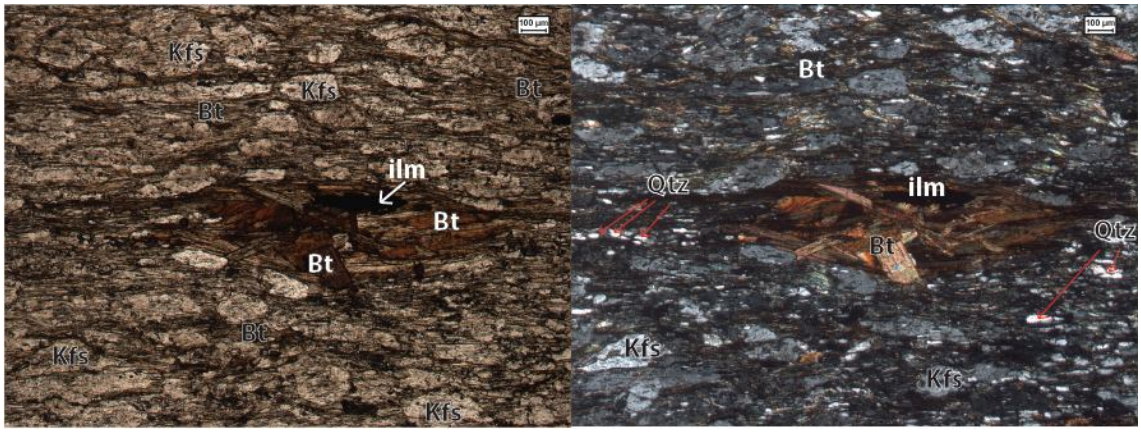

Figure 2.13 – *Matrix of sample 15E with biotite cluster in the centre. Note varying orientations of crystals making up the cluster. Bt: biotite, Ilm: ilmenite, Kfs: potassium feldspar. Left: ppl, Right: ppx.*

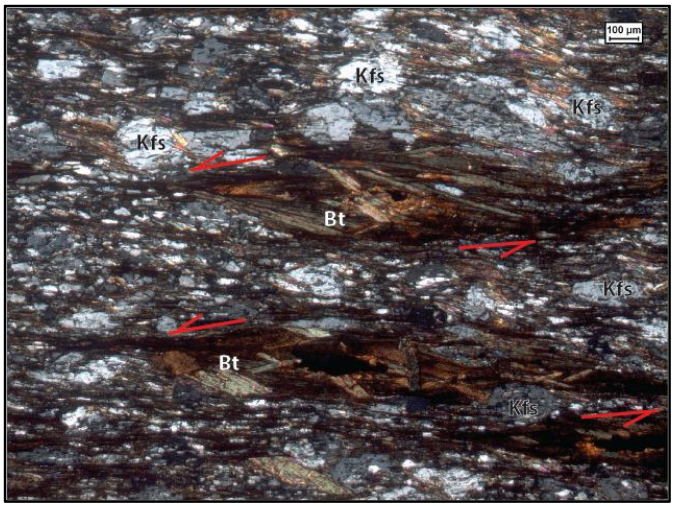

Figure 2.14 – *Biotite clusters of 15E with mineral fish structure suggesting sinistral shear sense (ppx).*

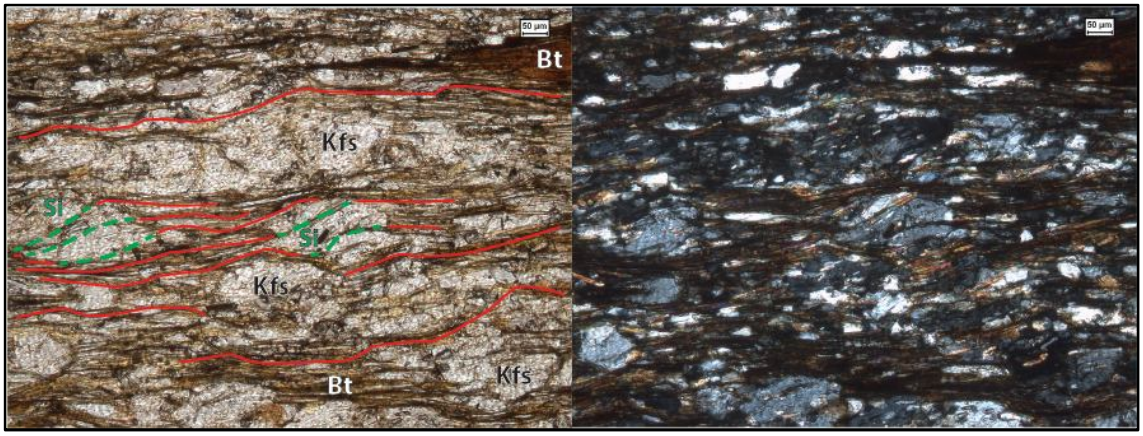

Figure 2.15 – *15E matrix with syntectonic k-feldspar crystals. Green: internal schistosity defined by biotite inclusions (Si), red: external matrix schistosity (Se). Left: ppl, Right: ppx.*

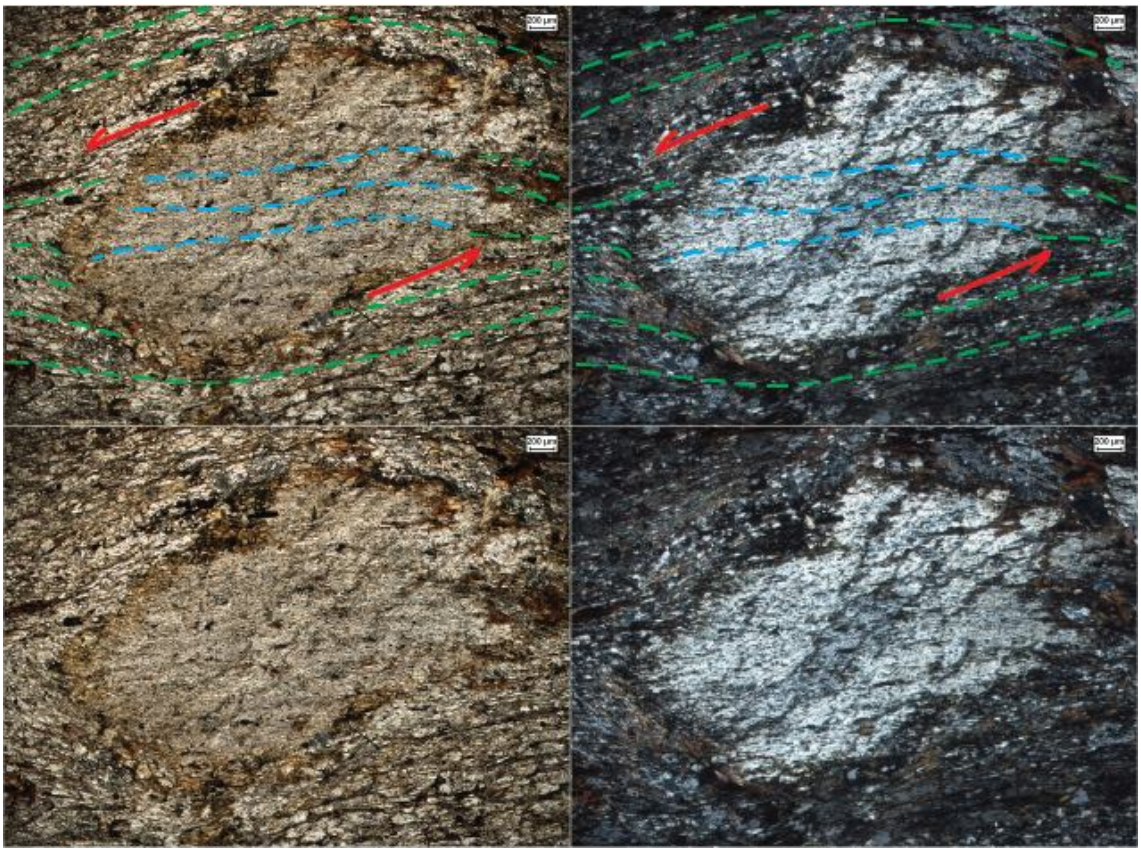

Figure 2.16 – *Microphotographs of sample 15E with cordierite porphyroblasts with subhorizontal S_i. Note the slight curvature of S_i and pinitized rims of cordierite. Blue: internal schistosity defined by biotite inclusions (Si), green: external matrix schistosity (Se). Red arrows show sinistral shear sense. Left: ppl, Right: ppx.*

Timing of metamorphic growth of minerals

Sample 15E				
Mineral	*Def. Phase:*		*D1*	
Biotite 1			----------	
Biotite 2			--------	----
Quartz		----------	----	----
K-feldspar			----------	
Cordierite			----------	
Andalusite				----------

Table 2.17 - *Paragenetic grid of 15E.*

Matrix **biotite** grows with a preferred orientation parallel to overall foliation, which suggests development during a deformation phase linked to either burial or shearing. **Clusters of biotite** grow with a generally ϕ-clast shape with wings parallel to matrix, indicating syntectonic growth. However, the clusters include numerous randomly-oriented biotite prisms and this may suggest an increase in temperature causing nucleated matrix crystals to continue growing during a post-deformational stage. **Quartz** is a relict mineral found in the matrix from the sedimentary protolith and probably recrystallized after burial. However, its presence in pressure shadows indicated probably recrystallization during deformation phase D1 and its presence in cordierite as a decay product of porphyroblast destabilization. **K-feldspar** is found in the matrix as a syntectonic mineral. Microstructures observed inside k-feldspar grains correspond to an S_i with a sigmoid shape that refracts when continuing into the matrix without truncation. This indicates syn-foliation growth also involving rotation of the clasts. **Cordierite** growth occurs syntectonically to D1, given the structures displayed by its internal foliation $\mathbf{S_i}$ and deformation of porphyroblasts into porphyroclasts. This will be further explained below. **Andalusite** grows after deformation phase D1 as it seems unaffected by deformation and the cleavage direction parallel to the long axis of andalusite prisms follows the same orientaton as matrix foliation S_e, indicating a typical post-kinematic microstructure.

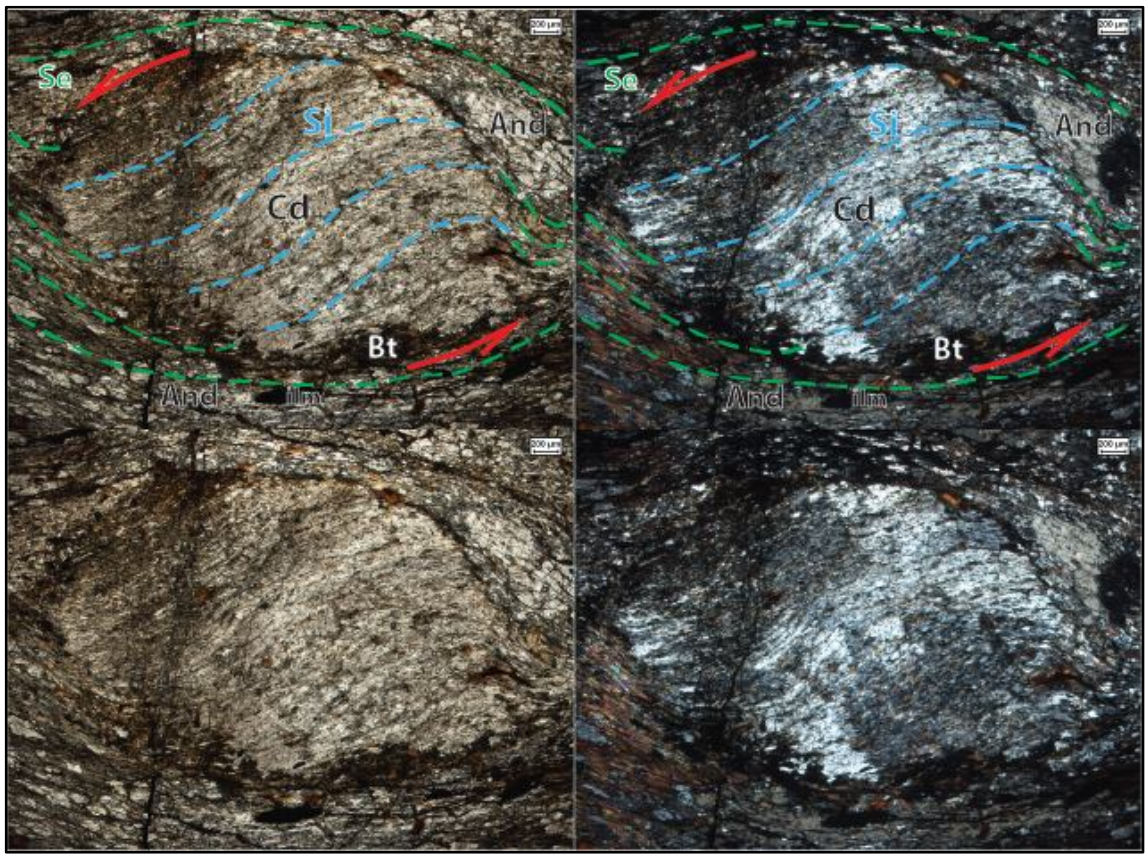

Figure 2.18 – *Microphotographs of sample 15E with cordierite porphyroblasts with s-shaped oblique S_i wrt matrix foliation. Note andalusite crystals around cordierite. Blue: internal schistosity defined by biotite inclusions (Si), green: external matrix schistosity (Se). Red arrows show sinistral shear sense. Left: ppl, Right: ppx.*

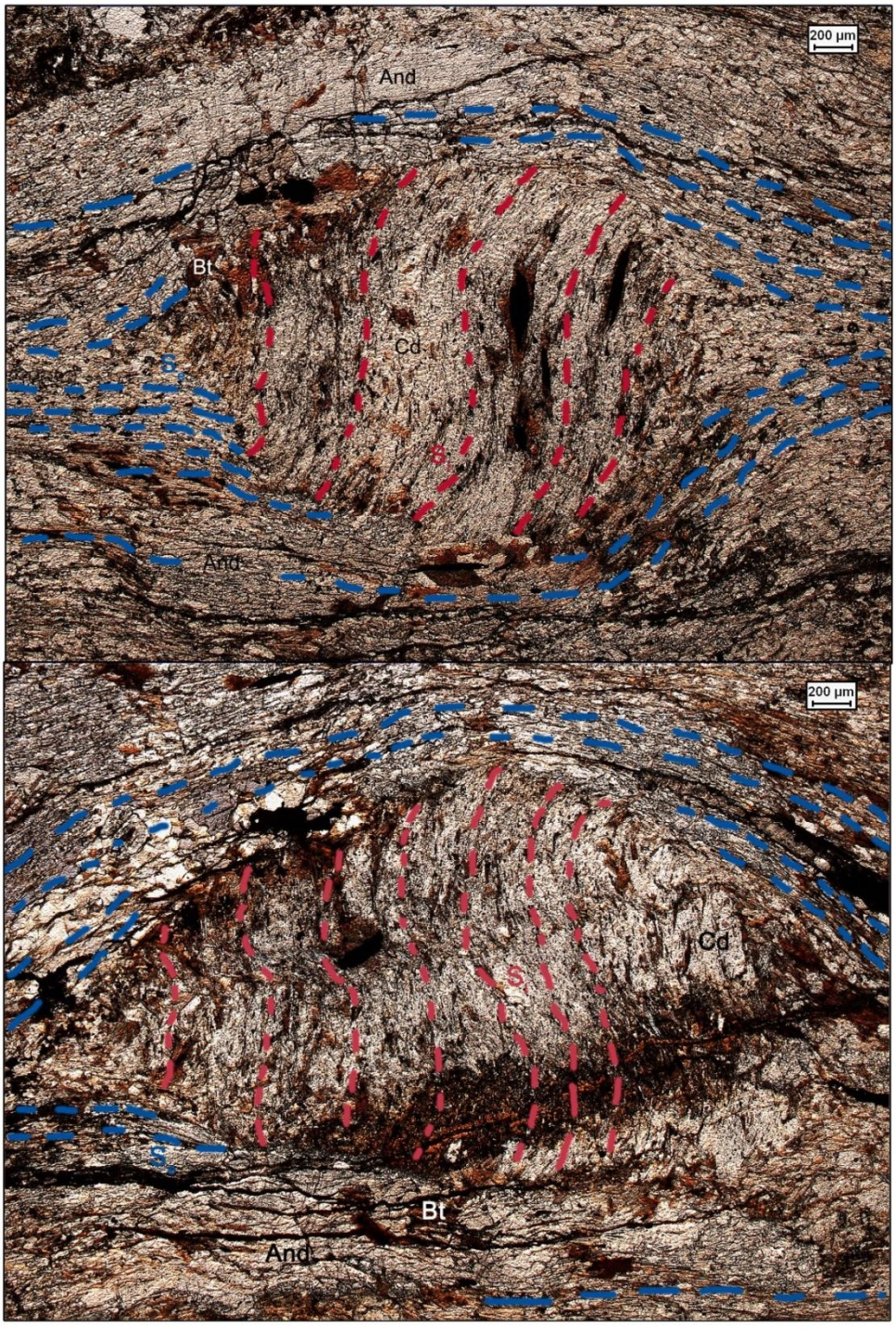

Figure 2.19a – *Microphotographs of sample 15E with cordierite porphyroblasts with s-shaped oblique S_i wrt matrix foliation. Note andalusite crystals around cordierite.*

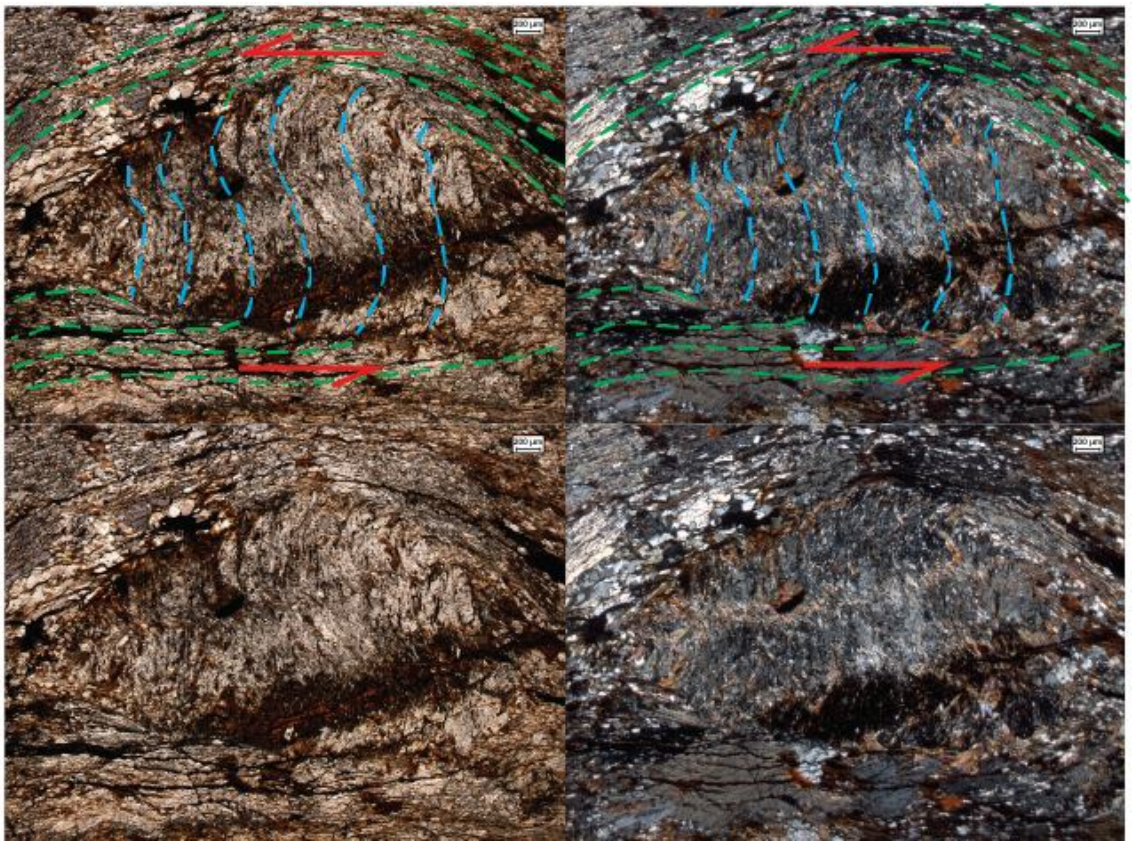

Figure 2.19b – *Microphotographs of sample 15E with cordierite porphyroblasts with S_i at 90° with external foliation. Note the curvature of S_i. Blue: internal schistosity defined by biotite inclusions (Si), green: external matrix schistosity (Se). Red arrows show sinistral shear sense. Left: ppl, Right: ppx.*

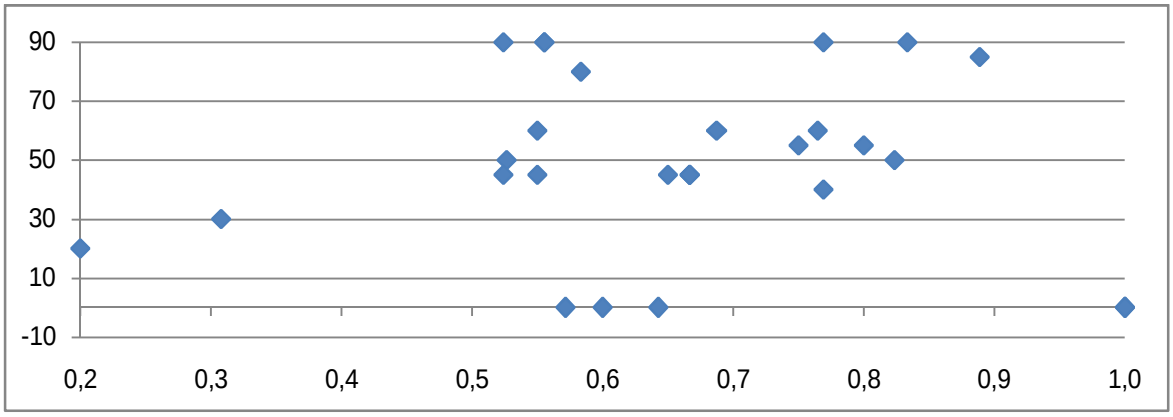

Figure 2.20 – *Graph showingrelationship between **x**: aspect ratio of porphyroclasts and **y**: angle between internal foliation **S_i** and external foliation **S_e**.*

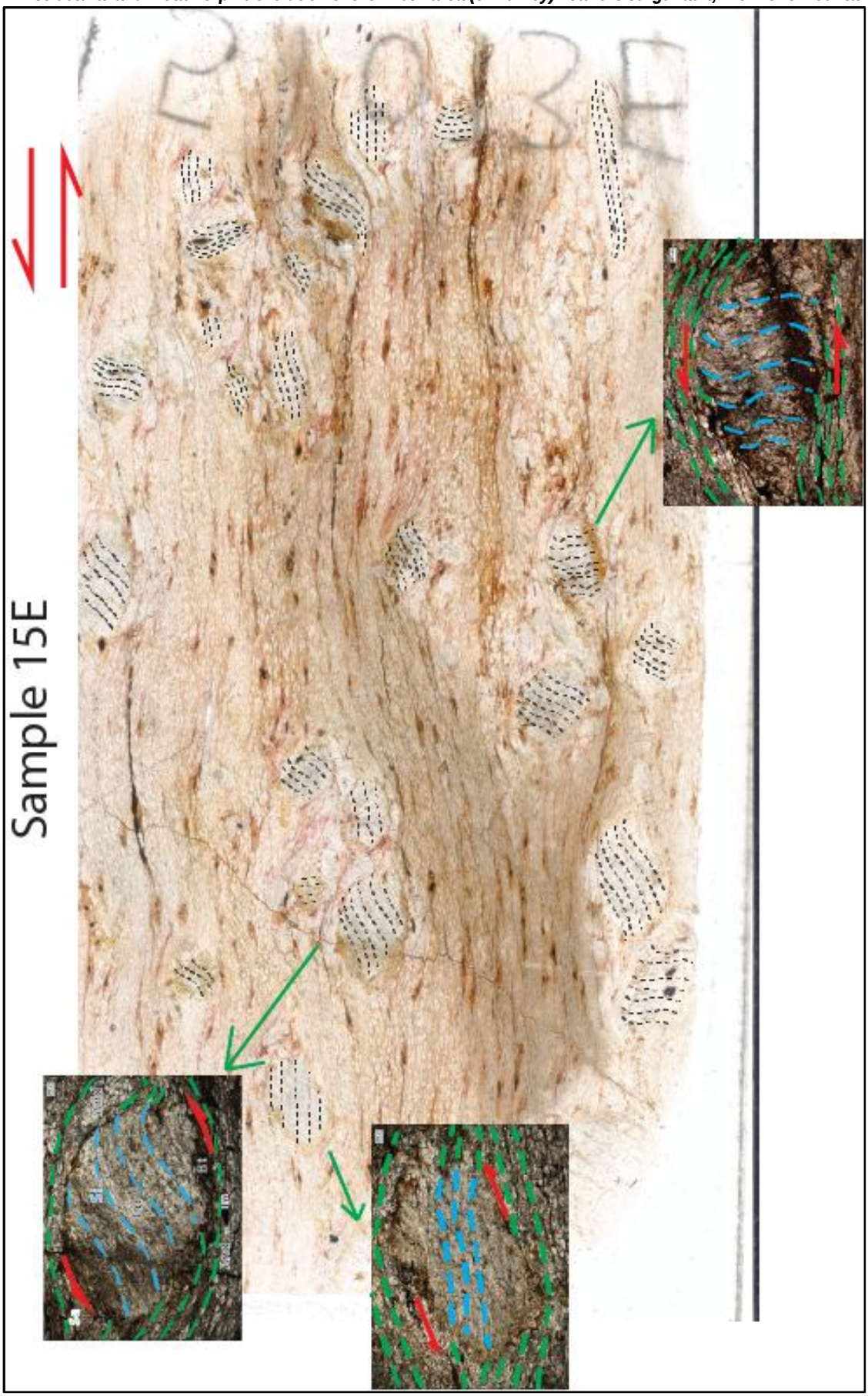

Figure 2.21 – *High resolution scan of thin section 15E highlighting internal schistosity of cordierite porphyroblasts (black dashed lines) and showing location correspondence with microphotographs.*

Cordierite porphyroclast analysis

Cordierite porphyroblasts grow syntectonically to deformation. This fact may is likely to involve rotation, as is the case of the k-feldspar clasts described above. Porphyroblasts are therefore deformed as they grow to the condition of porphyroclasts, displaying shear-related morphologies such as mantled porphyroclasts with strain shadows and truncated mineral fish. An analysis of the kinematics of deformation of these clasts has been carried out by measuring their aspect ratio and the angle between of internal schistosity S_i and matrix schistosity S_e (see Fig. 2.20 and Appendix Table 2). Crystal elongation direction is considered almost parallel to foliation throughout the thin section.

Uniformity criteria and arguments in favour of syntectonic growth

All cordierite porphyroblasts are within a millimetric size range with matrix foliation S_e wrapping around them and pressure shadows forming adjacent to them. They show sigmoidal S_i and deflection planes on the rims of the porphyroclast can often be seen.These porphyroblasts show clear signs of synkinematic growth (Figs. 2.16, 18, 19, 21) due to difference in competence between porphyroblast and matrix (Bell 1985). The reference frame for rotation is the horizontal that corresponds to matrix foliation defined by biotite crystals with a preferred orientation.

Analysis in terms of internal schistosity (S_i) orientations and aspect ratio

Internal foliation of cordierite porphyroblasts shows three main trends (as seen with the thin section scan Fig. 2.21):

a) S_i inclined with 20-60° azimuth, slightly curved to S-shaped.

b) S_i with an almost vertical orientation, in some cases curved or S-shaped

c) Horizontal and very slightly curved S_i.

A: Porphyroclasts with internal foliation oblique to matrix S_e have aspect ratios between 0.53 and 0.8, with the exception of two very elongated porphyroblasts with aspect ratios of 0.2 and 0.3, respectively. The porphyroclasts with S_i 45 and 90 to the matrix are likely to have rotated.

B: Clasts with vertical S_i have an aspect ratio between 0.53 and 0.89. Their higher angle to the matrix may indicate earlier rotation.

C: Porphyroclasts with horizontal S_i may have grown at a later stage of heat flow and will not have rotated (Passchier and Trouw, 2005). However, they also show a slightly assymetrically-curved S_i and therefore are also considered syntectonic. This group of porphyroclasts have an intermediate aspect ratio (around 0.6) and smaller grain sizes. According to Barker, straight S_i can be formed at low strain rates (1994). Therefore, cordierite porphyroblasts with horizontal S_i do not display a clearly characteristic synkinematic trend of inclusion trails, but can still be accepted as a possibility. Another hypothesis could classify this group as intertectonic, fossilizing a foliation formed by a deformation phase previous to D1. However, we have chosen the first hypothesis since most inclusion trails, although horizontal, have a slight curvature following the asymmetry of the other porphyroblasts. Porphyroclasts with $\mathbf{S_i \wedge S_e = 0}$ may also indicate resistance to rotation with some stretching and redistribution of material around their rims. This could indicate fast growth.

Those porphyroclasts with the lowest aspect ratios (i.e. narrow and long) are inferred to have become elongated and to have decreased their $\mathbf{S_i \wedge S_e}$ angle due to stretching during shear in

the same direction as matrix foliation. The arguments for this statement are morphological: they display a truncated mineral fish shape and proportions that are very far from those of a euhedral cordierite crystal. This result may indicate these porphyroblasts responded to shear by stretching after a small amount of rotation. Rotation is inferred from the difference in orientation between Si and Se. The tendency of these porphyroblasts to yield under a force indicate possible strength differences between these and other cordierite porphyroblasts. At some point the $\mathbf{S_i \wedge S_e}$ of these elongated porphyroclastswill have been between 90 and 30, as the other less stretched porphyroclasts. This analysis suggests two steps in the deformation process: rotation + stretching.

Given the lack of trend seen in Fig. 2.20 it is difficult to relate $\mathbf{S_i \wedge S_e}$ angle and aspect ratio to amount of rotation. For this correlation to make sense, extent of elongation due to strain after rotation should be quantified.

Shear sense

A sinistral shear sense is deduced from the shape of S_i within cordierite porphyroclasts and the arrangement of their clast wings and/or pressure shadows, and therefore counter-clockwise rotation (Figs. 2.16, 18, 19, 21).

Pure shear vs simple shear

In this lithology, cordierite porphyroblasts deform under the action of simple shear. This is due to the fact that there is a range of orientations for Si and a variety of stretch of lines. In simple shear stretch decreases considerably and after a certain threshold they start to extend (Passchier and Trouw, 2005). In pure shear, however, rotation of Si would never exceed 45°, which it does in the case of sample 15E and stretch generally increases constantly and would be less likely to cause the wide range of stretch found in the porphyroclasts of this sample.

2.1.2.6 - Hornfels (15D)

Distance from granite: in direct contact with small dike of granitic composition, 76.77 metres away from main intrusion body.

Description in hand specimen: Dark-coloured, massive rock in direct contact with a granitic dike. External colour is brown, violet, red and yellow. It is a highly dense rock with sharp edges. Some wavy compositional lamination and a foliation can be identified. Fresh cut shows bands of a dark mineral of about 1 mm grain size (60%), and white bands (white mineral, 40%) mottled with patches of a dark mineral (biotite). Biotite crystals do not have the same preferred orientations.

Mineral content

Major minerals: Quartz (15%), biotite (45%), (turned to hematite...metallic reddish brown in hand specimen., andalusite (30%), sillimanite (7%), muscovite (3%)

Secondary minerals: hematite and opaque minerals.

Microstructure

This lithology is heteroblastic with a matrix and porphyroblasts of a slightly larger grain size. The porphyroblasts of andalusite are from 1 to 3 mm in grain size. The matrix can be divided into two textural domains corresponding to two distinguishable grain sizes, one being around 0.2 mm and the other around 2 mm. Foliation is determined by biotite with a preferred orientation. However, in some areas of the sample it is randomly oriented. The former can be

found as an anastomosing foliation, with biotite wrapping around andalusite porphyroblasts. Biotite is also found as inclusions within andalusite grains (Figs. 2.22, 23, 24, 25).

Quartz shows an equidimensional habit with regular grain boundaries defining a polygonal microstructure. Biotite is found in bands. Andalusite is found as a porphyroblast of subhedralgrains and sometimes as clusters of smaller grains. It is pleochroic from light pink to colourless.

Sillimanite presents an acicular habit often found in fibrous clusters or above quartz and biotite grains.

This lithology shows a relict foliation that is almost completely overprinted by a randomly oriented microstructure, and therefore it is considered a hornfels.

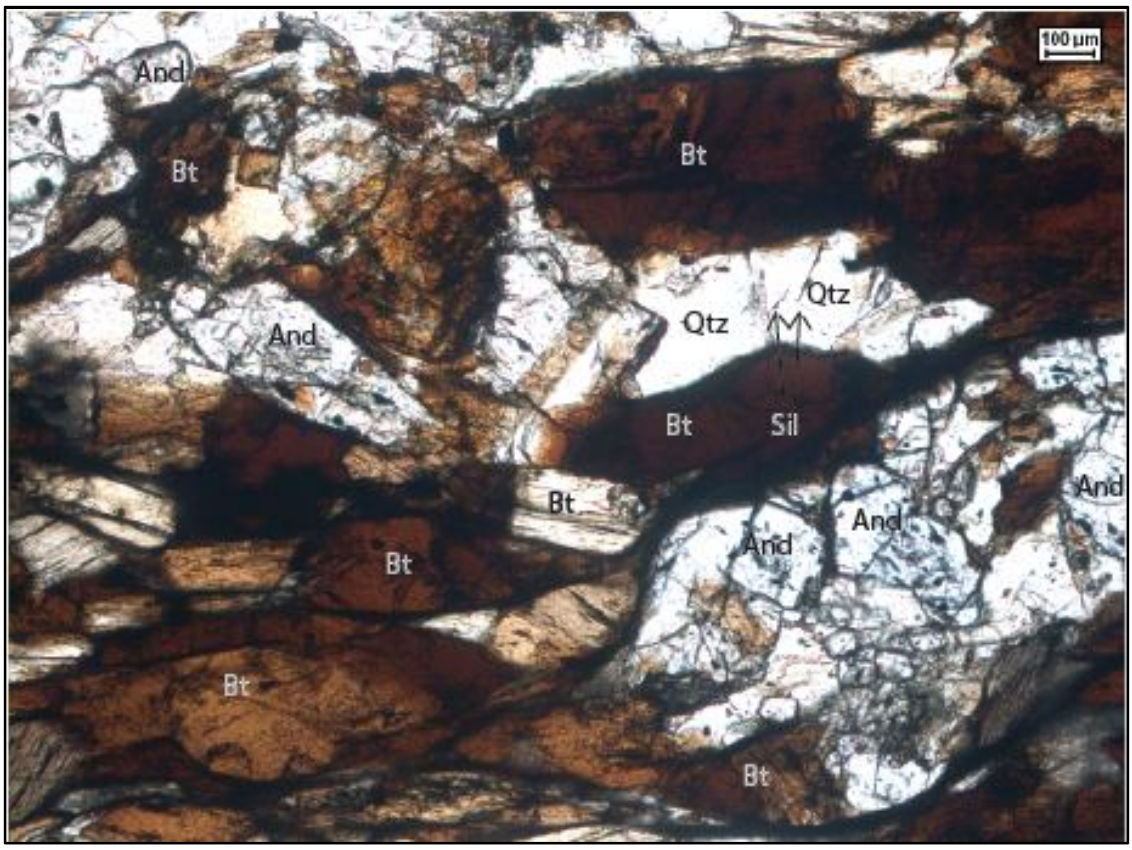

Figure 2.22 – *Microphotograph of hornfels (sample 15D) showing the assemblage bt-and-sil-qtz.*

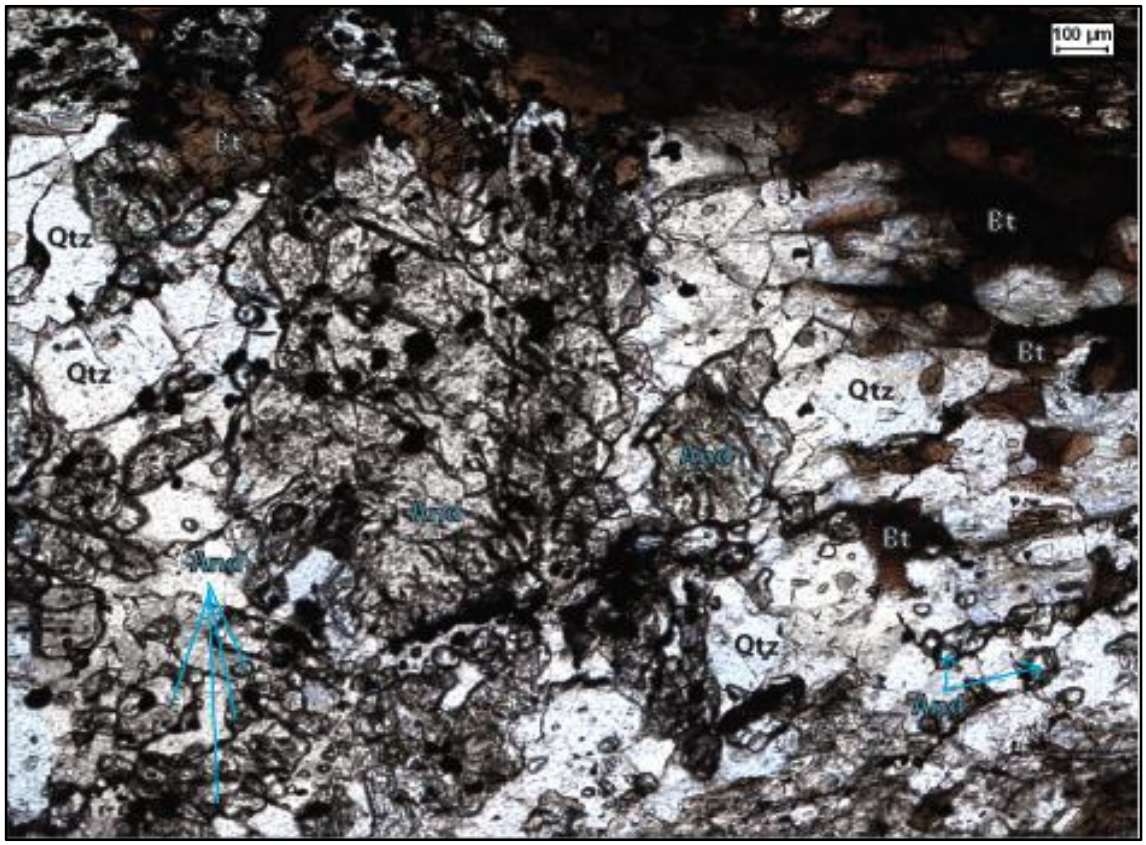

Figure 2.23 – *Microphotograph of hornfels (sample 15D) showing a large andalusite porphyroblast and fragments of the same mineralogy on a matrix of quartz and biotite.*

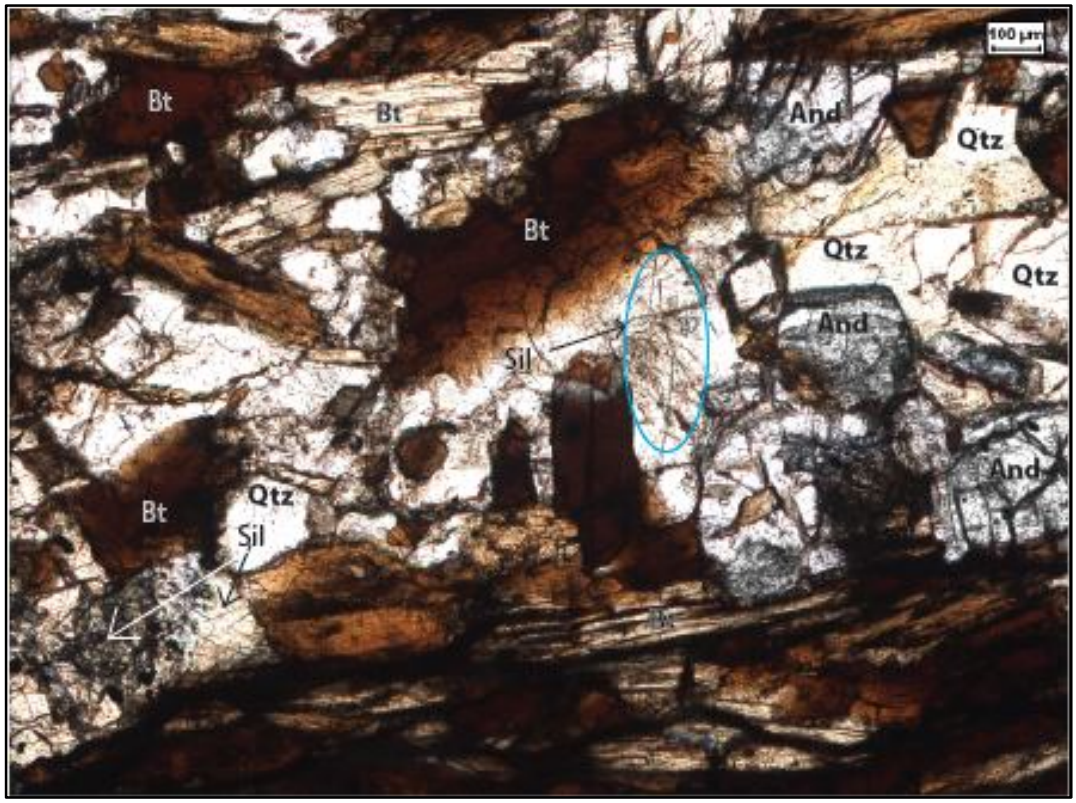

Figure 2.24 – *Microphotograph of hornfels (sample 15D). In this image sillimanite can be seen more clearly than in previous figures.*

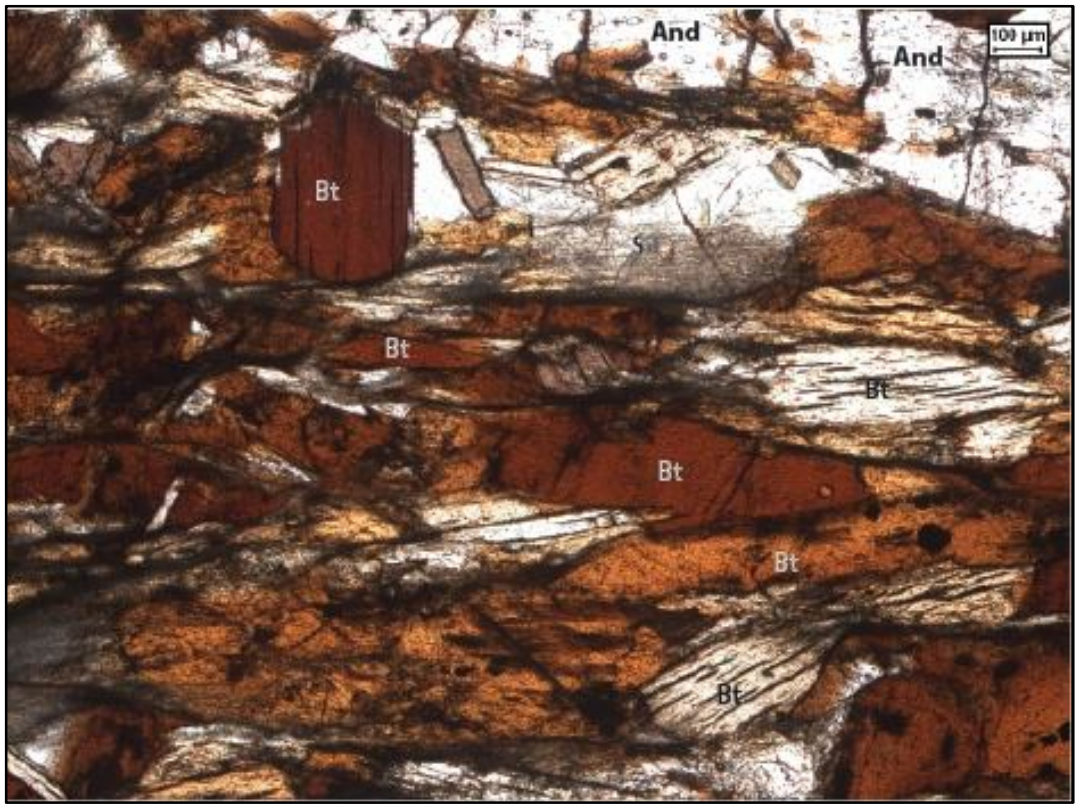

Figure 2.25 – *Microphotograph of hornfels (sample 15D).*

Stable mineral assemblage: bt qtz + bt + and+ms + sil

Facies: amphibolite facies/pyroxene hornfels facies (see Fig. 2.27).

Approximate stable P,T conditions (see petrogenetic grid, Fig. 2.28-2.29): (0.16 GPa, 650°C)

Timing of deformation and metamorphic growth

Sample 15D				
Mineral	*Def.*		*D1*	
Biotite			-----	--------
Muscovite				----------
Quartz		----------		
Andalusite				----------
Sillimanite				----------

Table 2.26 - *Paragenetic grid of 15D. The foliation seen in previous lithologies has virtually disappeared in this hornfels sample. The distribution of biotite in bands may indicate this mineral initially grew during deformation phase D1, with crystals arranged parallel to each other and not randomly scattered around the matrix. The incipient biotite crystals may have recrystallized with an increase in temperature and grown further into large and randomly oriented crystals using those already nucleated.*

2.1.2.7 - General observations on P,T conditions and mineral reactions

15G, 15B have passed the biotite isograd, where ms and bt form from destruction of chlorite at 440 ° C (Winter, 2001) **Chl + kfs = bt + ms (+qtz +H_2O)** and is therefore no longer in the greenschist facies.

All metapelites except 15H are found probably below 0.2 GPa due to the absence of staurolite at intermediate grades. In addition, all metapelites except 15H are found probably around or below 0.15 Gpa, since garnet is absent below this pressure at intermediate grades (Winter, 2001). Given the absence of garnet and staurolite, very low pressures can be inferred for the described lithologies. Therefore the action of batholith emplacement should account as trigger of metamorphic mineral reactions.

15E shows the action of reaction where ms is totally absent due to transformation to kfs and andalusite. Temperatures are around 650°C, since there is no longer any muscovite left but garnet has not formed yet either. This indicates the beginning of px-hornfels facies. As temperature increases, Cordierite may react with other minerals to form Andalusite The presence of andalusite crystals close to the rims of cordierite pophyroblasts indicates incipient nucleation around the latter.

The new formation of k-feldspar and absence of muscovite in sample 15E suggests the right conditions for the Tschermaks substitution to take place (Xu *et al.* 1994), with decay of muscovite and quartz in favour of k-feldspar and aluminosilicate. Reaction

ms + qtz = kfs + and + H_2O Temperatures are around 650 deg, since there is no longer any ms left but garnet has not formed yet either. This fact marks the beginning of px-hornfels facies (see AFM diagram, Fig. 2.30).

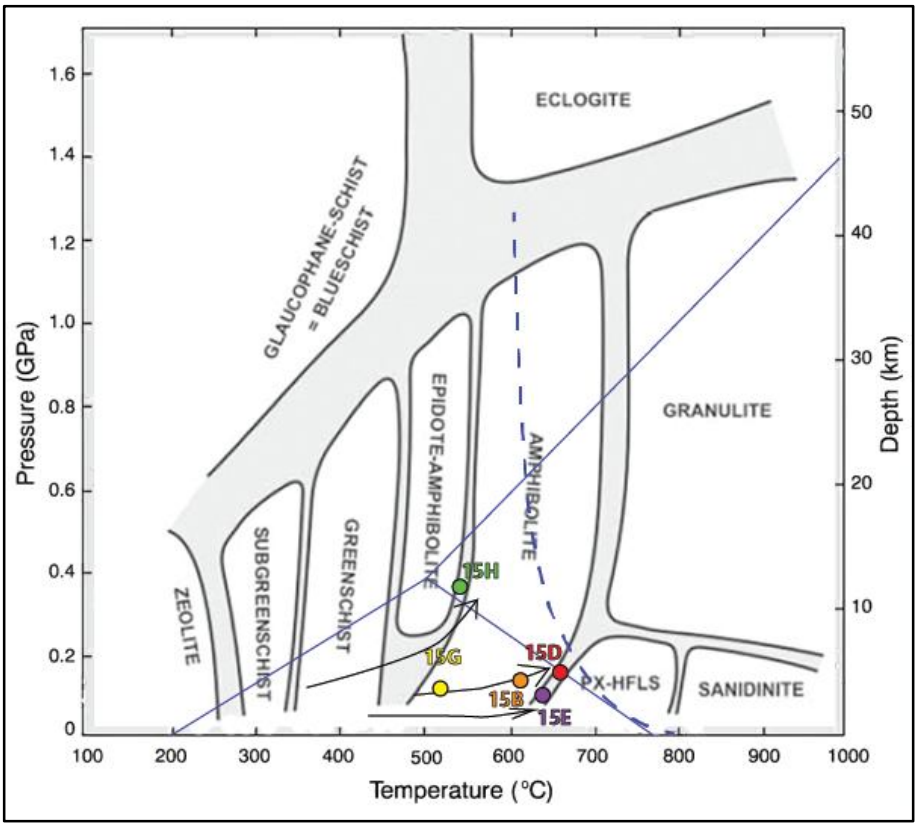

Figure 2.27 - *Facies diagram with P,T conditions of each of the sampled metapelitic lithologies, modified from Smulikowski et al. 2003.*

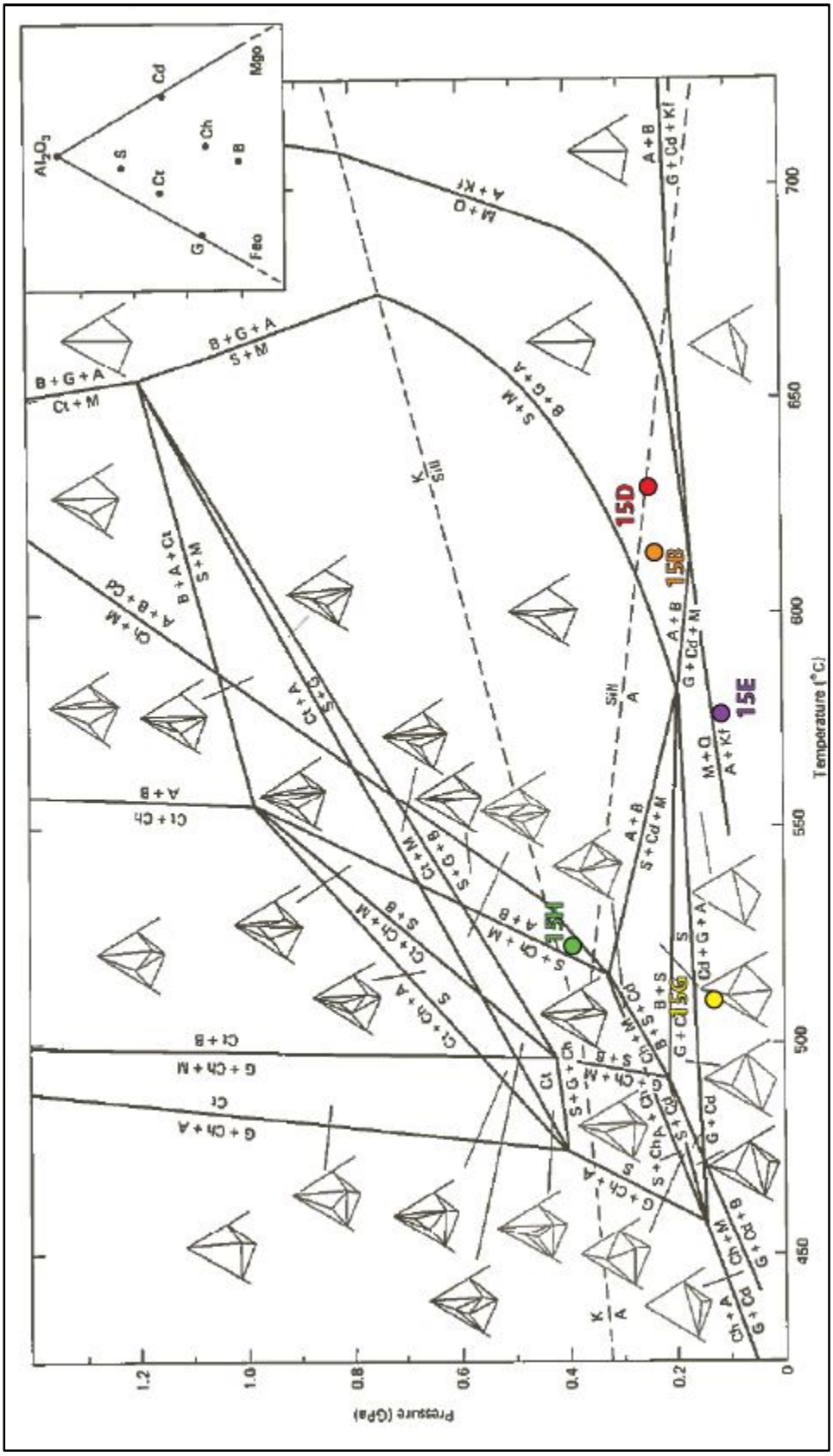

Figure 2.28 – *Location of samples on petrogenetic grid for metapelites by Philpotts (1990).*

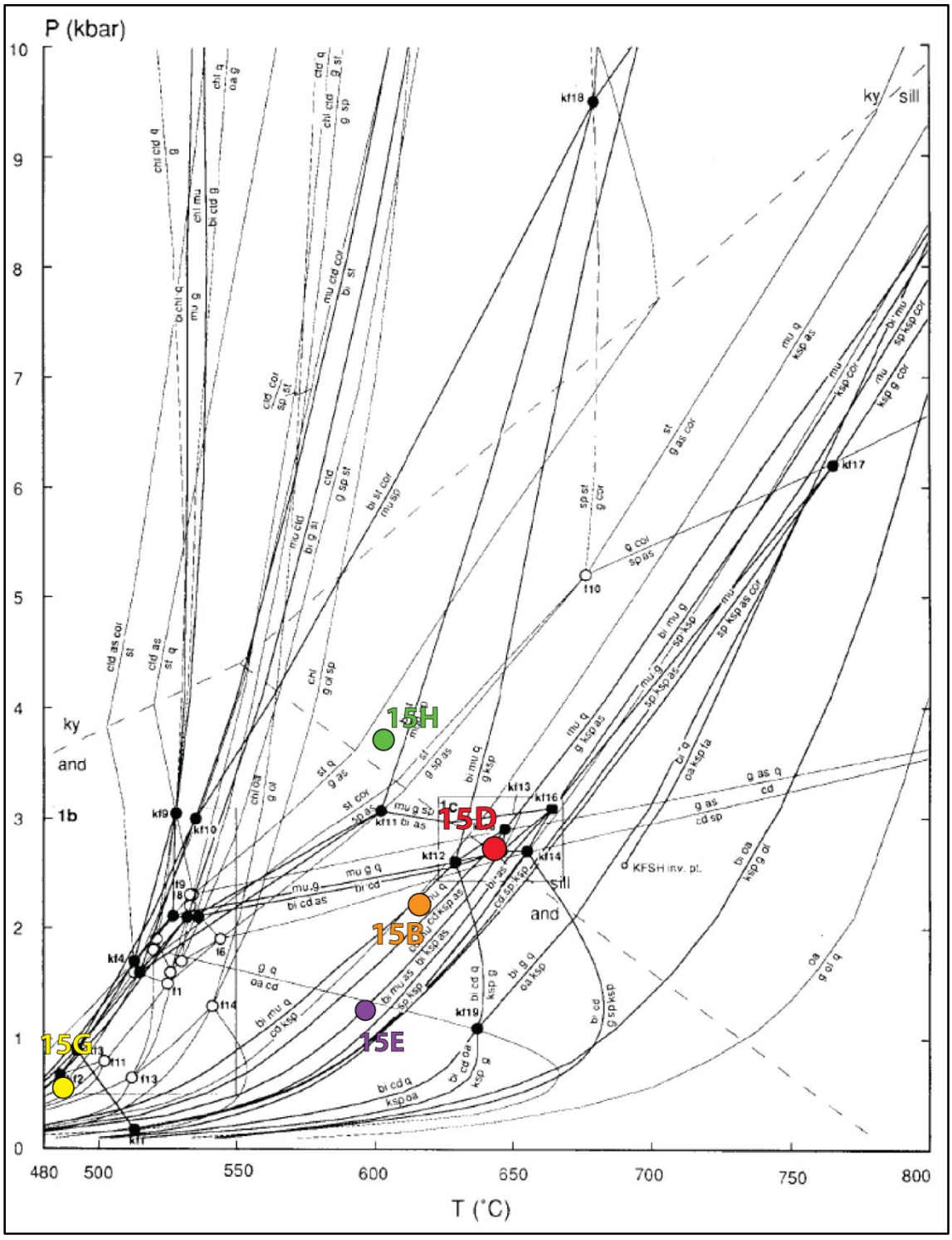

Figure 2.29 – *Location of samples on petrogenetic grid for metapelites by Xu et al. (1994).*

When projecting the different lithologies onto the petrogenetic grid of Philpotts 1990 (Fig. 2.28), just by looking at the reactions, the P,T conditions do not coincide with the same P,T conditions of the reactions described by Winter (2001). This is also the case when projecting the assemblages from the different samples onto the diagram of Xu et al. (1994), conditions vary depending on reactions considered and input data of petrogenetic grid.

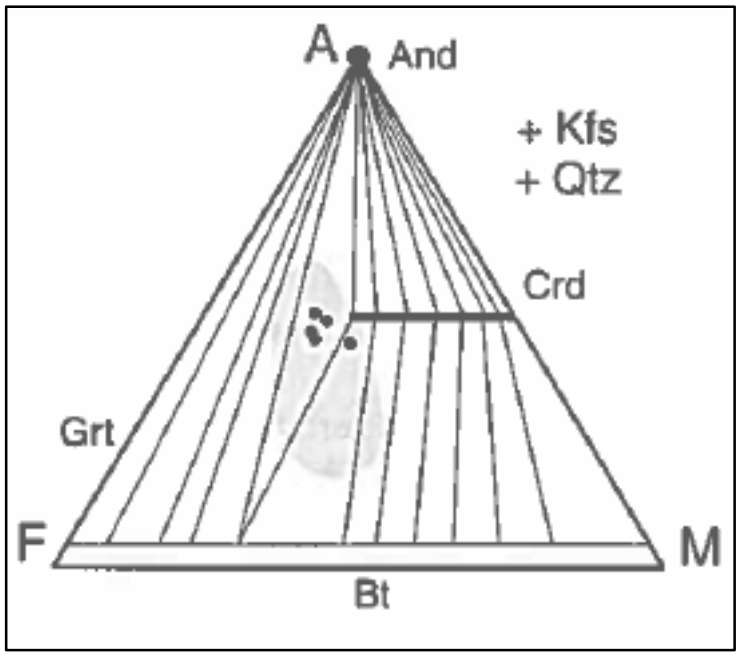

Figure 2.30 – *AFM diagram showing composition of sample 15E in the pyroxene-hornfels facies.*

2.1.3. Structural analysis

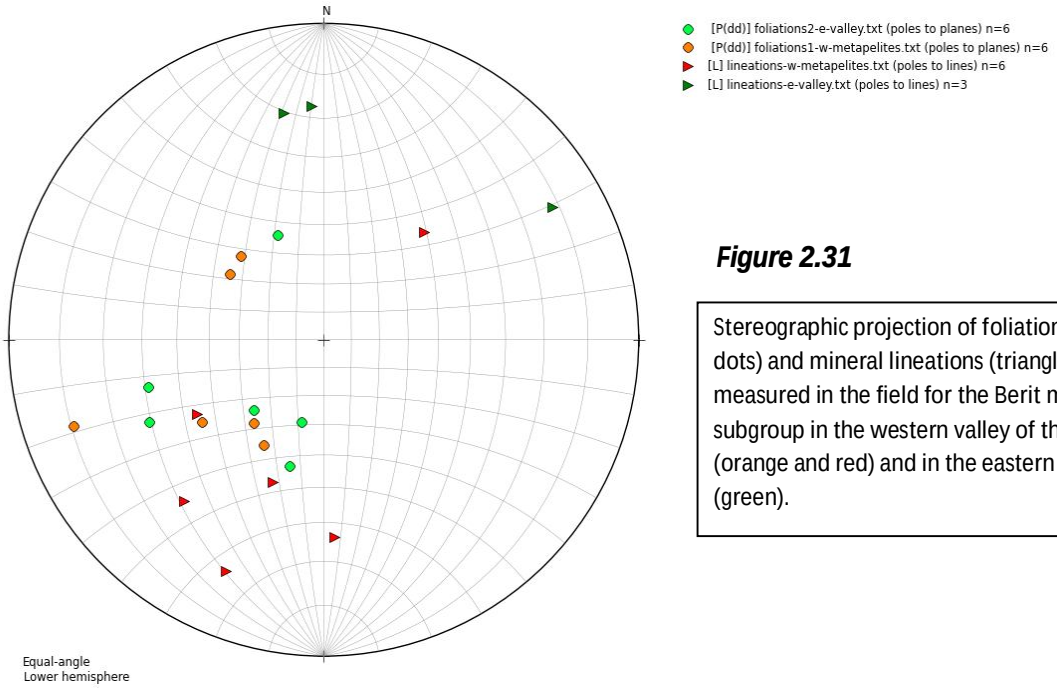

Figure 2.31

Stereographic projection of foliations (poles: dots) and mineral lineations (triangles) measured in the field for the Berit metapelitic subgroup in the western valley of the study area (orange and red) and in the eastern valley (green).

Mineral lineations mainly dip towards the SW in the W valley, whereas they dip N-NE in the E valley. Foliations are arranged around a small circle that dips SW, except for 3 that dip towards the NW. Mineral lineations are scattered dipping S, SW, N and NE.

Plane poles arranged around a small-circle-resembling curve represent measurements from flanks of a conical fold (ee). Since the 2nd eigenvector of the foliation coincides with mineral lineations in the eastern valley, these may correspond to the fold hinge. The other orientations of mineral lineations that don't coincide with the small circle or its hinge may correspond to lineations formed earlier than the conical fold. NW-dipping foliations may coincide with deformation from granite emplacement.

2.1.4.Discussion on metamorphism and intrusion sequence

There is not enough information to conclude whether the growth of minerals is actually due to the adjacent granitic intrusion. Given the nature of the mineral assemblages this is a low P and intermediate T sequence of rocks, but with not enough index mineral and textural variation to assess the gradual changes from an outer to an inner contact metamorphic aureole.

Given the situation of syntectonic growth of cordierite, increase in geothermal gradient could be interpreted to have had some relation to shear and subsequent thinning of the crust. By observing the map (Fig. 2.2.1 and 2.2.2) it is apparent that mineral lineation is more or less parallel to the contact between host rock and intrusion.This may correlate with the formation of oriented sillimanite in sample 15H further NW. The foliation recorded in sampled lithologies 15B and 15D could also be hypothetically related to intrusion emplacement. The same cannot be said, however, of the foliation recorded at sampling points 15G and 15F, which would be almost perpendicular to the edge of the batholith.Growth of cordierite syntectonically and further development of andalusite indicates late to post-tectonic emplacement of granite, which would fit in with the tectonic events described in the literature (see introduction).

Comparison of granite of the two valleys: The ages of the granites of the two valleys may be different. From the characteristics seen in the samples of these units, this study supports a hypothetical Late Cretaceous age for the emplacement of the granite of the eastern valley and a possible Eocene age for the granite of the western valley, given its less deformed characteristics (only by late brittle SFZ). However, according to Robertson *et al.* (2006) the granite of the western valley is Late Cretaceous in age.

2.2. Brittle deformation in the Ericek area

This section gives an overall account of the lithologies sampled in the vicinity of the Sürgu fault, SE Anatolia, South of the village of Ericek.The samples described include limestones and pyroclastic lithologies.Their location corresponds to the points in the map (Appendix 1). High resolution scans of each sample are available in the appendix.The classification used for fault rocks corresponds to IUGS (Brodie *et al.*2007).

2.2.1. Petrographic descriptions and fault rock classification

Jurassic limestone mesocataclasite(17G)

This unitcrops out in the vicinity of the main branch of the Sürgü fault zone in the North-West of study area.It corresponds to alimestone with sparite grains and a dark matrix of micrite. Sparite crystals are heterogeneous in grain size, ranging between 40 and 250 μm. Lamellar twinning in calcite crystals is curved in some cases and some grains present undulatory extinction. There are cracks running across the sample which contain clear sparite crystals, as well as microfaults separating domains of displaced material.

Interpretative comments: curved lamellar twinning indicates deformation. Recrystallization in cracks evidences the infiltration of calcite-rich fluids or dissolution of the host rock. Microfaults cause the strike-slip displacement of grains (Fig.2.32). The presence of micrite and the heterogeneity in calcite grain sizes are clear signs of the absence of metamorphism, however, a finer-grained matrix indicates possible grain-size reduction. For the presence of >50% of matrix surface and less than <90%, this sample will be termed a **mesocataclasite**.

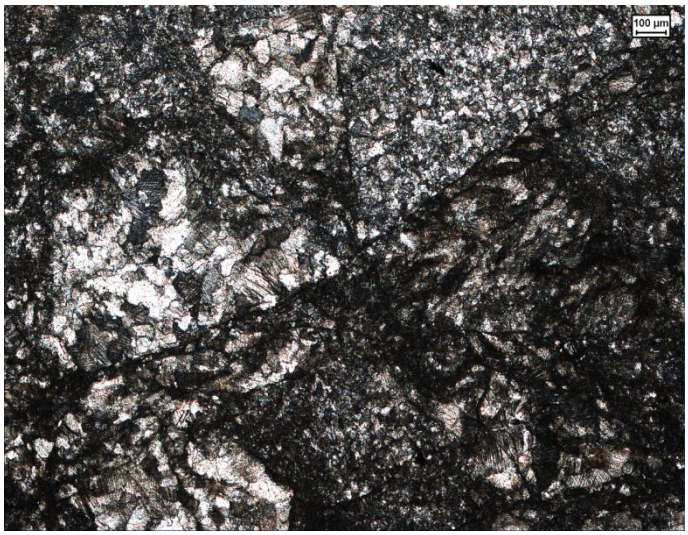

Figure 2.32 – *Jurassic limestone sampled in the vicinity of the Sürgü fault.*

Miocene limestone to fault breccia - 17B, C & D

Distance from fault of each sample:

This rock is made up of a matrix of sparitic and equidimensional calcite grains with regular grain boundaries of 30 to 100μm that define a polygonal microstructure.The matrix is cross-cut by veins, also containing calcite of larger grain size.Crystals found in veins are generally around 100 μm in grain size, but in some of the wider veins can be up to 0.4 mm. The largest vein that cross-cuts the matrix shows angular bends (Fig. 2.33).

17C and D are more strongly brecciated than 17B. They are made up of angular clasts (2-4 mm) of limestone parent rock in a clay matrix (Fig. 2.34).

Interpretative comments:in 17B this unit has undergone mild brittle deformation and aforementioned displacement of veins might be caused by the influence of the SFZ.On the other hand, 17C and 17D have suffered strong brittle deformation and are classified as**fault breccia**(>30% fragments).

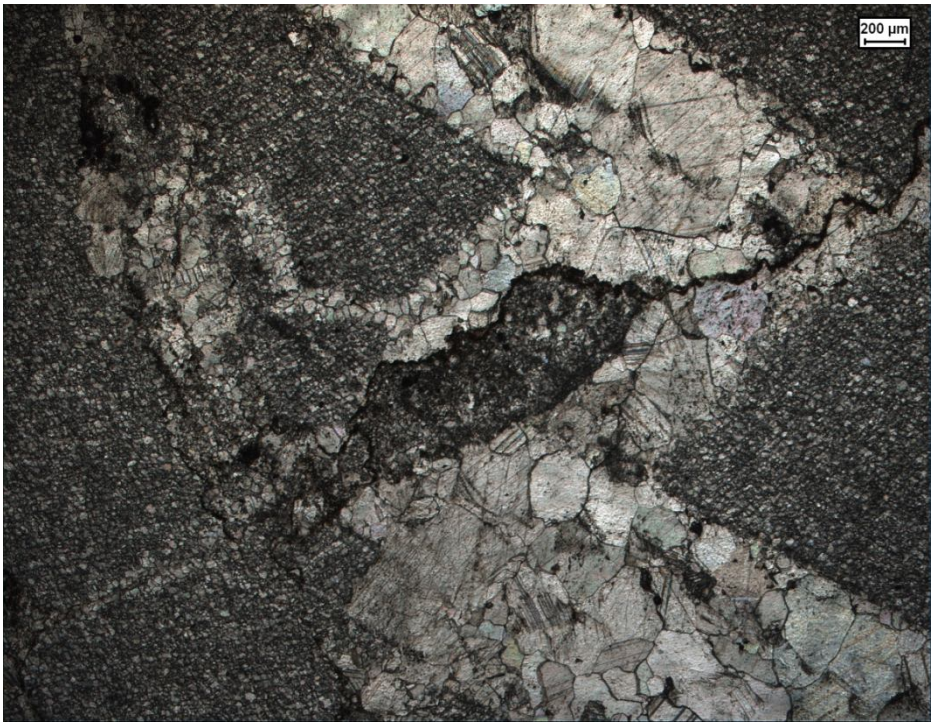

Figure 2.33 – *Miocene limestone sampled in the vicinity of the Sürgü fault (relatively underformed).*

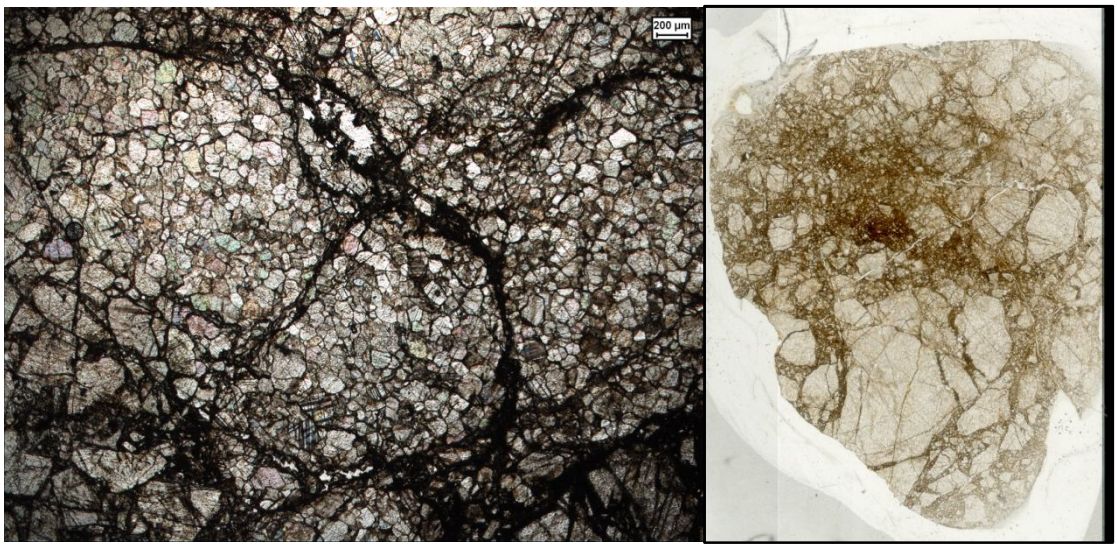

Figure 2.34 – *Miocene limestone sampled in the vicinity of the Sürgü fault (clear brittle deformation).Left: microphotograph, right: scan of the thin section (scale: horizontal margin=27 mm).*

2.2.2. Pyroclastic fault rocks – pseudotachylite or cataclasite?

Coarse ash tuff cataclasite (18H &18J)

Two samples collected from within the fault zone have been described and analysed for evidence of seismic creep using light microscopy and SEM. These samples correspond to a cohesive felsic-to-intermediate pyroclastic unit with granular texture, within the Maden group mentioned in the introduction. Veins and bands with textural differences are identifiable in the field at outcrop scale (Fig. 2.35) and have been chosen as study targets to assess fault-related deformation and confirm the presence or absence of pseudotachylites.

The analysis of these vein areas involves a comparison between structures characteristic of frictional melting, such as sub-veins with amorphous or devitrified textures, and others of ultra-cataclasis and comminution, such as brittle grain size reduction, undulatory extinction and presence of cohesive material and cracks.

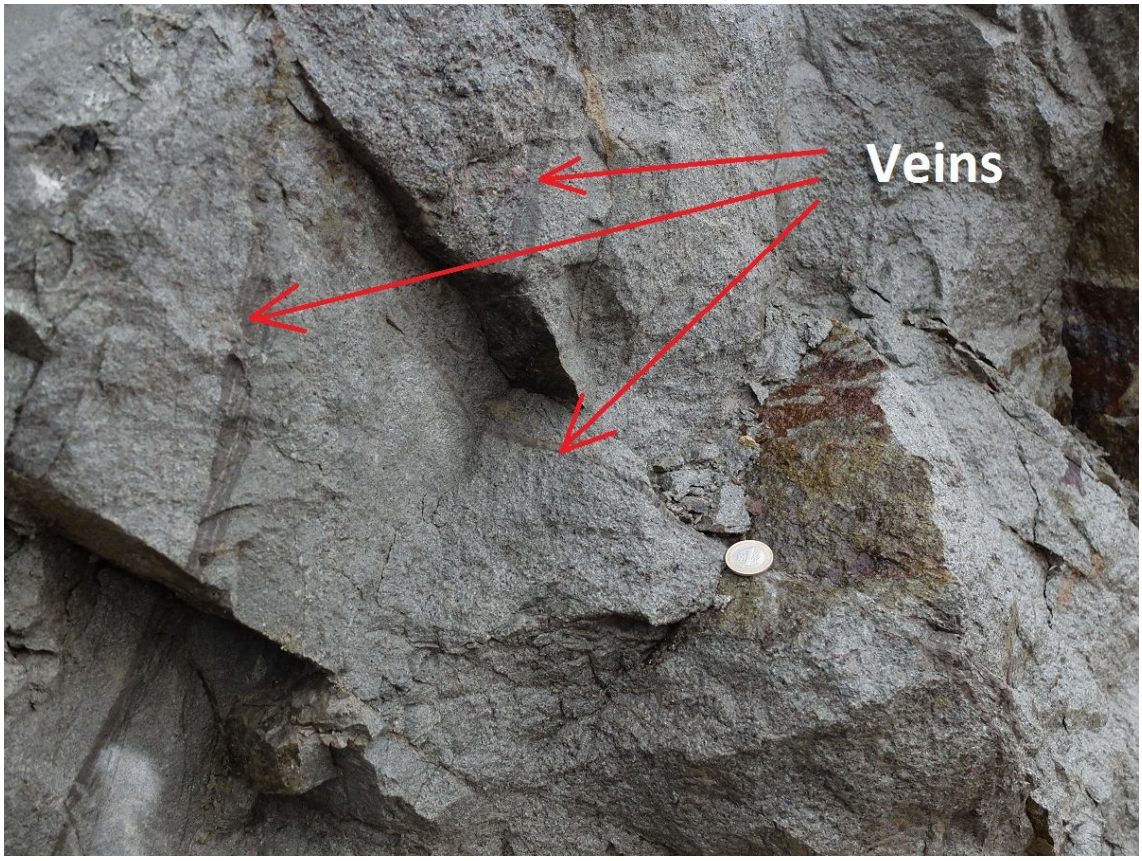

Figure 2.35 –*Eocene pyroclastic rock sampled in the vicinity of the Sürgü fault (veins pointed out).*

Petrography of protolith – coarse ash tuff

This lithology is integrated by a light grey cohesive fine-grained matrix of submillimetrical fragments of different compositions. Darker and finer-grained areas can be distinguished from the matrix. In addition, the latter is cross-cut by millimetric veins of darker appearance (Fig. 2.36). Both the veins and finer-grained areas are thought to be associated to concentration of deformation, being found within the fault zone.

The protolith of this deformed rock from the Sürgü fault zone is described as the least-deformed part of samples 18H and 18J: the coarser-grained matrix mentioned above, which is

nonetheless deformed to some extent. Classification of these specimens has been done on the basis of their pyroclastic textural characteristics as well as according to their composition.

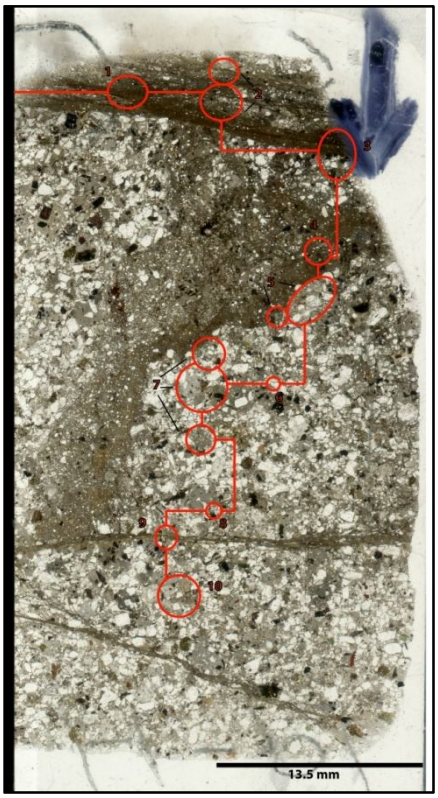

Mineral content: Plagioclase (30%), K-feldspar (sanidine, 15%), Orthopyroxene (3%), Hornblende (or other amphibole) (5%), biotite(7%), Quartz (2%), Silica glass fibres (18%), Feldspar glass fibres (20%), Apatite (trace).

Microstructure: This lithology is integrated by a granular matrix of coarse ash grains (0.3 to 1 mm) with xenoliths (around 1 mm) and xenocrysts of feldspar, plagioclase biotite, amphibole and orthopyroxene (0.15 to 1 mm in size).Plagioclase xenocrysts are zoned. Pumice fragments vary in composition (SiO_2 or Plag.-Feldspar). All fragments and crystals are randomly oriented. Many feldspar grains present undulatory extinction and/or cracks, especially when located close to a vein or higher deformation area. This lithology is dense and has little porosity (Fig. 2.37).

Due to its even proportions of pumice, crystal and lithic fragment content this lithology can be termed pumice-crystal-lithic coarse ash tuff (classification: Schmid, 1981).

Considering this units' compositional distribution it can be considered a **dacite** (see classification diagrams for volcanic rocks, Figs. 2.39&2.40: TAS diagrams –Le Bas and Streckeisen, 1991; QAPF –Streckeisen, 1978).

Figure 2.36 –*Thin section scan of coarse ash tuff 18H. Large version of the scan is available in the appendix.*

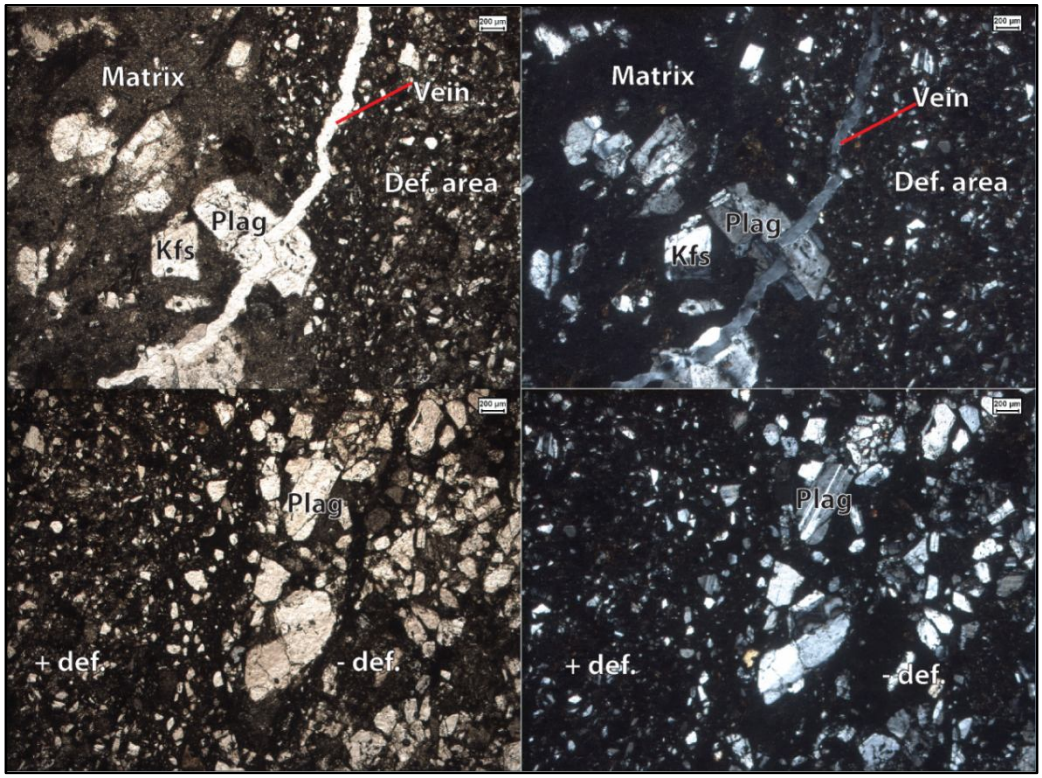

Figure 2.37 –*Microphotographs of coarse ash tuff 18H displaying xenocrysts, ash matrix and finer-grained deformed area.*

Chemical analyses

Sample 18H of the Maden unit was analysed with SEM to find out what type of tectonic structures related to the SFZ it contains. Qualitative and semi-quantitative analyses were carried out to confirm composition of mineral and lithic grains. More information on these results can be found in the appendix.

Amongst feldspar grains, the most common composition is of a mix of anorthoclase and oligoclase, as intermediate Na-K feldspar and Na-Ca plagioclase.Feldspar grains found in veins typically present orthoclase compositions including smaller-grained anorthite exsolutions within.

Hydrous phases were calculated by recalculating their formula adjusting oxygen estimates to the required amount (e.g. 20 oxygens for biotite).

Biotite, hornblende and orthopyroxene are the mafic minerals found as xenocrystalline phases in the matrix of this coarse ash tuff.

Some dark clasts in the matrix were found to contain quartz, most likely in very small fragments of glass: ash will trace amounts of impurities of other elements (e.g. Al, Na, K, Ti).

Quantitative analyses from vein areas proved more difficult to recalculate using the resulting cations. This may be induced simply by calculation error, however, the recurrence of this fact in vein areas may indicate incomplete restructuring of elements into crystalline shapes in their right proportions.

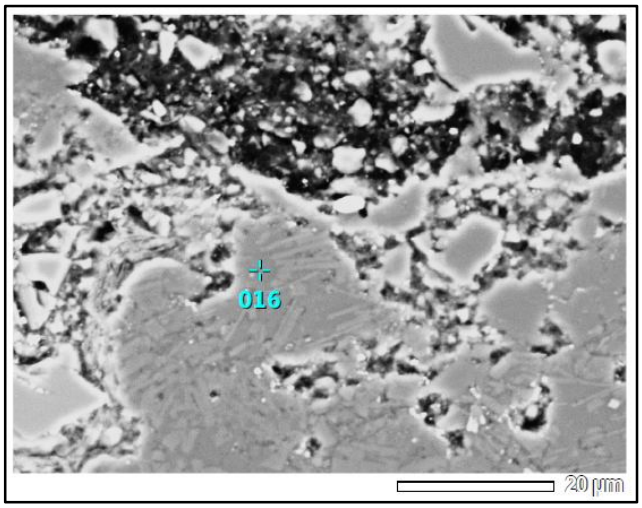

Figure 2.38 – *Feldspar grain from cataclasitic vein presenting exsolutions.*

Figure 2.39 *–(Right) TAS compositional diagram for volcanic rocks showing location of sampled rocks 18H and 18J with a green circle (Le Bas & Streckeisen, 1991).*

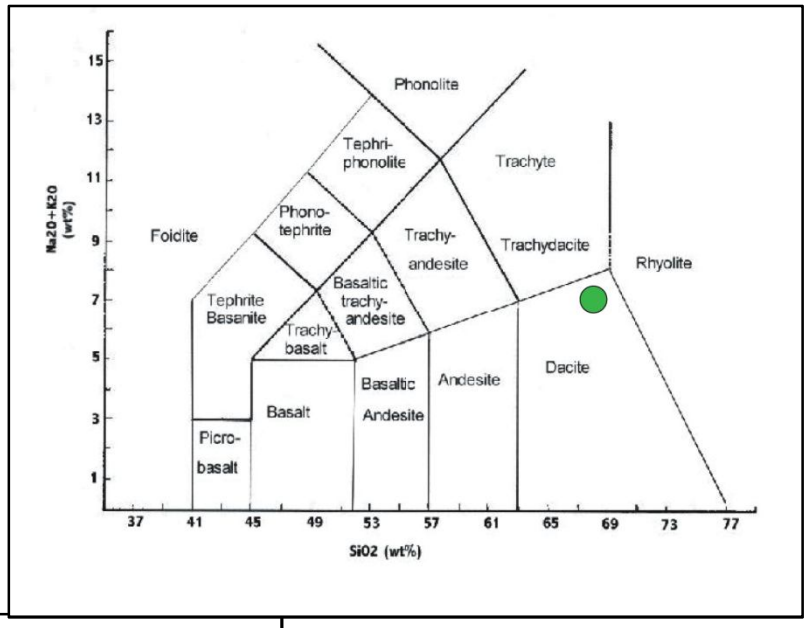

Figure 2.40 *–(Below)QAPF compositional diagram for volcanic rocks showing location of sampled rocks 18H and 18J with a green circle (modified from Streckeisen, 1978).*

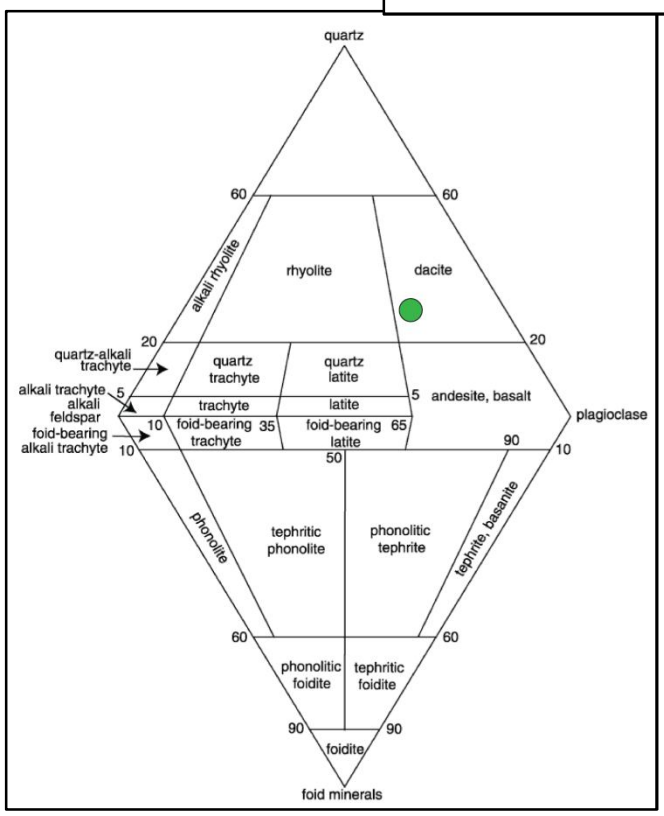

Petrogenetic origin

This lithology is an example of an intermediate magma. Dacitic compositions find their origin in plate convergence, when oceanic crust from a subducting plate is melted, fractionated to more felsic compositions and contaminated with acidic continental crust. In this context, this type of magmas originate above the Benioff zone by fractionation of the melted subducting slab (Ringwood, 1975).

Similar volcano-sedimentary units such as those corresponding to 18H and 18J are described in Robertson *et al.* (2006) as Middle Eocene. Kuscu *et al.* (2010) mentions two prominent intraplate magmatic events of calc-alkaline/alkaline nature in the area; one set in the Late Cretaceous and one in the Early to Middle Eocene, leading to different types of lithologies integrating plutonic, volcanic and pyroclastic units. See introduction for information on tectonic configuration associated to magmatism in SE Anatolia.

Pyroclastic flow deposits arise from collapsing domes, lahars, and different types of breccias. Most dacitic pyroclastic rocks originate from stratovolcanoes. With increasing silica content, extrusive magmas become more explosive (Winter, 2001).This fact fits in with the felsic composition of our samples and origin from an ash cloud.

Fault rock analysis

Pseudotachylites are evidence of seismic deformation. If glass becomes unstable, due to a change of pressure and/or temperature conditions, it will recrystallize resulting in an igneous texture. Pseudotachylites can be found at lithospheric depths of brittle deformational behaviour down until the transition between brittle and ductile behaviour. Pseudotachylites can be found along faults or in injection veins that have an almost perpendicular orientation with respect to the fault. Frictional melting can be identified in quenched vein boundaries, corona textures, a general glassy texture and flow-related structures (Mambane *et al.*, 2011).

Pec *et al.* (2012) suggest revising the idea of considering pseudotachylites as solid evidence for paleoseismicity, since their experiments at slow creep (and aseismic) also result in the formation of pseudotachylites. This gives pseudotachylites less reliability in identifying seismic creep.

The characteristic fine-grained textures found in pseudotachylites can make them hard to identify. In addition, pseudotachylites can be overprinted by later deformation, brittle or ductile, can make indetification even more difficult. Compositional differences of clasts inside and outside the vein may also be a way of discerning between pseudotachylite and cataclasite (Mambane *et al.*, 2011).

According to Passchier and Trouw (2005), cohesive cataclasite can be distinguished from undeformed part of the lithology due to its darker colour, as seen in 18H and 18J. Cataclasite would typically show a transition from smaller grains to increasingly larger grains from the vein to the less-deformed matrix. This is not alway the case of our samples and overall grain size variation is not very large. Cohesive cataclasite is thought to originate deeper than incohesive fault rocks.

Deformation indicators

The following is a list observations from the deformed area of 18H are descriptive of veins and potentially indicative of deformation mechanisms. An interpretation has been made for each of them, as an attempt to identify each characteristic to brittle-cataclasitic type of deformation or as a result of frictional melting.

Pseudotachylite indicators:

- The contact between veins and host rock is sharp in most areas of the sample. *According toKirkpatrick et al. (in press) this is characteristic of pseudotachylites.*

- Veins are proportionally richer in quartz and feldspars, whereas matrix also contains considerable amount of hydrous minerals, therefore composition is more uniform in the broken grains found in veins. *Less compositional variation in pseudotachylite areas can occur due to melt differentiation (Mambane et al., 2011). Fragments could account for quenched glass that later suffered brittle deformation.*

- *Sorting of brittle fragments is intermediate.*

- *Presence of orange veins of silicate composition.*

- *Presence of exsolutions as evidence of igneous recrystallization.*

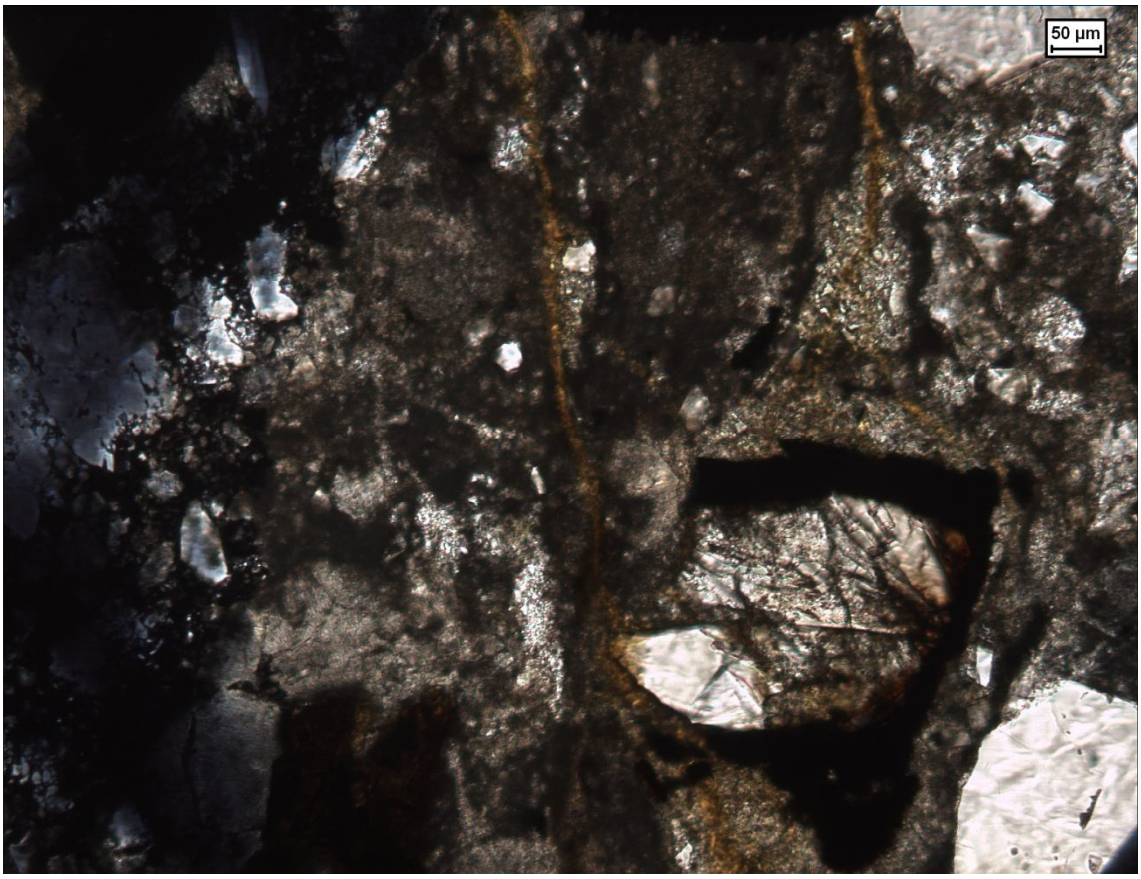

Figure 2.41 –*Microphotograph of sample 18H, zooming in on a narrow vein. Orange/light brown veins are visible.*

Cataclasite indicators (Passchier and Trouw, 2005)*:*

- Grain size reduction in vein areas.
- Poorly sorted grain sizes within veins (Figs. 2.42 & 2.43).
- Angular clasts (Figs. 2.42 & 2.43).
- Brecciated igneous xenocrysts.
- Wavy structure of some of the more highly deformed areas (veins), wider than straight veins: interpreted as oblique section of a cataclasitic zone (Fig. 2.36).
- Absence of igneous textures in 'vein' areas.
- Absence of a sharp transition between host rock and vein in some localized areas.
- Preservation of hydrous mineral in vein (biotite).
- Colour variations within vein (orange vein): from fluid infiltration during brittle faulting (Fig. 2.40).

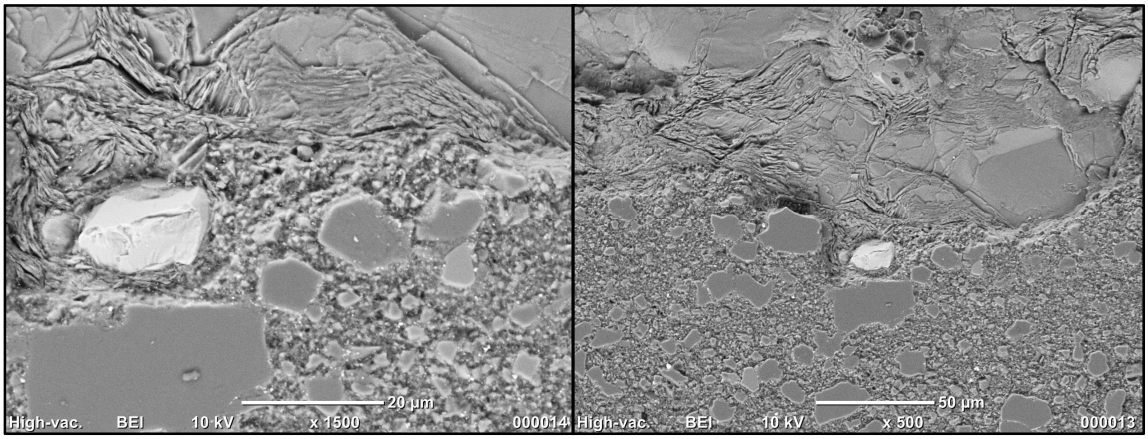

Figure 2.42 – *SEM image showinggrain size reduction from host rock (top) to deformed vein (bottom).*

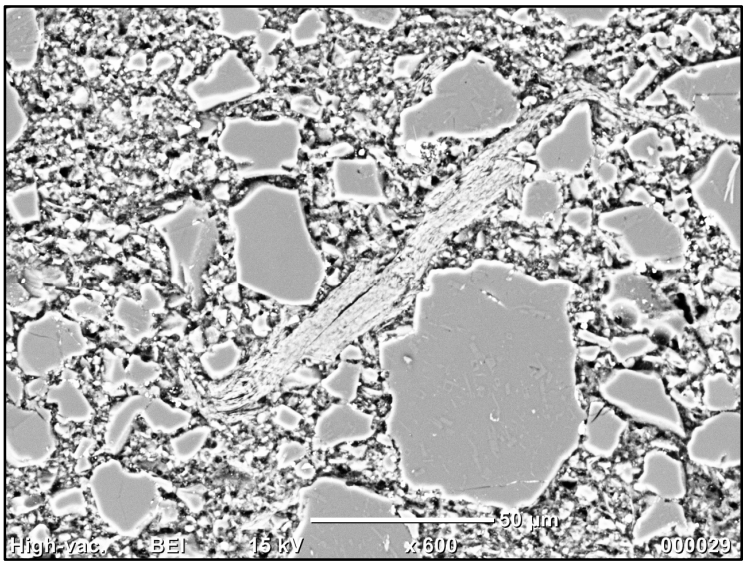

Figure 2.43 – *SEM image showingBiotite grain amongst matrix of feldspar and quartz fragments. Evidence of preservation of hydrous minerals (instead of going into a melt phase).*

Figure 2.44 – *SEM image showingrelatively poor sorting between fragments within deformed vein.*

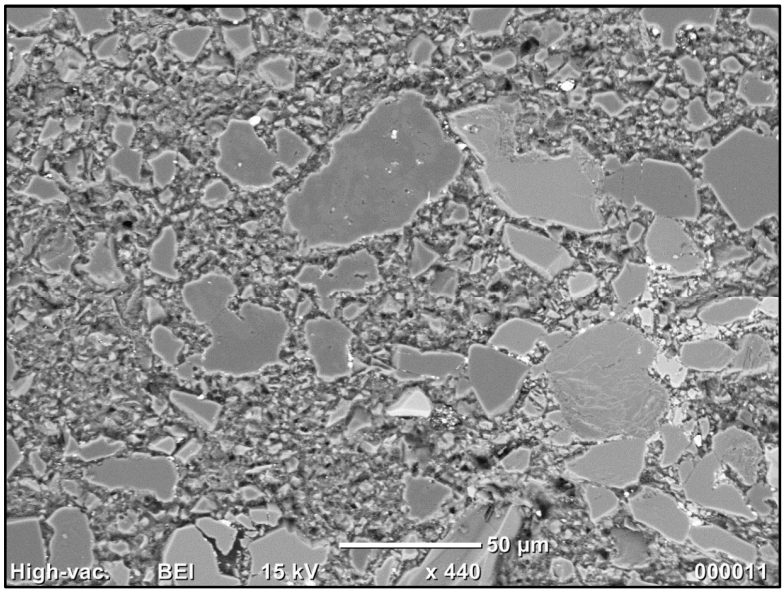

Ambiguous indicators:

- Differences in colour between areas of vein (brown and orange). *Colour zoning parallel to vein margins can be a consequence of quenching of melts (Kirkpatrick et al. in press)*

- Wavy structure of some of the more highly deformed areas (veins) and wider than straight veins. This structure could be interpreted as injection veins (morphology seen on the thin section scan, without microscope). Alternatively, this could indicate an oblique surface cut of a brittle deformation plane.

- Banding parallel to vein direction. This could initially be interpreted as zoning due to melt quenching (supporting pseudotachylite hypothesis), however, in this case analysis shows that banding is accounted for by changes in grain size (Passchier and Trouw, 2005), supporting cataclasite hypothesis.

- Embayed clasts in vein areas. *This could be a sign of melting (Kirkpatrick et al. in press). However, this could also be polishing from interstitial clay or debris being washed out (Fig. 2.44).*

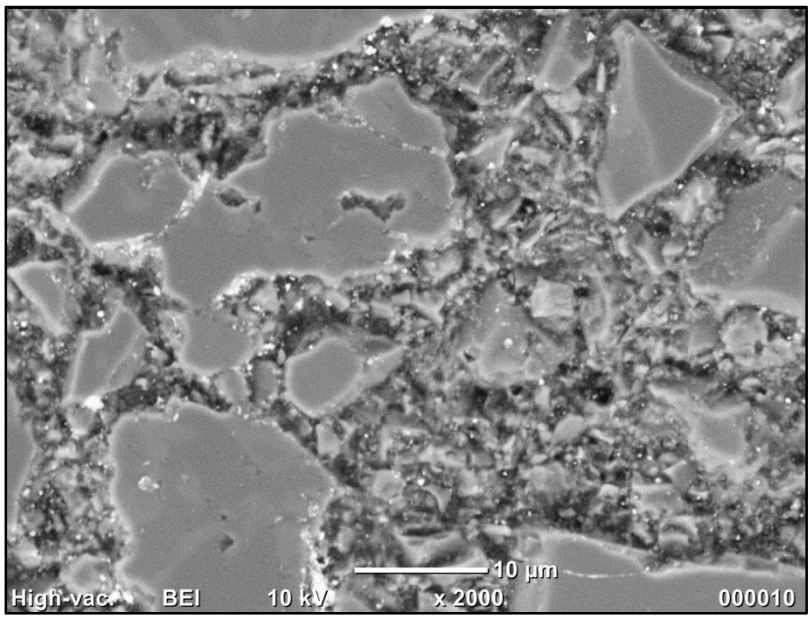

Figure 2.45 – *SEM image showingfragments from within a high deformation area. Embayed clasts are visible**.** Grains have an overall polished out appearance*.

Interpretation

Pseudotachylites deform more readily than host rock due to fine-grained material from fast crystallization or due to the metastability of amorphous phases (Kirkpatrick *et al.*, in press). Ductile flow can also concentrate in pseudotachylite veins. It is a possibility that further brittle deformation may have taken place later than pseudotachylite formation, due to exhumation and a transition to more surficial brittle conditions within the fault zone.

The dark colour of veins can be explained by textural differences, not compositional, specifically grain-size reduction.

The most striking microstructures displayed by this lithology are of cataclasitic nature (Figs. 2.43-2.45), however, some traits may point towards a relict and overprinted pseudotachylite (e.g. embayed clasts, exsolutions, etc.). Since grain-size reduction zones (finer-grained matrix and veins) correspond to less than 50% of the unit and brecciation of xenocrysts and clasts is

only visible microscopically, the samples from the Maden unit 18H and 18J will be classified as **protocataclasite**.

2.2.3. Structural analysis

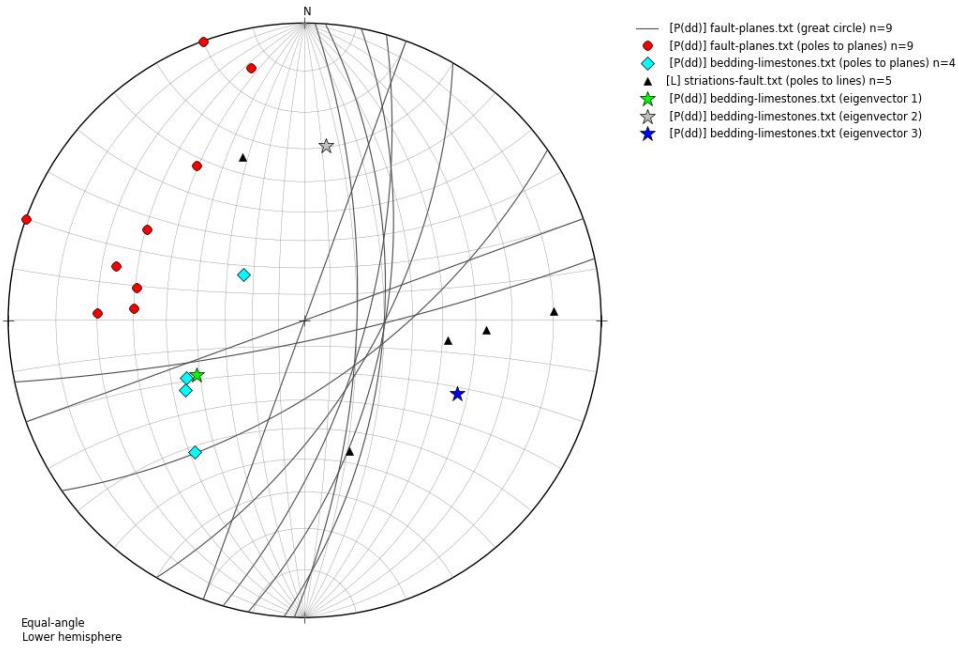

Figure 2.46 – *Equal-angle projection of measurements from limestone bedding and fault planes near Ericek village.*

Fig. 2.46 shows a stereographic projection of bedding in limestones (blue diamonds: poles) units adjacent to the SFZ near Ericek and fault measurements from different outcrops (red:poles, black lines: great circles). Black triangles correspond to fault striations. Limestone bedding dips moderately to the SE. Fault planes are vertical to dipping very strongly to the ESE. Fault striations dip towards the E, SE and NW.

Poles of limestone bedding planes follow a great circle, which probably indicated a cilindrical fold.

The variations in orientation of the fault can be correlated to the curvature seen on its surface trace on the map and to the fact that measurements were taken on different branches of the fault near Ericek. East-dipping fault striations indicate E-W-trending displacement, as seen on the map.

3. Discussion

Tectonic-scale implications

In the area of Ericek there is an emplacement of nappes as in other places in the area, intruded by granites and overlain by sedimentary and volcano-sedimentary units, finally cross-cut by the SFZ. The relation between intrusions and host rock are studied more in depth. Our findings fit in with previous studies that consider batholith intrusion as syn-orogenic and post-orogenic intrusion (Kuscu et al. 2010; Robertson et al. 2006). However, dating of units should be made to confirm whether granites from both valleys mentioned are actually coeval or not, even though they display different characteristics (one is affected by ductile deformation (E) while the is other is affected by brittle deformation (W)). There is no consensus in the literature about a constrained age for granite intrusion, since it happened episodically throughout the Alpine orogeny (Kuscu et al., 2010) and Karaoglan (2013) describes intrusions along the same strike-slip fault further NE as Eocene.

Metamorphism of pelites is found to be most likely caused by intrusion of the adjacent granitic body, resulting in intermediate to high-grade mineral assemblages. This takes place at the same time as ductile deformation and continues and after, confirming the late-to-post orogenic tendency in the area, mentioned above.

An explanation has not been found as to why magmatic intrusions are found close to the SFZ. This may be related to SFZ being a reactivation of an old suture (since the area has ophiolites it is likely that the suture was found here). If subduction initiated in the South, melts will have formed on the subducting slab, risen to the overlying mantle wedge and lower crust at a first point, and as subduction advanced, this melt source will migrate northward. Older melts will have more time to differentiate. This is also possibly why Kuscu et al. (2010) mention that magmatic suites get gradually more alkaline in a southerly direction.

Local implications

Metapelites of the Berit group are metamorphosed to phyllite condition unaffected bythe granite and to spotted schist and hornfels in areas closer to the intrusive batholith.These are also foliated and sheared withminerals in clast morphologies, both in the western and eastern valleys. In the western valley, bt-ms-and-qtz assemblages are described increasing to add cd + kfs, or sillimanite with increasing grade. One sample from this metapelitic unit in the west is found to be outside the aureole, this may be due to faulting separating the locality and the granite, since samples closer to the granite than 15H display more hornfels-like microstructures. As far as structure is concerned, foliation planes measured from the Berit pelitic subgroup display a conical fold morphology on the stereonet, which may be indicative of the presence of a sheath fold, typical of shear zones. Moreover, deformed clasts show evidence for simple shear.

Rocks sampled from the fault zone aredeformed in a brittle manner from Protocataclasite to Fault breccia, and with some indications of possible relict pseudotachylitic evidence.

According to the literature (Robertson et al., 2006), the SFZ is Plio-Quaternary in age and therefore cuts across all older structures and units described in this study. This is confirmed by the fact that sampled lithologies near the fault zone of different ages are deformed.

Fault activity in the area corresponds to the brittle domain with cohesive fault rocks. This indicates exhumation may have taken place after formation of these fault rocks, since they are

not formed at shallow levels as incohesive fault rocks. Fault motion is mainly E-W, as seen on the offset in lithologies mapped, confirmed by field measurements.

There is not enough evidence to confirm seismic vs aseismic activity in sampled fault rocks such as clear structures confirming frictional melting or recrystallization due to fault activity. However, limestones could be analyzed further in search for the latter type origin of recrystallization.

Exsolutions may indicate evidence for melting and recrystallization. In any case, pseudotachylitic structures were recorded in this lithology at some point, exhumation will have induced structures of a more cataclasitic nature, overprinting above pseudotachylite is however still a plausible hypothesis.If this hypothesis is confirmed, the fault will have undergone clear exhumation.

Despite the lack of concrete dating, exhumation is apparent in the study area due to surface exposure of granitic intrusions with overlying platform carbonates and later slope deposits. This indicates that uplift will have got the intrusions in contact with sediments (submarine or subaerial)before the Miocene.

4. Conclusions

- Late-to-post orogenic magmatic events generate contact metamorphism of intermediate to high grades, which takes place at the same time as ductile deformation and continues.
- Fault rock microstructures in lithologies sampled near the village of Ericek confirm activity of the SFZ on Jurassic, Eocene and Miocene lithologies. This confirms it is more modern that all the latter ages.
- Contact metamorphic assemblages include bt-ms-q-and, bt-ms-q-and-cd-kfs, bt-ms-q-and-sill, which are characteristic of low pressure and intermediate to high temperature.
- Cordierite is found to grow syn-foliation and andalusite, post-foliation. This fits in with a late-to-post orogenic intrusion.
- Granite intrusions of the Berit group from the two valleys of the study area are found to be compositionally and microstructurally different. Literature study does not clarify the ages of these particular outcrops separately (except Robertson et al. -2006- mention late Cretaceous at least for the western valley granite). However, given the nature, size and proximity of the intrusions, the same contemporary source for both of them could be a sensible hypothesis.
- Pseudotachylite veins have been searched for in pyroclastic fault rocks, however, fine-grained materials i veins have pointed towards grain-size reduction as principal deformation mechanism in this locality. However, some textures seen in coarse ash tuff samples may indicate relict pseudotachylite-derived structures, such as embayed clasts or igneous textures within broken vein materials.

References

Barker, A.J., 1994. Interpretation of porphyroblast inclusion trails:limitations imposed by growth kinetics and strain rates. J Metam.Geol. 12:681–694

Bell TH (1985) Deformation partitioning and porphyroblast rotationin metamorphic rocks: a radical reinterpretation. J Metam.Geol 3:109–118

Brodie, K., Fettes, D., Harte, B., & Schmid, R., 2007. Structural terms including fault rock terms. In: Recommendations by the IUGS Subcommission on the Systematics of Metamorphic Rocks. Web version of 01.02.07 Available at: www.bgs.ac.uk/scmr/home.html. Last visited: 18 June 2014.

Compton, R.R. (1962). Manual of field Geology.*John Wiley and Sons*, NewYork, U.S.A., 214pp

Borradaile, G. J., Bayly, M. B.&Powell, C. McA., 1982.Atlas of Deformational and Metamorphic Rock Fabrics. *Springer-Verlag, Berlin* ,551 *pp. et al.* 1982

Duggen, S., Hoernle, K., Van Den Bogaard, P. & Garbe-Schonberg, D. 2005. Post-collisional transition from subduction to intraplate-type magmatism in the westernmost Mediterranean: evidence for continental-edge delamination of subcontinental lithosphere. Journal of Petrology, 46, 1155–1201.

Göğüş, O.H., Pysklywec, R.N., 2008. Mantle lithosphere delamination driving plateau uplift and synconvergent extension in eastern Anatolia.*Geology*, 36,723–726.

Göncüoglu, M.C., 2010. Introductionto the geology of Turkey : geodynamic evolution of the pre-Alpine and Alpine terranes. Ankara, *General Directorate Mineral Research and Exploration*, Monography series 5, 66 pp.

Karaoğlan, F., Parlak, O., Robertson, A., Thöni, M., Klötzli, Urs, Koller, F., Okay, A.I., 2013. Evidence of Eocene HT/HP metamorphism of ophiolitic rocks and granitoid intrusion related to Neotethyan subduction processes (Doğanşehir area, SE Anatolia). *Geological Society,* London, Special Publications, 372.

Kirkpatrick, J.D., Rowe, C.D., (in press). Disappearing ink: How pseudotachylytes are lost from the rock record, Journal of Structural Geology, http://dx.doi.org/10.1016/j.jsg.2013.03.003

Koç, A., Kaymakcı, N., 2013. Kinematics of Sürgü Fault Zone (Malatya, Turkey): A remote sensing study. *Journal of Geodynamics*, 65, 292–307.

Kuscu, I., Gencalioglu, Tosdal, R.M., Ulrich, T.D., Friedman, R., 2010. Magmatism in the southeastern Anatolian orogenic belt: transition from arc to post-collisional setting in an evolving orogen. In: Sosson, M., Kaymakci, N., Stephenson, R. A., Bergerat, F. & Starostenko, V. (eds). Sedimentary Basin Tectonics from the Black Sea and Caucasus to the Arabian Platform. The Geological Society of London, Special Publications, 340, 437–460. DOI: 10.1144/SP340.19 0305-8719

Le Bas, M.J & Streckeisen, A.L., 1991.The IUGS systematics of igneous rocks. J. Geol. Soc. London 148, 825-833.

Mambane, P.W., Hein, K.A.A., Twemlow, S.G. & Manzi, M.S.D., 2011.Pseudotachylite in the South Boundary Fault at the Cooke Shaft, Witwatersrand basin, South Africa. South African Journal of Geology, Vol. 114.2, 109-120, doi:10.2113/gssajg.114.2.109

Maden Tetkik ve Arama Enstitüsü (MTA), 1994. Geological map of Turkey, scale 1:100,000, n. 123 (Elbistan).

Nalbant, S.S., McCloskey, J., Steacy, S., Barka, A.A., 2002. Stress accumulation and increased seismic risk in eastern Turkey. Earth and Planetary Science Letters, Vol. 195, issues 3–4, 291–298. DOI: 10.1016/S0012-821X(01)00592-1

Perinçek, D., Kozlu, H., 1984. Stratigraphy and structural relations of the units in the Afşin-Elbistan-Doğanşehir region (Eastern Taurus). In: O, Tekeli., and M. C, Göncüoğlu, (eds.), Geology of the Taurus Belt, 182-198.

Passchier, C.W., Trouw., R.A.J., 2005. Microtectonics, 2nd revised and enlarged edition. *Springer*, Berlin-Heidelberg, 366 pp.

Powell, C.McA., 1979. A morphological classification of rock cleavage. Tectonophysics, 58, 21-34.

Ringwood, A.E. (1975) Composition and Petrology of the Earth's Mantle. McGraw Hill, USA, 617 pp.

Robertson, A.H.F., 2002. Overview of the genesis and emplacement of Mesozoic ophiolites in the Eastern Mediterranean Tethyan region.*Lithos*, 65, 1–67.

Robertson *et al.*, 2006. The Berit transect of the Tauride thrust belt, S Turkey: Late Cretaceous–Early Cenozoic accretionary/collisional processes related to closure of the Southern Neotethys. *Journal of Asian Earth Sciences*, 27, 108–145.

Schmid, R., 1981. Descriptive nomenclature and classification of pyroclastic deposits and fragments: Recommendations of the International Union of Geological Sciences Subcommission on the Systematics of Igneous Rocks. Geology.The Geological Society of America. Boulder. Vol. 9, p. 41-43.

Şengör, A.M.C., Görür, N., Şaroğlu, F., 1985. Strike-slip faulting and related basin formation in zones of tectonic escape: Turkey as a case study. In: Biddle, K. T., Christie-Blick, N. (eds.). Strike-slip Deformation, Basin Formation, and Sedimentation. Society of Economic Paleontology & Mineralogy, Special Publications, 37, 227–264.

Streckeisen, A. L., 1978. IUGS Subcommission on the Systematics of Igneous Rocks.Classification and Nomenclature of Volcanic Rocks, Lamprophyres, Carbonatites and Melilite Rocks.Recommendations and Suggestions.Neues Jahrbuch für Mineralogie, Abhandlungen, Vol. 141, 1-14.

Winter, J.D., 2001.An Introduction to Igneous and Metamorphic Petrology.*Prentice Hall*, New Jersey, 697 pp.

Wortel, M. J. R. & Spakman, W. 2000.Subduction and slab detachment in the Mediterranean–Carpathian region. Science, 290, 1910–1917.

Xu, G., Will, T.M., Powell, R., 1994.A calculated petrogenetic grid for the system K20-FeOMg0-AI2O3-SiO2-H20, with particular reference tocontact-metamorphosed pelites. J. Metam. Geol.,12, 99-119

Yılmaz, Y., Yifgitba, E., Gen, C., 1993. Ophiolitic and metamorphic assemblages of southeast Anatolia and their significance in the geological evolution of the orogenic belt.*Tectonics*, vol. 12, 5, 1280-1297.

Appendix

1. Map

2. Field photos

3. Field measurements

4. Scans of thin sections

5. Porphyroclast analysis

6. SEM imagery

7. SEM chemical data

1.1 Map

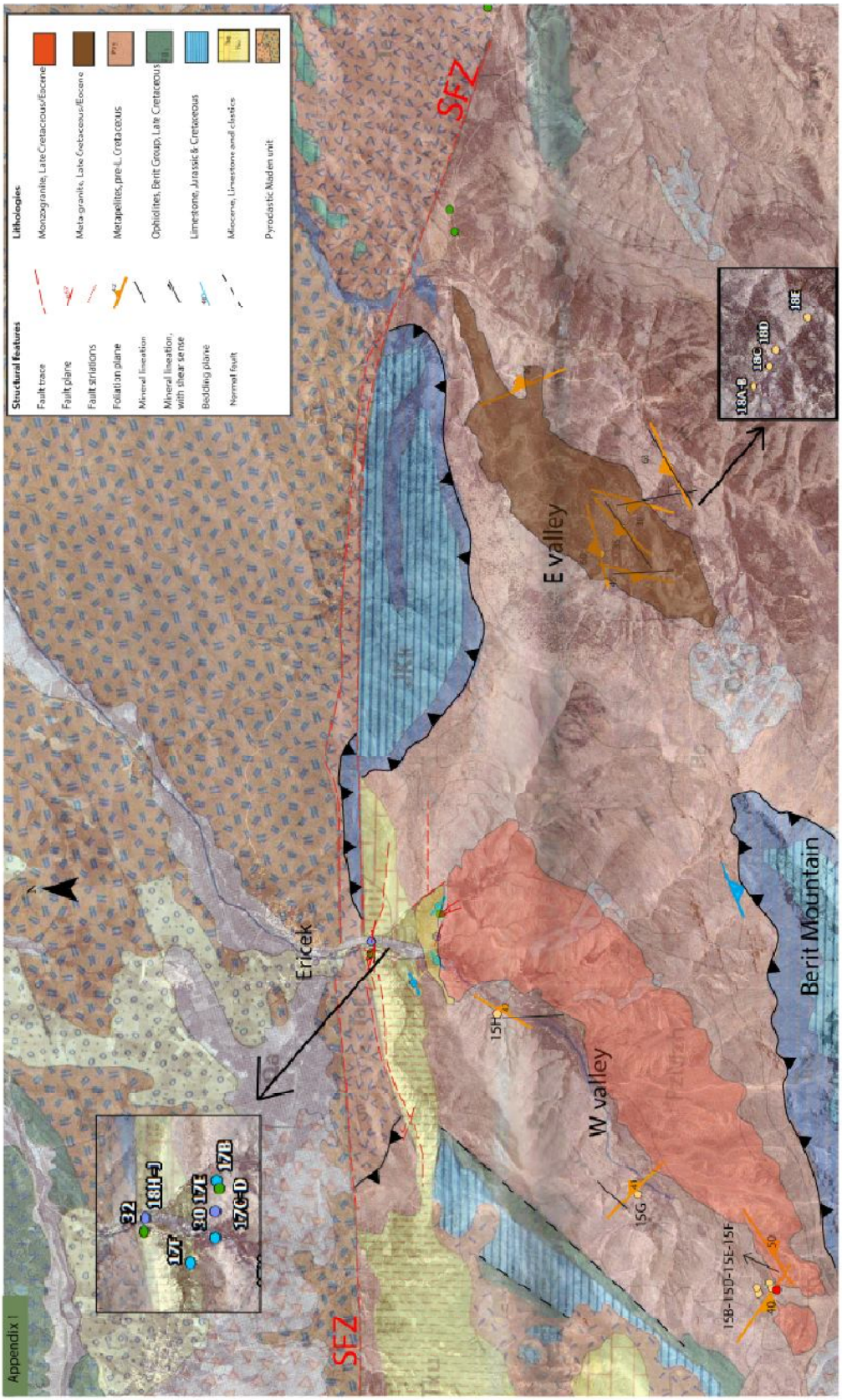
Structural features
Fault trace
Fault plane
Fault striations
Foliation plane
Mineral lineation
Mineral lineation, with shear sense
Bedding plane
Normal fault
Lithologies
Monzogranite, Late Cretaceous/Eocene
Meta-granite, Late Cretaceous/Eocene
Metapelites, pre-L. Cretaceous
Ophiolites, Berit Group, Late Cretaceous
Limestone, Jurassic & Cretaceous
Miocene, Limestone and clastics
Pyroclastic Maden unit
SFZ
SFZ
Ericek
E valley
W valley
Berit Mountain
15H
15G
15B-15D-15E-15F
18A-B
18C
18D
18E
0
0.75
1.5
3 Kilometers
Geological Map of the study area. - A.M. Currin Sala, MSc Thesis
Appendix I

2. Field photos

15B (above). 15D (below)

15E (above). 15F (below)

15G (above). 17D (below)

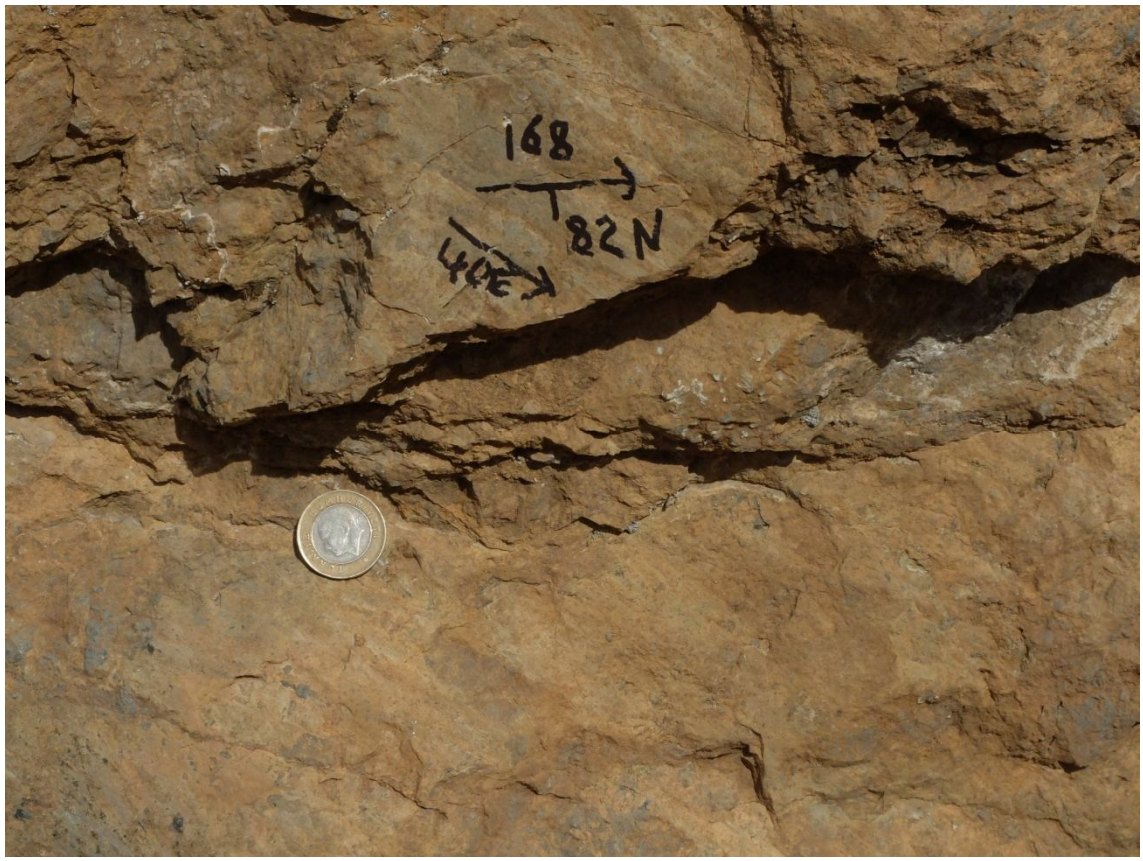

17E (above). 17C (below)

17D (above). 17H (below)

18B (above) 18C (below)

18D (above) 18 E (below)

18F (above) 18J (below)

3. Field measurements

Latitude	Longitude	Photo	Type of measurement	Photo orientation	rock type	Measurements	sample	Date
38,028919	36,833846	7	foliation + lineation	(view to NW)	HG schist - zoom on foliation plane	Foliation: N71/80S, Lineation (pitch): 49W (L in trend and plung	15-B	15/10/13
38,02843	36,83355	8	contact schist/granite	(view to NE)	contact between schist and granite (steep)	steep contact (oriented ~N60/almost vertical)		15/10/13
38,029192	36,834548	10a	foliation + lineation		schist close to contact with dyke	Foliation schist: N56/50SE, L(pitch): 24S		15/10/13
-	-	10b	contact schist/granite		contact dyke/schist	contact: ~N89/vertical		15/10/13
-	-	10e	foliation + lineation		contact schist/dyke (oriented sample)	F: N40/38SE, L: N24)	15-D	15/10/13
38,030264	36,833102	11			oriented fold + Hornfels/schist with Cordierite and Andalusite - sample not oriented (not in-situ)		15-E	15/10/13
38,03046	36,83384	12	foliation + lineation		Foliated and Lineated impure marble with potential px	(F:N125/40SW, L:N200, Top N)	15-F	15/10/13
38,04285	36,84561	13	foliation + lineation	(view to NW)	Dark schist	Oriented sample (F:N135/41NE, L:N43)	15-G	15/10/13
38,05775	36,86852	14	foliation + lineation	(view to NW)	Foliated green/grey schist	Foliation: N30/42E, Lineation: N177	15-H	15/10/13
38,064042	36,88228	27a	bedding		Miocene Limestone	bedding: N127/29NE (view to E)		17/10/13
-	-	27b	bedding		Miocene Limestone	(N127/29NE)	17-B	17/10/13
	36,881315	28d	fault plane	(view to NNE)	Fault zone in limestone	fault zone (~N160/vertical)	17-C	17/10/13
-	-	28e	fault plane+ striations		Fault surface with striations	(Fault plane: N168/82N; striations (pitch): 40E)		17/10/13
-	-	28f	fault plane	(view to NNE)	Fault zone in limestone	(~N168/82N)	17-D	17/10/13
-	-	28g	fault plane+ striations	(view to ESE)	Fault surface with striations	(Fault plane: N145/65N, striations (pitch): 30W)		17/10/13
38,064104	36,878481	29c	green surface		granite -zoom to the greenish surfaces, possible fractures with chlorite (view to NNE)	greenish surfaces ~110/vertical)	17-E	17/10/13
-	-	29d	veins on green surface	(view to NNE)	granite - pinkish veins	veins ~N94/60N)		17/10/13
38,064049	36,875317	30a	bedding	(view to W)	Miocene limestone (same loc. 16)	Bedding of Miocene limestone on top (N60/50N)		17/10/13
-	-	30c	bedding	(view to W)	layered unit: porous beds of calcite/hornblende?	N40/60N		17/10/13
38,06638	36,87231	31	bedding	(view to S)	Bedded Miocene unit above the limestone (volcanic or sedimentary?)	bedding: N64/48N	17-F	17/10/13
38,07081	36,8759	32	fault plane	(view to W)	Surgu fault separating JK limestone (N) with Miocene "volcanics" (S)	Fault plane: N101/60N		17/10/13
38,07074	36,8776	33m	fault plane+ striations		Fault plane in JK limestone	fault plane N106/67N; striation (pitch): 28E		17/10/13
-	-	33n	fault plane+ striations		fault plane	(FP:N120/63N, striation (p): 40E)	17-G	17/10/13
-	-	33q	fault plane+ striations		sheared dark/brown/orange material within gauge	Fault plane: N92/70N, striation (pitch): 10E	17-H	17/10/13
38,04808	36,92846	34a	cleavage	(view to NE)	granitic body - well developed cleavage and penetrative foliation	cleavage N75/60N (view to NE)		18/10/13
-	-	34e	foliation + lineation	(view to NE)	zoom to penetrative foliation	Foliation: N15/45W, Lineation: N357	18-B	18/10/13
38,04611	36,93183	35	foliation + lineation	(view to NE)	Fine grained quartzite (mylonitic?)	(F: N45/35W, L: N55)	18-C	18/10/13
38,0453	36,93438	36	foliation + lineation	(view to N)	Clear foliation LG metapelite - qtz rich ribbons	oriented: (F: N15/30W, L: N350)	18-D	18/10/13
38,04134	36,9397	37	foliation + lineation	(view to NE)	Alternation marble and schist - "calcschist"?	Foliation (F: N65/63NW, L: N60)	18-E	18/10/13
38,057	36,95034	38	foliation	(view to N)	Foliated LG pelites and carbonates	(F: N156/40NE)	18-F	18/10/13
	36,87758	39c	random surface		~0.5cm thick mylonitic band - orientation could correspond to conjuguate of fault plane??	measure from rock -(random oriented surface: 49/59W)	18-H	18/10/13
-	-	39h	random surface		wider zone (few mm) with finer grain that could be a more distributed shear zone	measure from rock -(random oriented surface: 140/54W)	18-J	18/10/13

4. Scans of thin sections -PPL

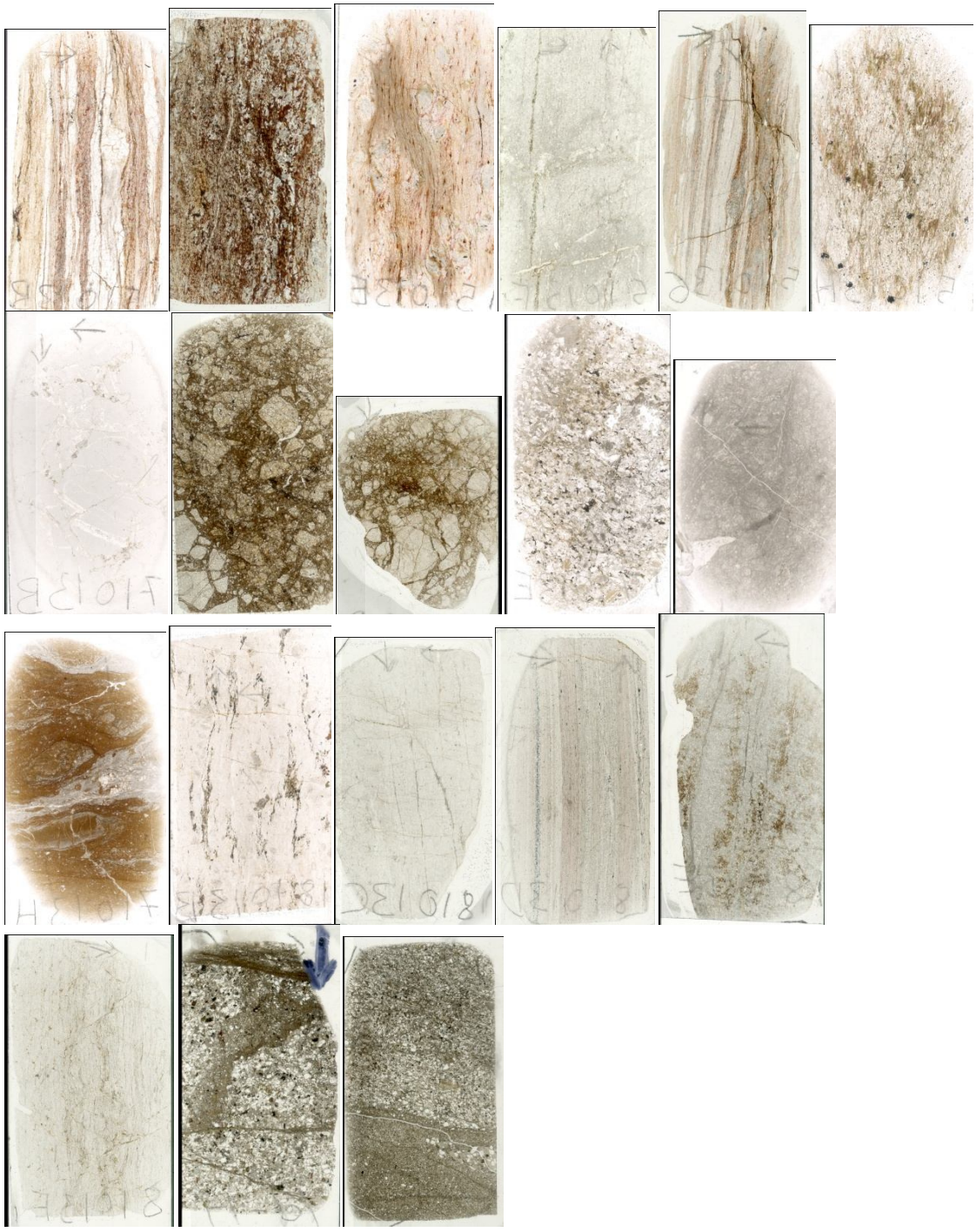

Scans of thin sections –PPX

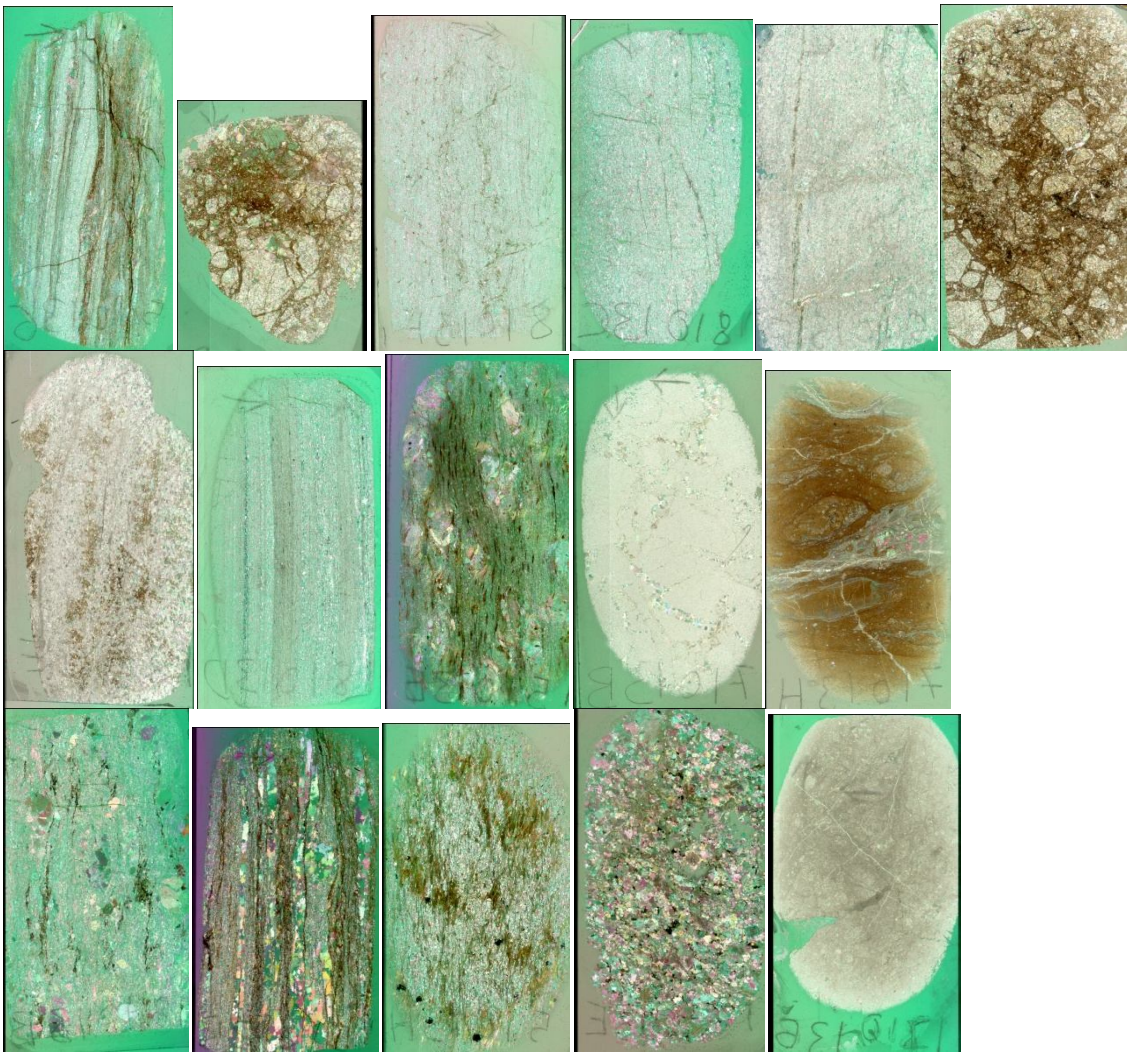

5. Porphyroclast analysis

Porphyroclast	Size along (mm)	Size across (mm)	Aspect ratio	Aspect ratio	$S_i \wedge S_e$ (°)	crystal elongation $\wedge S_e$ (°)	sense of rotation (el)	Si observations	clast wings	Si 45 deg to right	Type of clasts	Aspect ratio lower than 0.6
1	1,2	0,8	2/3	0,67	45	45	ccw	sigmoidal	Y	Y	sigma-type (not mantled)	
2	2	1,6	0,8	0,80	55	0				Y		
3	4	2,2	0,55	0,55	60	30	cw	crenulated	Y	Y	sigma or mienral fish	0,55
4	2,6	2	10/13	0,77	90	0 (or 45?)	(cw)	sigmoidal (s)	Y	Y	sigma-type	
5,1	1,5	1,5	1	1,00	0	0		wraps around on outside		H		
5,2	2,4	2	5/6	0,83	90	45	cw	convex to right	irregular	V	delta-type	
5,3	1	1	1	1,00	0	0				H		
6	1,8	1,2	2/3	0,67	45	45	ccw	sigmoidal (s)	Y	Y	sigma-type	
7	1,2	0,8	2/3	0,67	45	0		sigmoidal (s)	(z sigmoid mantle around clast)	Y	sigma-type	
8	2,4	1,4	7/12	0,58	80	40	cw	sigmoidal (s)	Y	Y	sigma-type	0,58
9	4	2,4	0,6	0,60	0	0		straight		H		
10,1	2,8	1,6	4/7	0,57	0	0		wavy	N	H (a bit wavy)		0,57
10,2	3,8	2	10/19	0,53	50	50	ccw	sigmoidal (s)	Y	Y	mineral fish	0,53
10,3	2	1,1	0,55	0,55	45	30	ccw	sigmoidal (s) & wavy	?	Y	mineral fish	0,55
11	5,2	1,6	4/13	0,31	30	30	ccw	sigmoidal (s)	Y	Y (very flattened)	mineral fish	0,31
12	2,4	1,8	0,75	0,75	55	45	cw	sigmoidal (s)	Y (small)	Y	sigma-type	
13	2,8	1,8	9/14	0,64	0	45	cw		Y	H	sigma-type	
14,1	4	2,6	0,65	0,65	45	30	cw	sigmoidal (s)	Y	Y	sigma-type	
14,2	1,8	1	5/9	0,56	90	0		straight	not clear	V		0,56
15	2,6	2	10/13	0,77	40	20	cw	sigmoidal (s)	not clear	Y		
16	1,8	1,6	8/9	0,89	85	30 (not sure)	cw	convex to right	not clear	V		
17	6	1,2	0,2	0,20	20	20	ccw			Y (very flattened)	mineral fish	0,2
18	3,6	2	5/9	0,56	90	45	ccw	crenulated	Y	V	fi-type	0,56
19	3,4	2,6	13/17	0,76	60	50	cw	sigmoidal (s)	Y	Y	sigma-type	
20	3,4	2,8	14/17	0,82	50	50	cw			Y	sigma-type	
21	4,2	2,2	11/21	0,52	90	40	cw	sigmoidal (s)		V		0,52
22	4,2	2,2	11/21	0,52	45	45	ccw	sigmoidal (s)	Y	Y	mineral fish	0,52
23	3,2	2,2	11/16	0,69	60	45	cw	sigmoidal (s)		Y		

5. SEM imagery

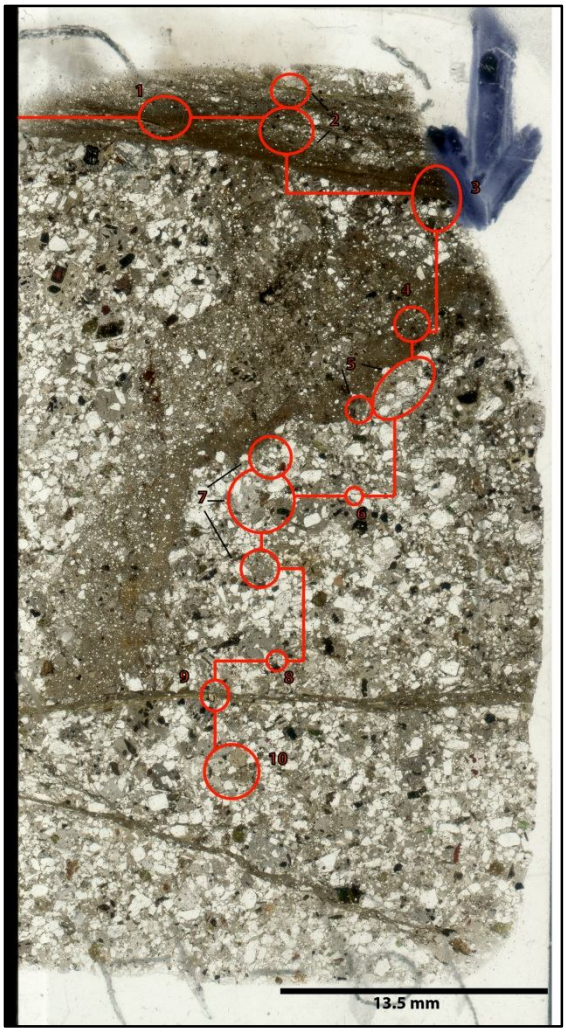

Fig. 1 - Analysis points: circles (or groups of circles) 1 to 10.

All the following images are "upside down"

Dates: Day1 (03-14) - Day 2 (20-03-14) – Day 3 (26-03-14).

Circle-1

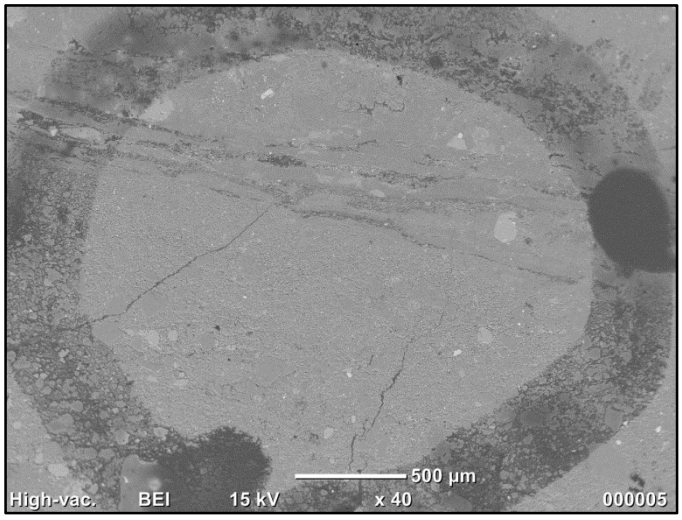

Fig. –2 - Circle 1 with vein in the middle (image **05** – name in folder: **D2-C1-1**). (orientation upside down). This circle is found within the dark vein at the top of the sample (see fig –x- top, with circle locations). Some streaks can be seen in the same direction of the vein elongation (so veins within the vein). The rest of the material appears to be made up of angular clasts of different shapes and sizes.

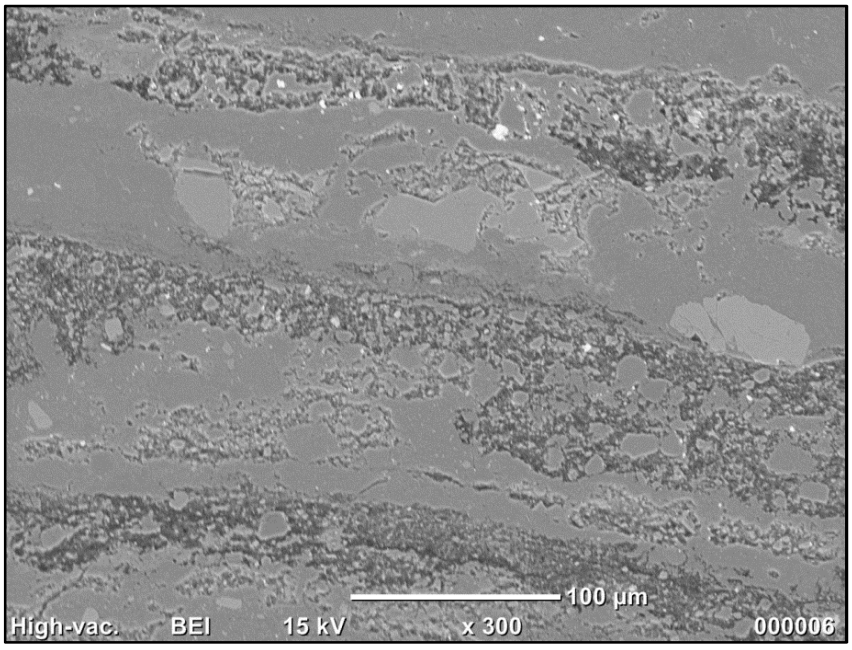

Fig. –3 – Circle 1. Close-up of vein indicated in previous image (Fig. X). (image **06** – name in folder: **D2-C1-2**). (orientation upside down). The darker areas correspond to material that has been polished out from the relief created by the lighter phase (therefore space with deeper finer-grained material: int. presence of clay). The lighter part of the vein is made up of a

uniform mass the microstructure of which is not clearlyvisible (70% surface), with two or three other different phases in this same unit (with preserved relief). Clasts of the predominant light phase can be found within the polished out trench-like sections, (40-50% of trench area). These clasts are subrounded, well sorted, with some clasts of grain sizes ranging approximately from 2 to 10 microns and another class of smaller grain size.

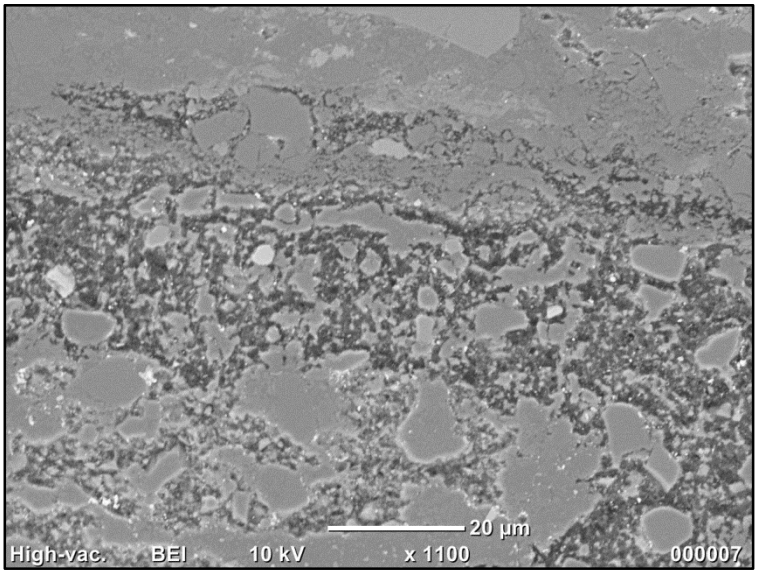

Fig – 4- This backscattered electron image (image **07** – name in folder: **D2-C1-3**)shows a close-up of the previous (Fig. X) where one of the aforementioned trench-like bodies is zoomed into. Here the clasts appear subrounded to rounded but with different aspect ratios. They seem eroded and polished out. Some of these clasts present embayments. Here we can see that the edges of the lighter-coloured plateau also show some polished out areas (although not as deep).

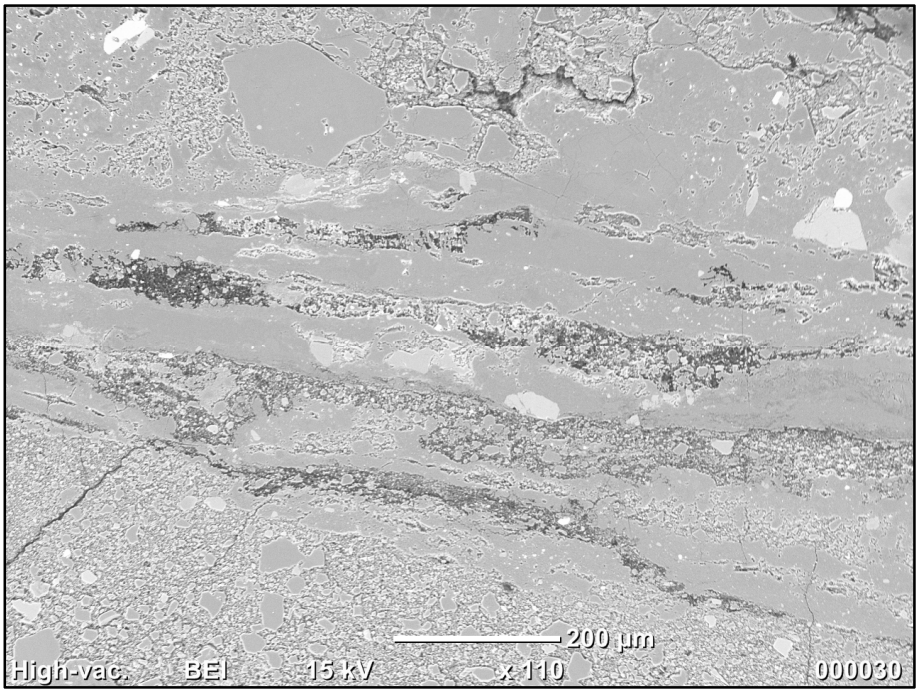

Fig. 5 - image (image **30** – name in folder: **D3-C1-1,** circle 1 revisited)

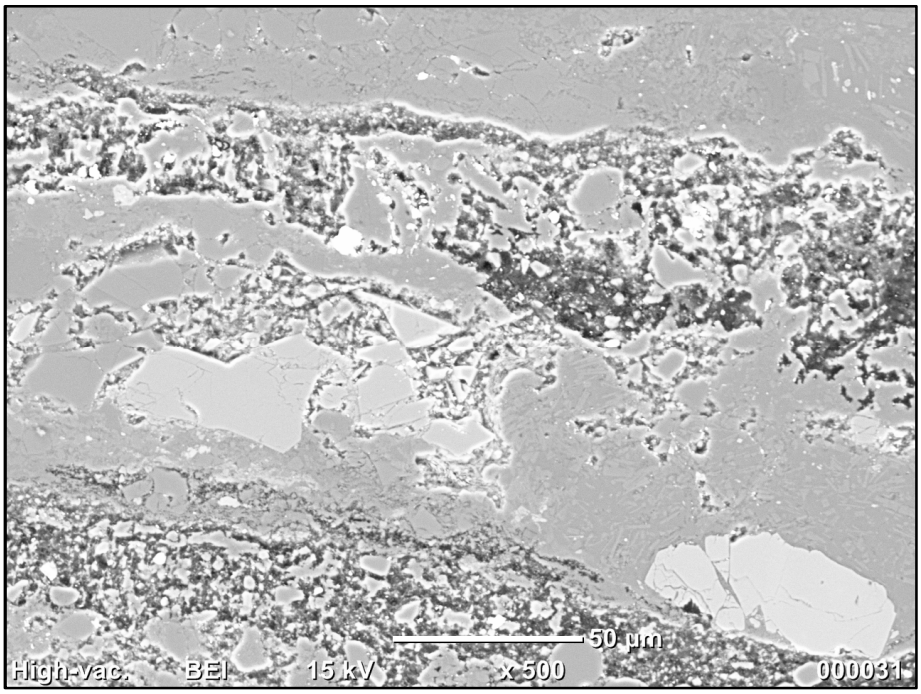

Fig. 6 - image (image**31** – name in folder: **D3-C1-2**).

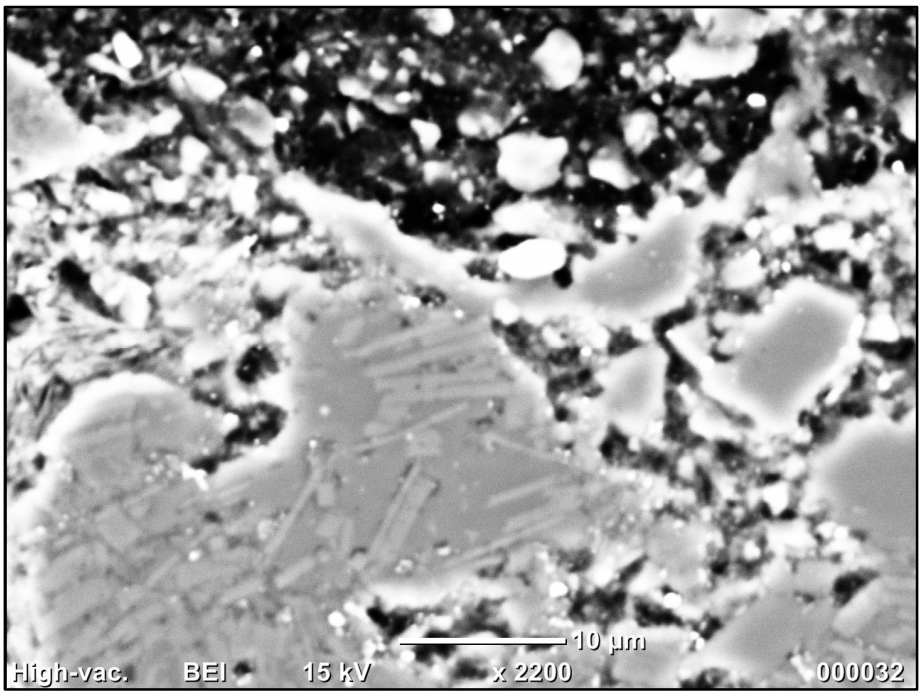

Fig. 7 - image (image**32** – name in folder: **D3-C1-3**).

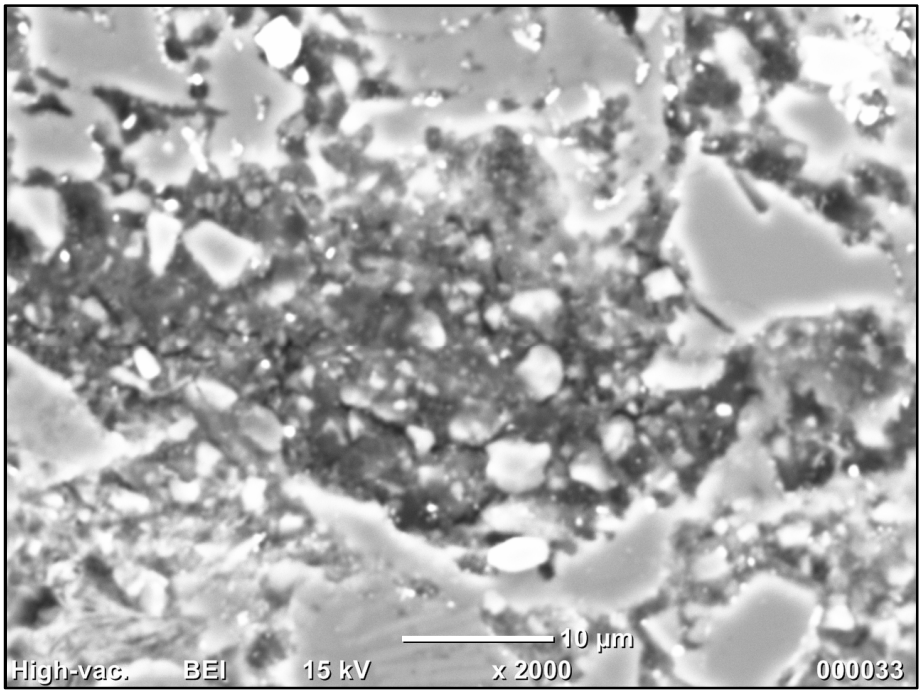

Fig. 8 - image (image**33** – name in folder: **D3-C1-4**).

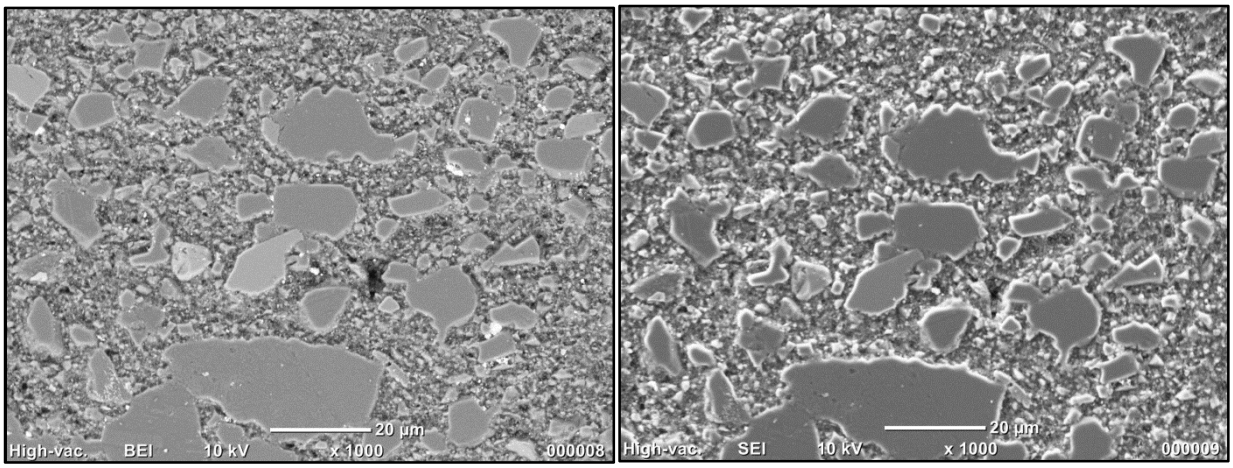

Fig 9a and 9b– BSE (backscattered electron) and SE (secondary electron) images (image **08** & **09** – name in folder: **D2-C2-1**&**D2-C2-2**) of circle 2, zooming into a trench area (darker part) within the vein. As in circle 1, subrounded, polished-out fragments and some embayed clasts can be observed.

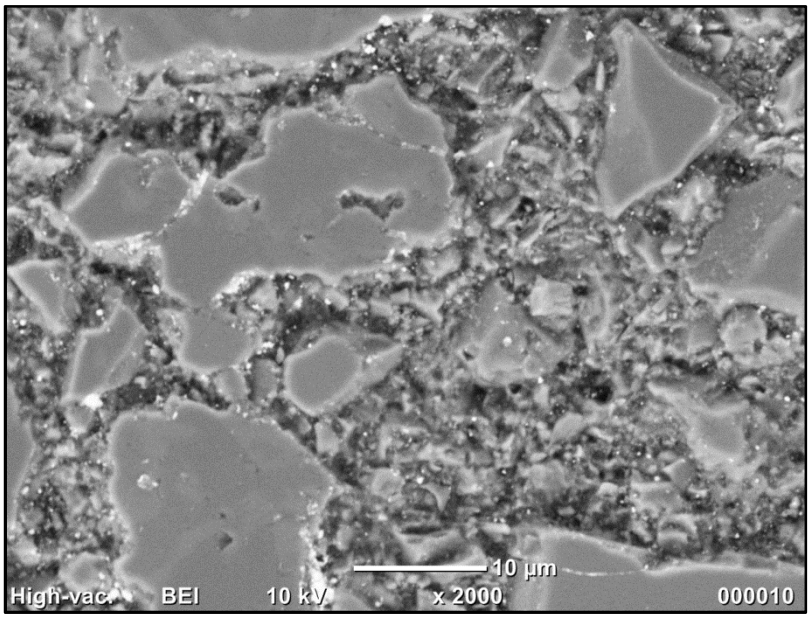

Fig. 10 – Close-up of previous image (Fig. X) where the darker area where relief appears to have been removed is visible. Finer-grained material can be identified in the matrix, angular fragments of around 1-2 microns. (image **10** – name in folder: **D2-C2-3**).

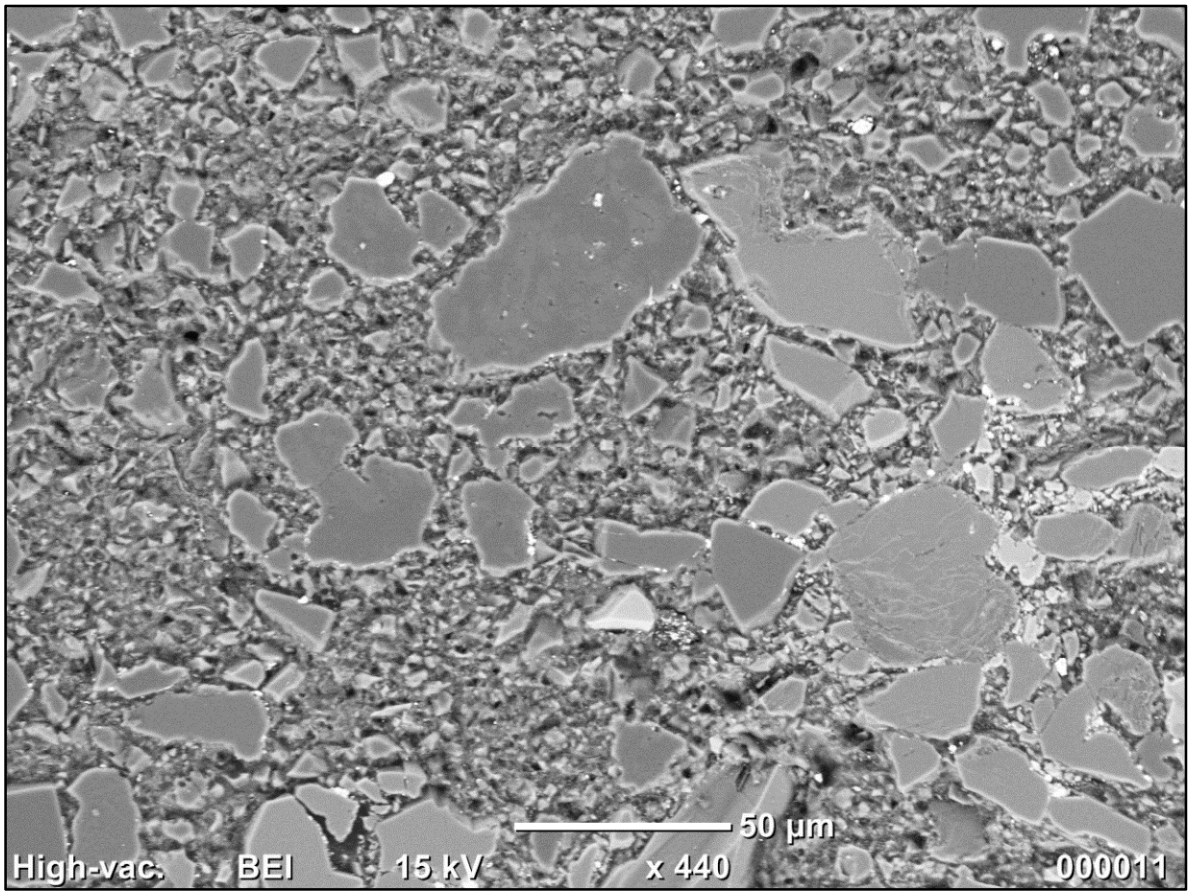

Fig. 11- This BSE image in circle 2 on a different area (not in the narrow vein area that we've been analysing so far) shows the larger clasts are subrounded and the smaller are angular. Embayed clasts are also visible. There are three major trends in grain size. Some of the larger fragments present internal cracks.

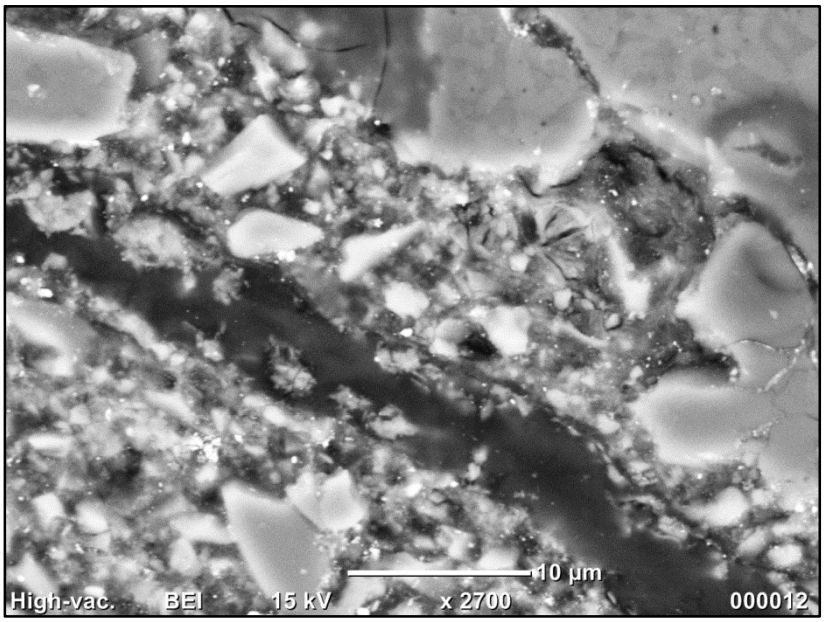

Fig. 12 – This BSE image (image **12** – name in folder: **D2-C2-5**) is a close-up located in circle 2b. The same heterogeneities in grain size and shape as in the previous image (Fig –X) are present here. There is a dark vein cross/cutting the image. (I think it´s a crack-hole-void, zooming in does not clarify anything, perhaps SE photographs should be taken, as well as analyses on the vein=crack itself', especially as some grains are surrounded by this black area/material). The large grains on the top/right of the image present inclusions or an exsolved phase within (plag and k-felds). Grains look polished out as in the previous images, there is one notable cluster of grains with a radial arrangement of cracks.

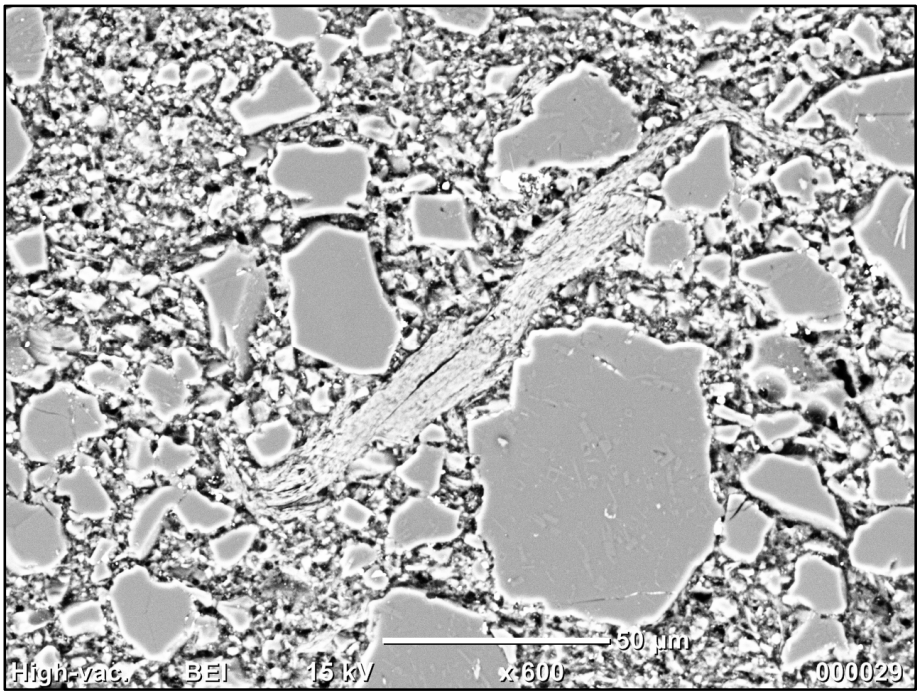

Fig 13 – BSE image (image **29** – name in folder: **D3-C2b**)of circle C2b where a elongated mineral (biotite) is found in between more equidimensional feldspar grains. The elongated mineral curves around some mineral grains at the edges.

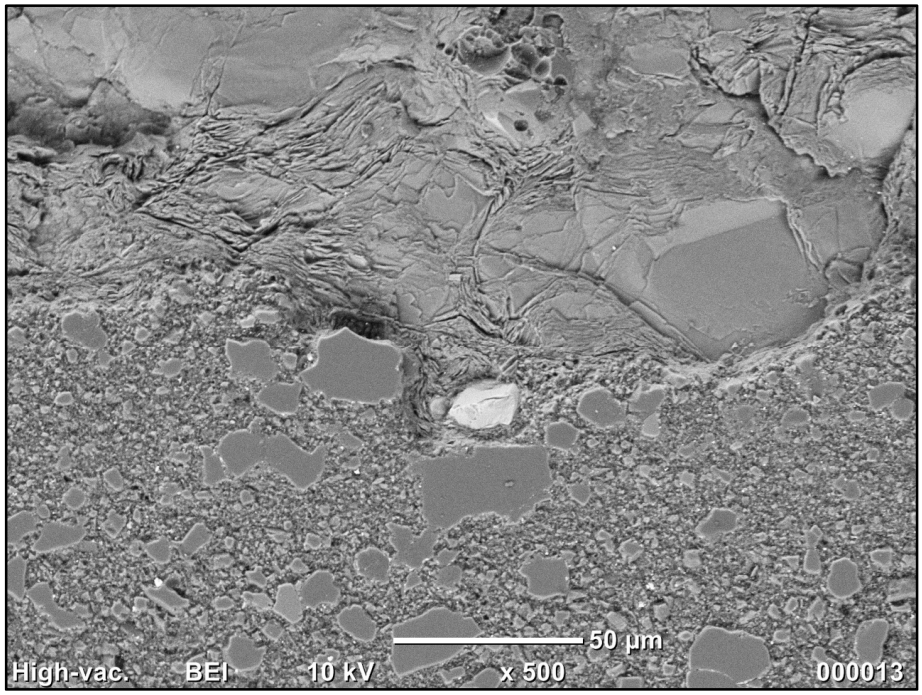

Fig 14 – This is a BSE image (image **13** – name in folder: **D2-C3-1**) of an area where the vein is in contact with the host rock. Here the vein is adjacent to a platy mineral (biotite as seen in thin section) and the contact is sharp. The vein shows its typical matrix composition of subangular and subrounded veins of different sizes.

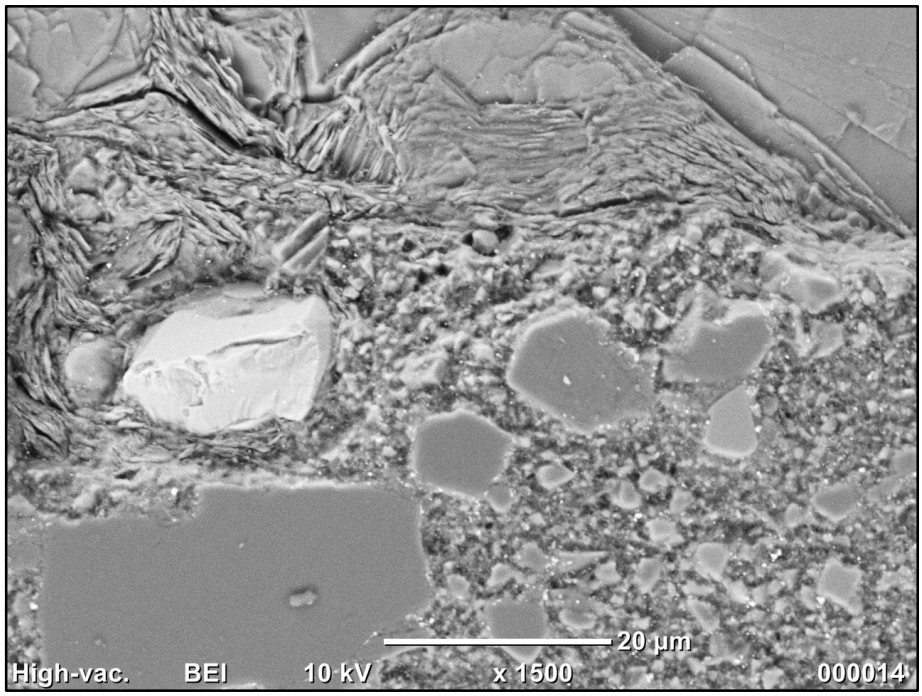

Fig. 15 – This is a BSE image (image **14** – name in folder: **D2-C3-2)** of the contact displayed in the previous image (Fig. X), with increased magnification.

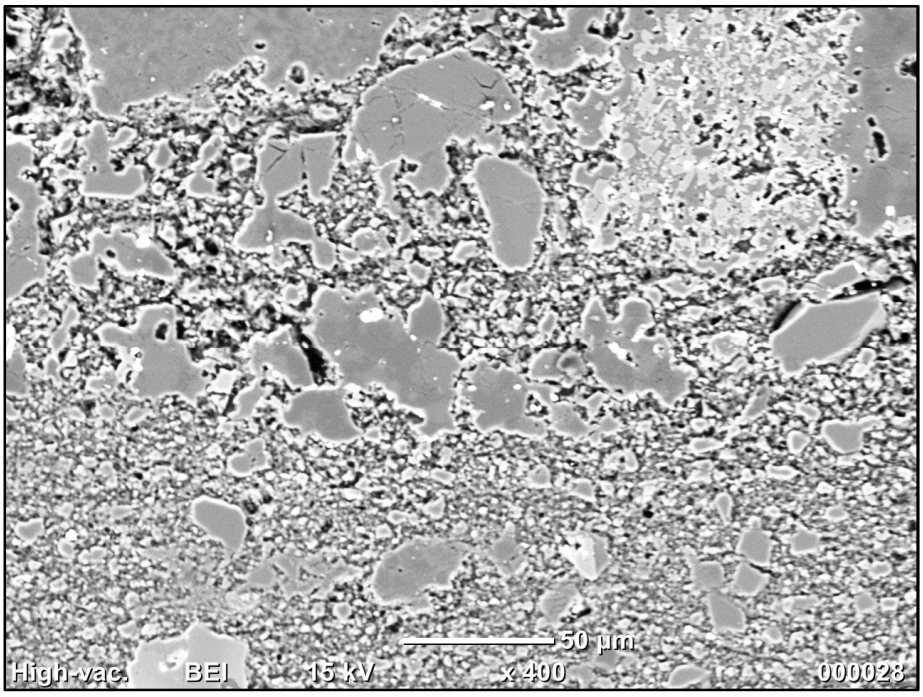

Fig. 16 – This BSE image (image **28** – name in folder: **D3-C3**) shows an area of circle C3 where host rock (top) is found in contact with vein (bottom). In this case, as opposed to other areas of the sample where the two domains meet, the transition is not exactly sharp.

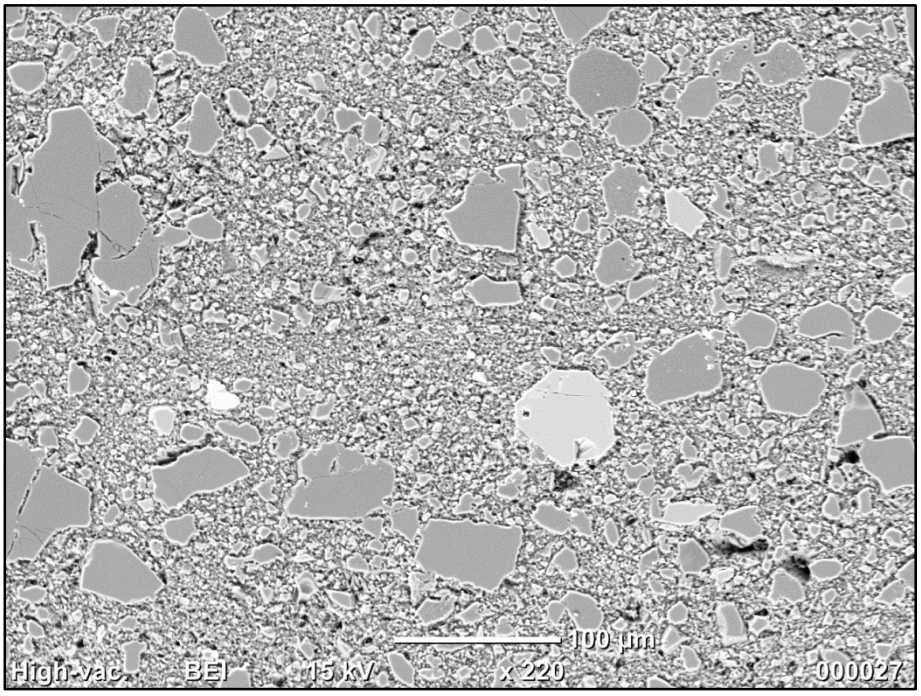

Fig. 17 – BSE image of matrix of darker vein area in circle C4 (image **27** – name in folder: **D3-C4-1**).

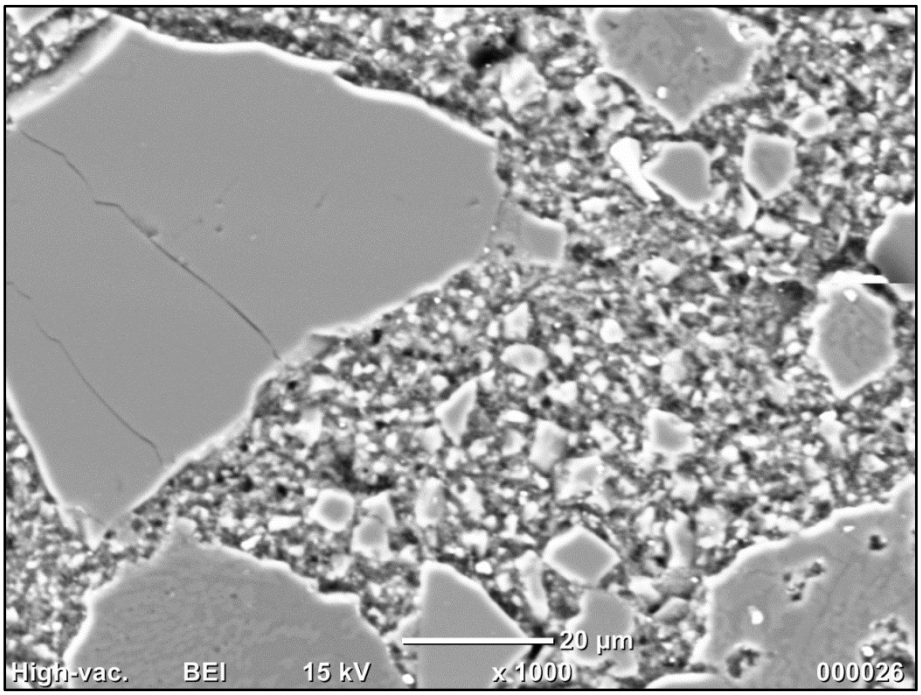

Fig. 18 – BSE image of vein area at C4 (image **26** – name in folder: **D3-C4-2**), zoom in on centre of previous image (Fig. X). There seems to be more of a heterogeneity of clast size than in C1 and C2 (?)

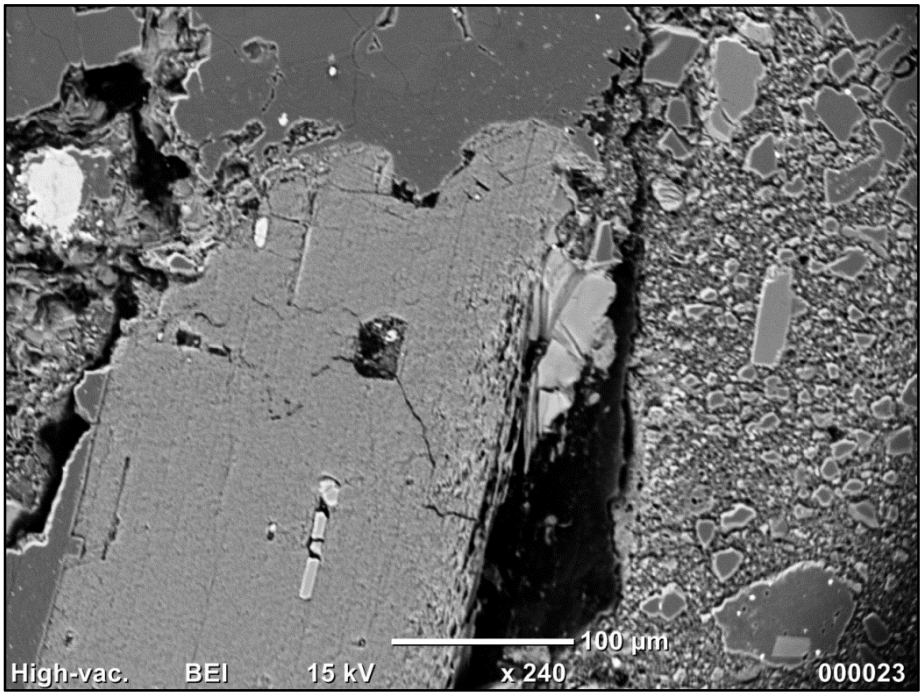

Fig. 19 – This BSE image shows a biotite grain of the host rock in contact with a darker vain area in circle C5b (image **23** – name in folder: **D3-C5b-1**). The difference in grain size between the host rock and the vein is clearly illustrated in this image. The separation in between the two domains is sharp (and there is a crack in between. the analysis of the crack shows very low and unclear peaks.)

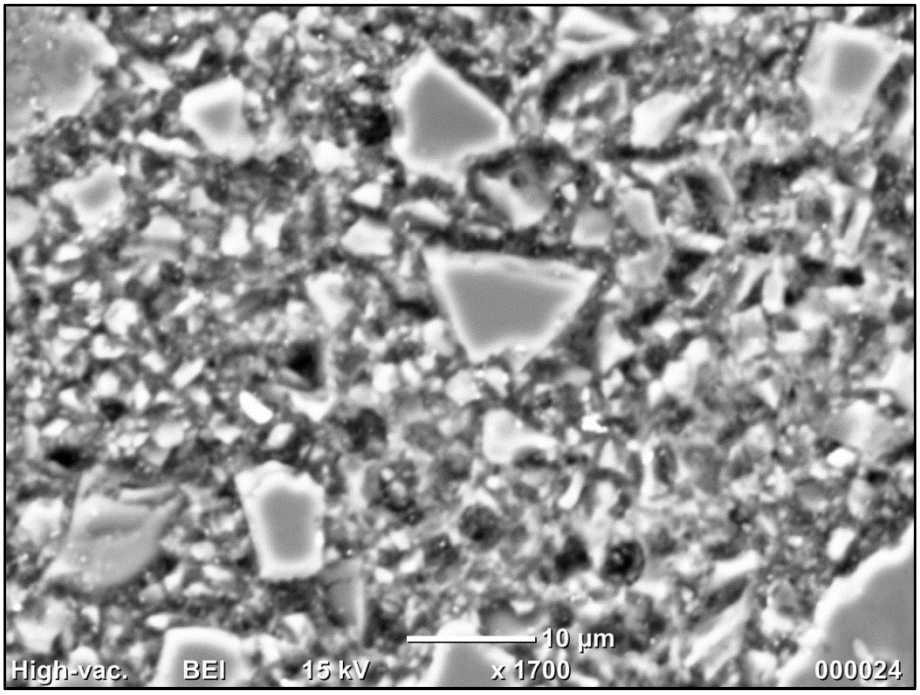

Fig. 20 – BSE image (image**24** – name in folder: **D3-C5b-2**). Close-up of vein area in circle C5b. Again, the fragments look angular and polished out.

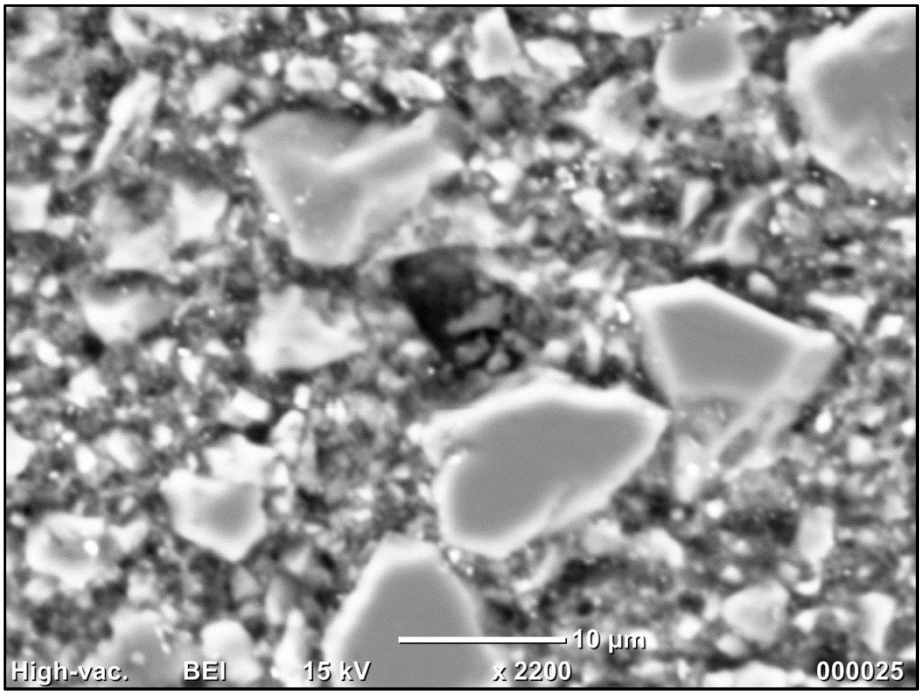

Fig. 21 – This BSE image (image **25** – name in folder: **D3-C5b-3**)shows the same area as the previous picture (Fig. X) with more zoom (not very well focussed).

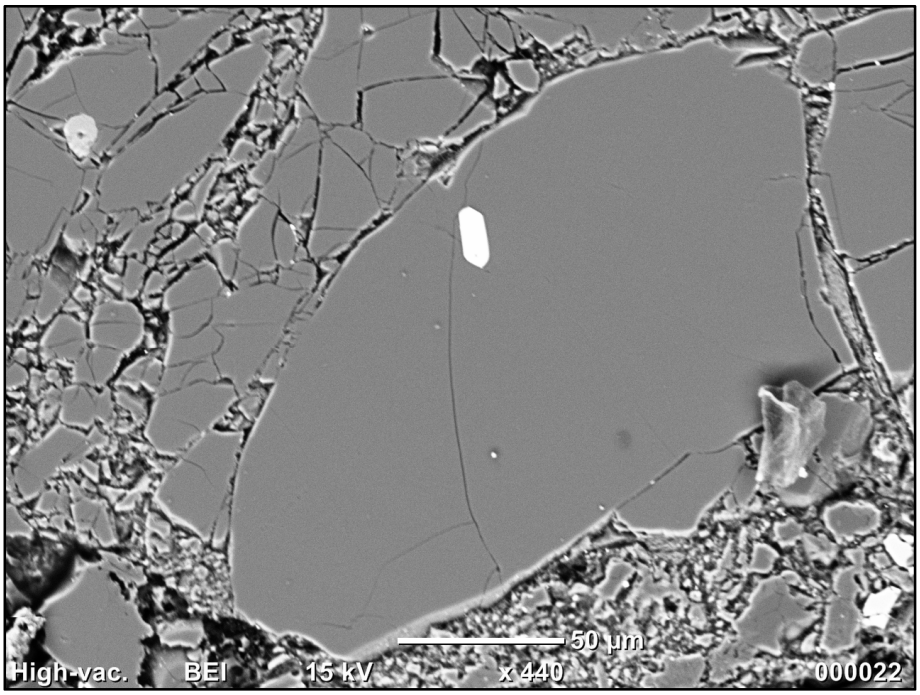

Fig. 22 –BSE image of a feldspar grain in the host rock with an apatite inclusion. The grains in this image show clear signs of brittle deformation (image **22** – name in folder: **D3-C6**).

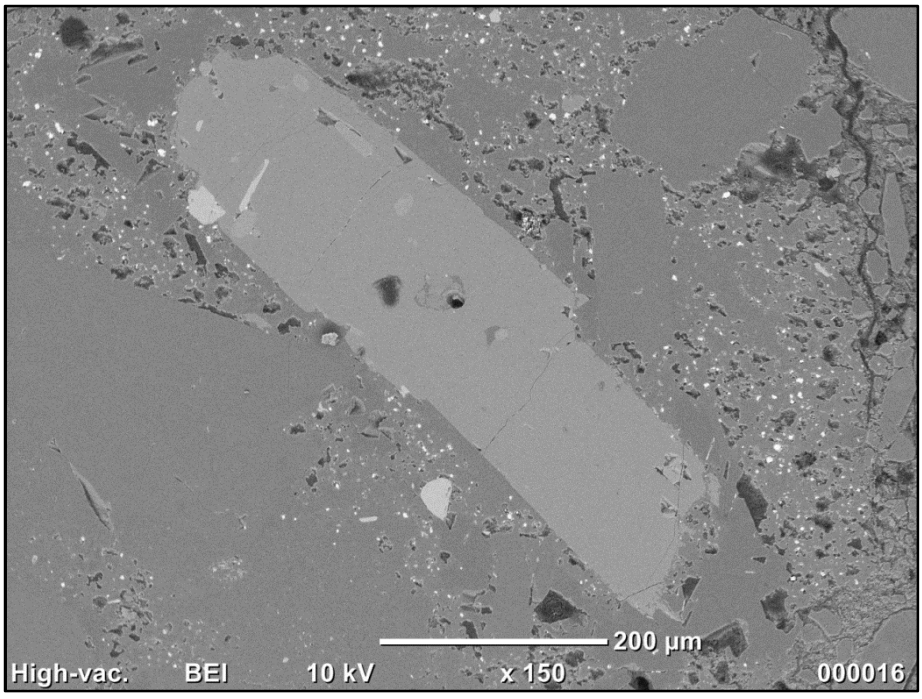

Fig. 23 – This is a BSE image of an area of sample 18H found outside the 'vein' areas in circle 7a (image **16** – name in folder: **D3-C7a-1**). The target of this image is the elongated mineral visible in the centre and the matrix surrounding it, with the purpose of assessing the composition of the host rock.

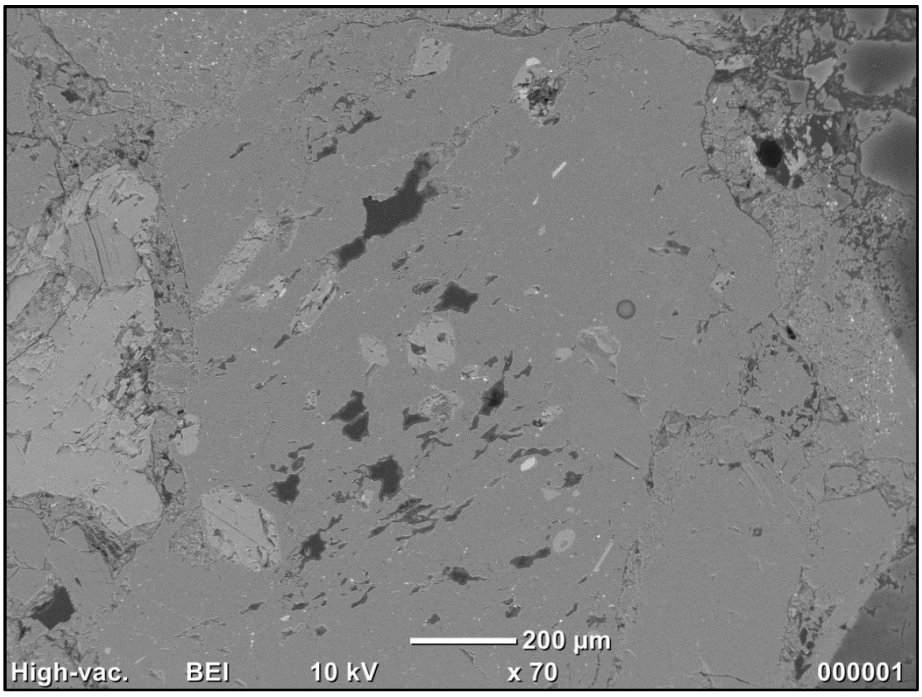

Fig. 24 – BSE image (image**01** – name in folder: **D1-C7b-1**). Within host rock matrix, grain with inclusions and matrix of thin lath-like structures uniform in composition according to analyses. Int. This is likely compacted ash with xenoliths (visible matrix: compacted ash made up of thin glass laths?)

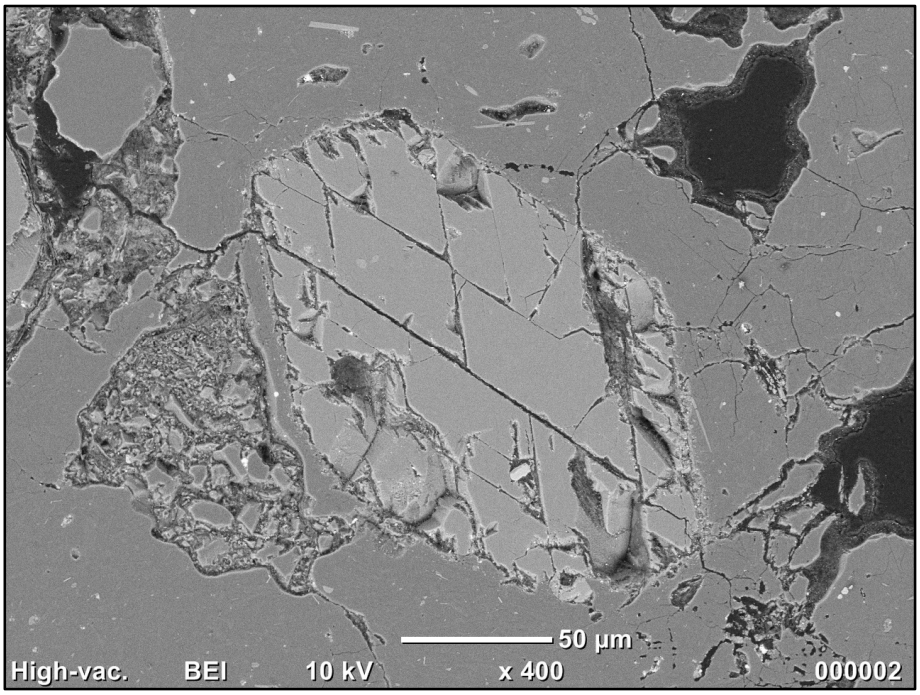

Fig. 25 – BSE image (image**02** – name in folder: **D1-C7b-2**). Zoom in on previous image, amphibole inclusion in clast.

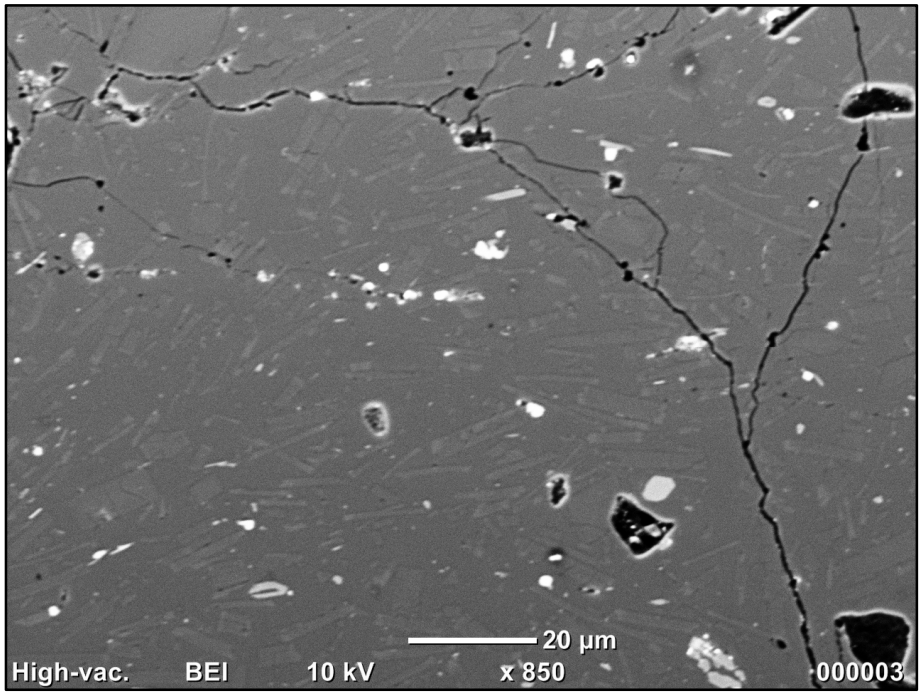

Fig. 26 – BSE image (image **03** – name in folder: **D1-C7b-3**) of the matrix which makes up most of a clast in circle C7b. The lath-like structures are visible, which represent a different composition of feldspar with respect to the darker area (matrix).

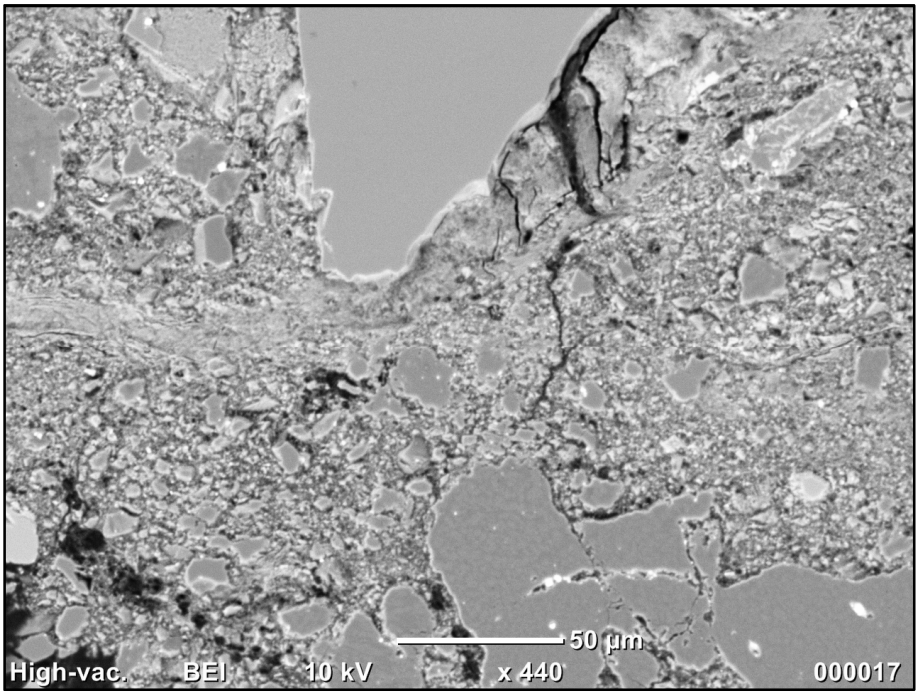

Fig 27 - BSE image (image 017 – in folder D3- C9 -1) showing a narrow vein towards the bottom of the thin section. This shows a similar microstructure to circle C1, C2, C3, C4. In addition, this image displays a meandering vein that is light orange in plane polarized light.

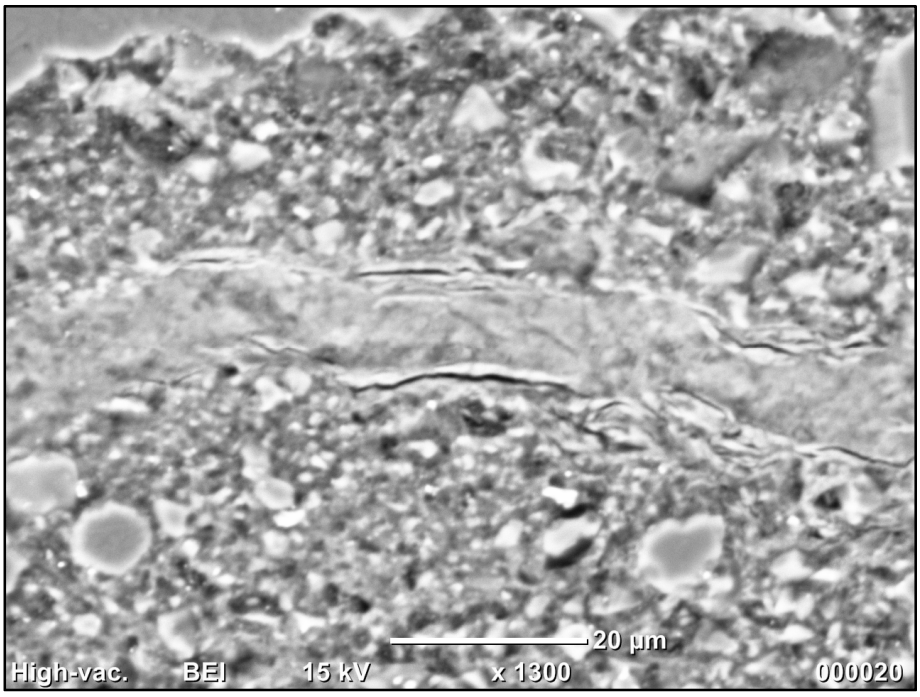

Fig.28 - BSE image (image 020 – in folder D3- C9 -4) showing a close-up of the vein mentioned in the caption of the previous figure (Fig. X).

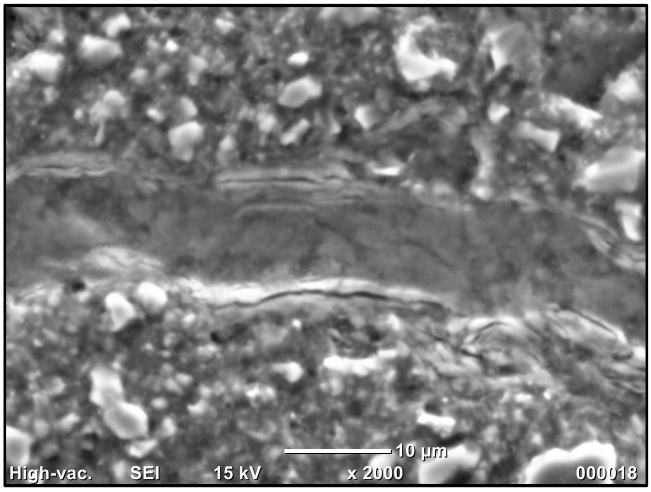

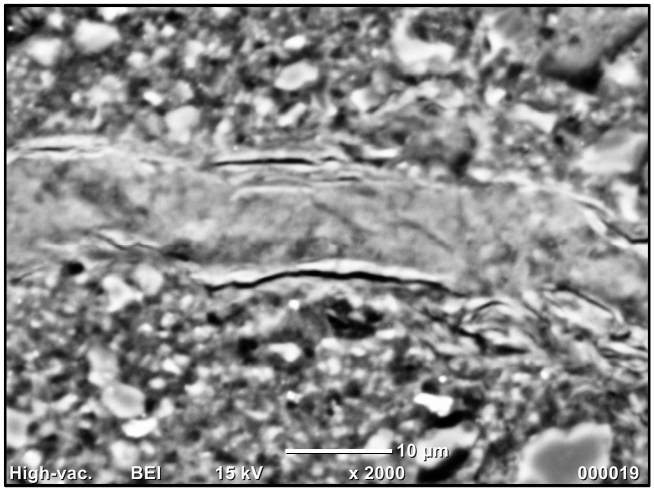

Figs. 29a and b - (image 018 and 019 – in folder D3- C9 -2 and D3-C9-3) SE and BSE images, respectively, of the vein shown in figs. X and X (2 previous). Some internal structure is visible.

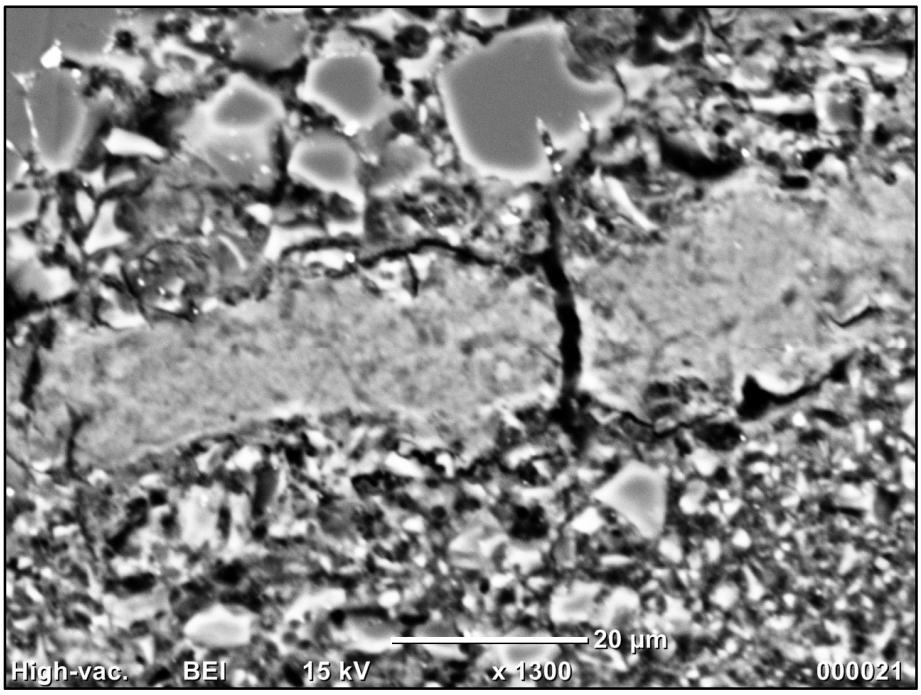

Fig. 30 – BSE image (image 021 – in folder D3- C9 -5) of a different area of the vein mentioned in the 3 previous images.

7. SEM chemical data

Chemical analyses of sample 18H (cations)

Analysis	Na	Mg	Al	Si	K	Ca	Fe	Ti	Mn	Ba	Tb	p	Total cations	Mineral
1	0,75	0,72	2,28	8,97	0,67	0,59	0,63							amphibole
2	1,66		4,26	7,81	0,13	1,1								
Min D5	0,5		0,12	8,49		0,14	2,47	0,01			2,64			
day2-1	1.19		2.53	9.54	1.04								14.31	alk feldspar
day3-1	0.14	2.80	2.80	6.09	2.38	0.03	2.28	0.83					17.08	bt
day3-2	0.73		2.66	9.47	0.67	0.32	0.04						13.89	alk feldspar
day3-3	0.37		2.19	9.87	0.96	0.18	0.05	0.04					13.66	alk feldspar
day3-4	0.31	2.32	2.02	6.66	0.20	2.56	1.76	0.38					16.21	
day3-5	0.01	0.05	0.06	0.35	0.07	8.71	0.06					5.74	15.05	apatite
day3-6		3.44	0.10	8.17		0.22	3.79	0.02					15.75	orthopyroxene
day3-7	0.96		4.45	7.57	0.14	1.57	0.07						14.76	plagioclase
day3-8	0.22	0.16	0.16	10.51	0.18	0.31	0.15	0.04				0.01	12.95	
day3-9	0.10		1.82	10.32	0.83	0.05	0.08	0.01					13.22	
day3-10	0.93		3.07	9.07	0.42	0.49	0.04	0.01					14.04	feldspars
day3-11	0.11	2.48	2.48	6.12	2.49	0.06	2.64	0.77				0.02	17.15	bt
day3-12	0.15	0.11	2.29	8.44	0.72	1.71	1.00	0.19				0.03	14.62	anorthite
day3-13	0.05		1.56	10.53	0.74	0.01	0.12	0.03					13.04	k-felds
day3-14	0.77		3.04	9.06	0.73	0.48	0.05	0.01					14.15	alk feldspar
day3-15	0.04	0.01	0.21	11.78	0.07	0.02	0.01	0.02					12.16	qtz/silica glass
day3-16		2.91	0.05	8.22	0.01	0.19	4.35						15.74	orthopyroxene
day 1- 2	1.66		4.26	7.81	0.13	1.10							14.96	plagioclase
day 1- 3	0.10		1.81	10.48	0.49	0.04							12.91	impure quartz
day 1- 4	0.47	3.15	1.62	6.97	0.14	1.77	1.92	0.25					16.28	hornblende
day 1- 5	0.72		2.26	9.77	1.44								14.18	k-felds
day 5 -1	0.01	0.49	0.54	10.08	0.14	0.23	2.21		0.02				13.73	alsil Fe-Mg
"	0.06	0.47	0.55	10.17	0.12	0.24	1.94	0.03					13.60	alsil Fe-Mg
day 5 - 2		1.93	1.83	8.62	0.86		1.53		0.01	0.11			14.90	
"	0.09	2.04	1.86	8.36	0.80	0.16	1.54	0.15					15.00	
day 5 -3		2.26	1.58	8.09	0.65		1.59	0.62					14.82	
"	1.79	0.05	4.57	7.65	0.12	0.76	0.02	0.02	0.03				15.01	

Chemical analyses of sample 15E (cations)

File name - PDF	Na	Mg	Al	Si	K	Ca	Fe	Ti	Mn	Ba	Tb	P	Total cations	Cations recalculated	Mineral
View002_0000201		1.17	3.91	5.58	2.51		3.32								
View002_0000202	0.27		3.26	8.77	2.66		0.01	0.03					15.01		Orthoclase
View002_quant-TiFeO			0.31	0.14			6.22	8.47					15.19		Ilmenite
View003_0000303	0.14	0.17	5.71	6.95	1.77		0.25	0.04					15.07		
View003_0000304															
View004_0000401	0.09	1.17	5.70	6.38	0.04	0.09	1.29	0.01	0.04	0.01			14.81	11	Cordierite
View004_0000402		1.43	4.13	5.76	2.46	0.02	3.11	0.25	0				17.15	16	Biotite
View005_0000501	0.01		10.96	3.65		0.08	0.08	0.05					14.83		Andalusite
View005_0000502	0.03	1.38	3.73	5.86	2.51	0.04	2.95	0.47	0.04	0.07			17.07		Biotite
View005_0000503	0.01	1.37	3.56	5.82	2.46	0.03	3.18	0.57		0.06			17.06		Biotite
View005_0000504		0.04	0.30	0.31	0.04	0.04	5.80	8.42	0.12	0.02			15.07		Ilmenite
View005_0000505	0.01	1.31	5.83	6.35			1.24						14.74		Cordierite
View006_0000601	0.04	1.33	5.74	6.39	0.01		1.22		0.05				14.77		Cordierite
View006_0000603		1.48	3.90	6.05	2.23		2.77	0.32	0.03	0.01			16.79		Biotite?
View006_0000604	0.13	0.07	6.77	6.20	2.12	0.02	0.17	0.03					15.51		Potassium feldspa
View007_0000701	0.20	0.02	3.23	8.74	2.89				0.02	0.03			15.15		Potassium feldspa
View007_0000703	0.06	1.26	3.71	5.85	2.43	0.05	2.97	0.55		0.03			16.92		Biotite
View008_0000801	0.03	1.19	3.68	5.73	2.65		3.37	0.53		0.06			17.24		Biotite
View009_0000901	0.28	0.03	3.14	8.86	2.65	0.03		0.01					15.01		K-feldspar
View009_0000902	0.21		3.20	8.80	2.76	0.03	0.03	0.01		0.02			15.06		K-feldspar
View009_0000903	1.63		3.72	8.56	0.09	0.44							14.44		Albite
View0011_00001101	0.04		10.34	4.09	0.04	0.02	0.23			0.02			14.78		Aluminosilicate?
View0011_00001102	0.06	1.16	5.65	6.47	0.03		1.29	0.03		0.01			14.71		Cordierite
View0011_00001103		1.34	3.66	5.88	2.47		3.08	0.53	0.02	0.02			17.00		Biotite